

# Feedback Control of a Tunable Laser for Cavity Optomechanics

---

*Jinqiang Ning, Tianchang Gu, and Zhijie Wang*

*Advisors: Prof. Yuxiang Liu and Prof. Yiming Rong*

*Dept. of Mechanical Engineering, Worcester Polytechnic Institute, Worcester, MA*

## **Abstract**

Precision tuning and measurements of a tunable laser wavelength is a challenging but important capability that is necessary for various applications including laser spectroscopy and nanophotonics. In this project, the team developed a LabVIEW-based software for convenient, intuitive, and multi-functional feedback control of a New Focus 6700 Tunable Laser System™, which is one of the leading tunable laser systems in the world. By controlling the motor scan of the laser cavity in the wide range and piezo scan in the narrow range, the wavelength tuning of the laser was fully controlled by the developed software with a resolution of a few picometers. More importantly, the team built a low-cost, high-accuracy, fiber-based Mach-Zehnder interferometer that can be used to both measure the laser wavelength and sense strain and stress on one of the interferometer optical paths. As a demonstration of the developed laser control system, a microscale cavity optomechanical device was optically characterized. By coupling light through a micrometer-sized fiber taper into the cavity optomechanical device while monitoring the transmission optical power, the developed system enabled the measurements of high optical quality factor (on the order of  $10^5$ ) of the microscale device. The project not only has served as an educational practice on various physics and engineering topics through both hands-on experience and software control of equipment, but also results in a fully developed control and measurement system for the tunable laser, which will benefit the future cavity optomechanics research at WPI.

# Table of Contents

<b>Abstract</b> .....	1
Table of Figures .....	4
Table of Tables .....	7
<b>1 Introduction</b> .....	8
1.1 Rationale .....	8
1.2 State of the Art.....	10
1.3 Goal and Objectives .....	12
<b>2 Working Principles and Characterization Results of the Equipment</b> .....	15
2.1 Fundamentals of Laser .....	15
2.2 Equipment Overview .....	15
2.3 Fiber Optical Coupler .....	18
2.4 Photon Detector.....	19
2.5 New Focus Laser Source .....	21
2.6 Optical Interferometers .....	26
2.6.1 Working Principles for Two Beam Interferometers.....	27
2.6.2 Two Beam Interferometers: Michelson Interferometers .....	27
2.6.3 Two Beam Interferometers: Mach-Zehnder Interferometers .....	29
2.6.4 Multiple Beam Interferometers: Fabry-Pérot Interferometers .....	31
2.6.5 Calculation of Interference .....	32
2.6.6 Calculation of interference for Fabry-Pérot Interferometers .....	35
2.7 Fourier Transform .....	36
2.8 Wavelength Calculation based on Adjacent Peaks of the Spectrum .....	37
<b>3 Experimental System Setup</b> .....	39
<b>4 Development of Software Control of the Tunable Laser with LabVIEW Codes</b> .....	42
4.1 Flowchart of Laser Feedback Control .....	42
4.2 Front Panel of Laser Feedback Control .....	44
4.3 Back-end of Laser Feedback Control.....	49
4.4 USB communication syntax and protocols .....	58
<b>5 Operating Protocol and Results of Tunable Laser Control</b> .....	61
5.1 Physical Connections of the System .....	61
5.2 Procedure of LabVIEW Control of Tunable Laser.....	61

5.3 Calculation of $\Delta L$ .....	66
5.4 Spectral Measurement Results of Laser Control of Motor Scan with LabVIEW .....	68
5.5 Spectral Measurement Results of Laser Control of Piezo Scan at 1280nm with LabVIEW .....	71
5.6 Spectral Measurement Results of Laser Control of Piezo Scan at 1300nm with LabVIEW .....	75
5.7 Spectral Measurement Results of Laser Control of Piezo Scan at 1320nm with LabVIEW .....	77
5.8 Curve Fitting to Determine the Optical Path Difference.....	79
5.9 Spectral Measurement Results of Disk Resonator with LabVIEW .....	82
<b>6 Error Analysis</b> .....	<b>87</b>
<b>7 Conclusion</b> .....	<b>91</b>
Bibliography .....	92

## Table of Figures

Figure 1.1.1. Schematic Diagram of Littrow Prism Tuning Mechanism [2] .....	9
Figure 1.1.2. Schematic Diagram of Birefringence Tuning Mechanism [3].....	9
Figure 1.2.1. Littrow Configured ECDL with Fixed Output Beam Direction, Based on the Design of Arnold, Wilson, and Boshier [6].....	10
Figure 1.2.2. The Optical Scheme of the Experimental Setup for Measurement of the Mode-Hop Free Tuning Range, Scanning of Absorption Spectrum of Molecular Iodine Vapors and Frequency Noise Properties. ....	11
Figure 1.2.3. Schematic Diagram of a Fabry-Perot cavity with harmonically bound end mirror [11] .....	12
Figure 1.3.1. System Schematic Diagram.....	13
Figure 2.1.1. Stimulated Emission Theory .....	15
Figure 2.2.1. 2x1 Optical Coupler [12].....	16
Figure 2.2.2. Cross Section of Optical Fiber [14].....	17
Figure 2.2.3. Internal Reflection of Optical Fiber [16].....	17
Figure 2.4.1. Photodetector Working Principle [17].....	19
Figure 2.4.2. THORLABS In Gas PDA20C Photodetector [18] .....	20
Figure 2.4.3. PDA20C Responsivity [18].....	20
Figure 2.4.4. PDA20C Responsivity (Zoom-in) [18] .....	21
Figure 2.5.1. Controller Block Diagram [19].....	21
Figure 2.5.2. Laser head [20].....	22
Figure 2.5.3. New Focus Laser Cavity Diagram [19].....	23
Figure 2.5.4. Diffraction-Grating Theory [21].....	24
Figure 2.6.1. Principle of Superposition of Waves [24] .....	26
Figure 2.6.2. Examples of Interference Spectral Plot [25].....	26
Figure 2.6.3. Michelson Interferometer Setup and Path of light in the interferometer [26] .....	28
Figure 2.6.4. Michelson Interferometer Fiber Setup Schematic Diagram .....	29
Figure 2.6.5. Mach-Zehnder Interferometer Working Principle [27] .....	29
Figure 2.6.6. Mach-Zehnder Interferometer Fiber Setup Schematic Diagram [28].....	30
Figure 2.6.7. Fabry- Pérot Interferometer Working Principle .....	31
Figure 2.6.8. Schematic Diagram of Fabry- Pérot Interferometer Classical Setup [29] .....	32
Figure 2.6.9. Fabry- Pérot Interferometer Fiber Setup.....	32
Figure 2.6.10. Schematic Diagram of Fabry–Pérot Interferometer Working Principle .....	35
Figure 2.8.1. Actual System Setup.....	39
Figure 2.8.2. Schematic Diagram of System Setup .....	40
Figure 2.8.3. Laser Source System .....	40
Figure 2.8.4. Mach Zehnder Interferometer Setup.....	41
Figure 4.1.1. Detailed System Flow Chart.....	43
Figure 4.2.1. LabVIEW Program Front View.....	44
Figure 4.2.2. While Loop .....	45
Figure 4.2.3. Case Structure.....	45
Figure 4.2.4. Event Structure .....	46
Figure 4.2.5. Stacked Sequence Structure.....	46
Figure 4.2.6. LabVIEW Subprogram of Wave Generation .....	47

Figure 4.2.7. Generated Waveform (Triangle Wave, Sine Wave and Saw-tooth Wave) .....	47
Figure 4.2.8. Signal produced from DAQ box, controlled by LabVIEW, measured by an oscilloscope. .	48
Figure 4.2.9. LabVIEW Subprogram of Signal Acquisitions .....	48
Figure 4.2.10. Measurement of Generated Signal and Reference of Generated Signal.....	49
Figure 4.3.1. Event Structure Drop Down Menu .....	50
Figure 4.3.2. Timeout Event in Event Structure .....	50
Figure 4.3.3. Wavelength Shift and Cursor Operation Event Case.....	51
Figure 4.3.4. Graph Data Output.....	51
Figure 4.3.5. Left Shift Situation .....	52
Figure 4.3.6. Detail Cases in the Sequence Structures.....	53
Figure 4.3.7. Right Shift Situation .....	53
Figure 4.3.8. Detail Case in Right Shift Wavelength Calculation .....	54
Figure 4.3.9. Cursor Operation Situation.....	54
Figure 4.3.10. Details of Sequence Structure in Cursor Operation Situation .....	55
Figure 4.3.11. Details of the Second While Loop.....	55
Figure 4.3.12. Details of the Third While Loop.....	56
Figure 4.3.13. Wave Generation .....	56
Figure 4.3.14. Data Acquisition .....	57
Figure 4.3.15. Data Displays.....	57
Figure 4.4.1. Front Panel of USB Communication Subroutine .....	58
Figure 4.4.2. Back Panel of USB Communication Subroutine.....	59
Figure 4.4.3. USB Command for Lambda Track.....	60
Figure 4.4.4. USB Command for (a) Current Sensing. (b) Power Sensing. (c) Cavity Temperature Sensing. (d) Diode Temperature Sensing. (e) Piezo Voltage Sensing. (f) Wavelength Sensing. ....	60
Figure 5.1.1. Physical Connection of the Laser Controller.....	61
Figure 5.2.1. Front Panel Screen Capture .....	62
Figure 5.2.2. Laser Power Mode and Control Buttons Panel.....	62
Figure 5.2.3. Basic Information Panel .....	63
Figure 5.2.4. Power, Current and Wavelength Setting Panel.....	63
Figure 5.2.5. Wavelength Scan Range Setting Panel.....	64
Figure 5.2.6. Wavelength Scan Velocity and Number Setting Panel .....	64
Figure 5.2.7. Piezo Modulation Setting Panel .....	64
Figure 5.2.8. Piezo Scan Reference and Feedback Graphs.....	65
Figure 5.2.9. Wavelength Vs Piezo Graph.....	65
Figure 5.2.10. Voltage Vs Wavelength Graph.....	66
Figure 5.4.1. Forward Motor Scan with Interferometer Intensity vs. Wavelength.....	68
Figure 5.4.2. Forward Motor Scan without Interferometer Intensity vs. Wavelength.....	69
Figure 5.4.3. Reverse Motor Scan with Interferometer Intensity vs. Wavelength.....	69
Figure 5.4.4. Reverse Motor Scan without Interferometer -Intensity vs. Wavelength .....	70
Figure 5.5.1. Forward Piezo Scan - Intensity vs. Piezo Voltage at Wavelength 1280 nm .....	71
Figure 5.5.2. Forward Piezo Scan without Interferometer at Wavelength 1280 nm - Transmission Intensity vs. Piezo Voltage .....	72
Figure 5.5.3. Reverse Piezo Scan Intensity vs. Piezo Voltage at Wavelength 1280nm.....	73
Figure 5.5.4. Forward Piezo Scan Wavelength vs. Piezo Voltage at Wavelength 1280 nm .....	73

Figure 5.5.5. Reverse Piezo Scan Wavelength vs. Piezo Voltage at Wavelength 1280 nm .....	74
Figure 5.6.1. Forward Piezo Scan Wavelength vs. Piezo Voltage at Wavelength 1300 nm .....	76
Figure 5.6.2. Reverse Piezo Scan Wavelength vs. Piezo Voltage at Wavelength 1330 nm .....	76
Figure 5.7.1. Forward Piezo Scan Intensity vs. Piezo Voltage at Wavelength 1320 nm.....	77
Figure 5.7.2. Reverse Piezo Scan Intensity vs. Piezo Voltage at Wavelength 1320 nm.....	77
Figure 5.7.3. Forward Piezo Scan Wavelength vs. Piezo Voltage at Wavelength 1320 nm .....	78
Figure 5.7.4. Reverse Piezo Scan - Wavelength vs. Piezo Voltage at Wavelength 1320 nm.....	78
Figure 5.8.1. Sine Wave Fitting for Forward Piezo Scan at Wavelength 1280nm .....	80
Figure 5.8.2. Sin Wave Fitting for Forward Piezo Scan at Wavelength 1300nm.....	80
Figure 5.8.3. Sine Wave Fitting for Forward Piezo Scan at Wavelength 1320nm .....	81
Figure 5.9.1. Nanophotonic Device (Disk Resonator).....	83
Figure 5.9.2. Forward Motor Scan with Disk Resonator Intensity vs. Wavelength .....	84
Figure 5.9.3. Forward Piezo Scan at 1286nm Intensity vs. Wavelength .....	84
Figure 5.9.4. Backward Piezo Scan at 1286nm Intensity vs. Wavelength.....	85
Figure 5.9.5. Q factor calculation (W is the bandwidth and f0 is the center frequency) .....	86

## Table of Tables

Table 2.3.1. Coupler's Splitting Ratio .....	19
Table 5.3.1. Measurement of Full Piezo Scan Range .....	66
Table 5.3.2. The Calculation of Wavelength .....	67
Table 5.3.3. The Result for Peaks Length Difference Calculation .....	68
Table 5.6.1. Forward Piezo Scan Intensity vs. Piezo Voltage at Wavelength 1300 nm .....	75
Table 5.6.2. Forward Piezo Scan Intensity vs. Piezo Voltage at Wavelength 1300 nm .....	75
Table 5.8.1. Fitted Sine Waves Data Sheet at Various Wavelength .....	81
Table 5.8.2. Forward Scan Peaks Data Sheet at Various Wavelength .....	81
Table 5.8.3. Calculations of Delta L .....	82
Table 5.9.1. Error of delta L .....	88
Table 5.9.2. Error Analysis of Delta L .....	89

# 1 Introduction

## 1.1 Rationale

Laser is an optical light-emitting device based on stimulated emission principle. In stimulated emission process, an incoming photon interacts with excited atom leading to two identical photons emitted. The energy is transferred from atomic electrons to electromagnetic field to create a new identical photon as incoming photon. Another essential element in the laser is the media for resonance. The resonance happens only when certain wavelength light is confined in the media, and accumulates its energy and intensity from the resonances. Among many type of lasers, tunable laser stands out due to its tunable wavelength, which could be widely applied in spectroscopy, photochemistry and other emerging areas.

Tunable laser's wavelength can be selected by precisely and mechanically changing cavity length for the light resonance. Cavity length is defined as the distance between the two ends of the media where light with certain wavelength can travel forward and backward inside. In addition, there are three common tuning mechanisms for the tunable laser: Littrow prisms, diffraction gratings, and birefringent filters. Our tunable laser device is based on the agile tuning mechanism of diffraction grating, which suppresses the cavity-length-dependent tuning behavior. Besides diffraction grating tuning, Littrow prism is a retro-reflecting dispersing prism arranged in the way that the incident light beam entering at the Brewster angle undergoes minimal deviation and hence maximum dispersion [1]. By rotating Littrow prism, the coating on the inclined surface reflects laser light with certain output frequency.



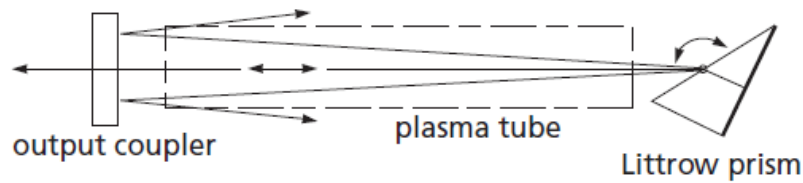


*Figure 1.1.1. Schematic Diagram of Littrow Prism Tuning Mechanism [2]*

A birefringence filter is another optical tuning mechanism. Birefringence is an optical property of materials that has different refractive index depending on polarization and light propagation direction. As shown in Figure 1.1.2, light inputs and passes through crystal material that has birefringent property. The output lights are separated into two rays: ordinary ray and extraordinary ray depending on crystal structure.

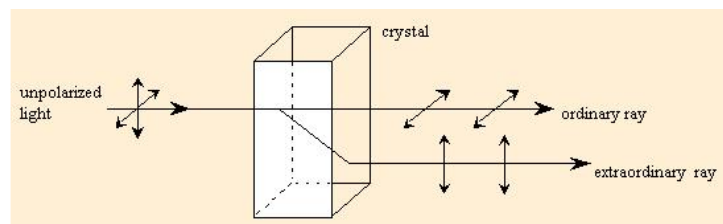


*Figure 1.1.2. Schematic Diagram of Birefringence Tuning Mechanism [3]*

However, the challenges are fine tuning of tunable laser and precise measurement of laser output. Most current tunable lasers can only be controlled by embedded processor inside the controller or simple controlling software program. The internal control processor can only process coarse motor scanning, set static internal mirror position, set some basic properties of the laser diode, like laser power, current. The program provided by the company (Newport, Inc.) in the WPI Optomechanics Lab is not functional enough to conduct cavity optomechanical research, although Newport is one of the major providers of research-grade tunable lasers in the world. As a result, a tunable laser is a powerful tool but cannot fully apply its potential use due to the lack of functions



With the improvement of computer engineering technology, there is a boost in the field of control of tunable laser. In 2015, Tuan Pham Minh \*, Václav Hucl, Martin Čížek, Břetislav Mikel, Jan Hrabina, and Šimon Řeřucha developed a tunable laser diode with Distributed Bragg Reflector structure, butterfly package and fibre coupled output. The experimental scheme was setup as shown in Figure 1.2.2. The work presents the way to developing the narrow-linewidth operation the DBR laser with the wide tunable range up to more than 1 nm of the operation wavelength at the same time [7].

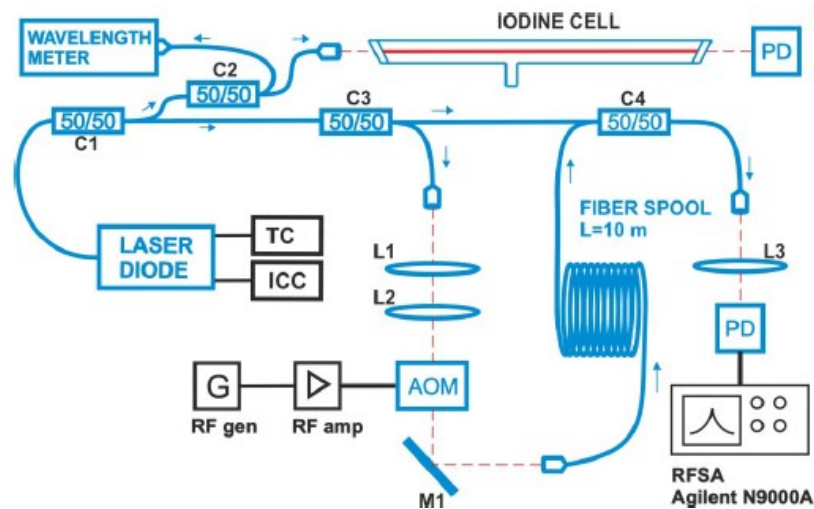
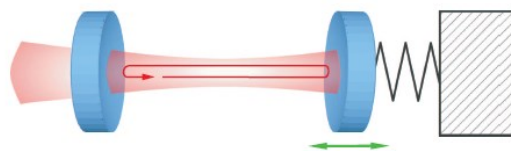


Figure 1.2.2. The Optical Scheme of the Experimental Setup for Measurement of the Mode-Hop Free Tuning Range, Scanning of Absorption Spectrum of Molecular Iodine Vapors and Frequency Noise Properties.

C1 - C4 – splitters, L1 - L3 – Lenses, RF gen – RF generator, RF amp – RF amplifier, RFS – RF signal analyzer, AOM – acousto-optic modulator, PD – Photodetector, TC – temperature controller, ICC – Injection current controller, M1 – mirror [7].

Although the tunable laser hardware has been evolved to a very high level, but the control of the tunable laser is unintuitive, complicated and lack of functions. And the resolution of wavelength for most tunable laser is up to 0.1nm. These constraints particular limit the development of many emerging area, for example, cavity optomechanics.

As we mentioned above, cavity optomechanics is a burgeoning branch of physics that studies the interaction of optics and mechanics through radiation pressure. A typical cavity optomechanical device is shown in Figure 1.2.3, which contains coupled optical resonators and mechanical resonators. The input laser wavelength can be red or blue detuned from the optical resonance, meaning the input wavelength is longer or shorter than the resonance but still on the shoulders of the resonance. Red detuning could be used to explore the quantum effects of these devices, such as slow light, ground-state cooling of nanoscale objects and electromagnetically induced transparency, while blue detuning enables the parametric amplification where mechanical resonator is optical excited by the input light. Both red and blue detuning could be applied to microelectromechanical systems (MEMS) for precise displacement sensing up to the resolution of sub  $\text{fm}/\text{Hz}^{1/2}$  [8]. For a typical cavity optomechanical device, the optical quality factors of  $10^5$  to  $10^6$  (at room temperature) can be achieved. If the laser is operating at about 1300 nm, the resolution of wavelength control is, therefore, a few to tens of picometers [9,10]. As a result, precision wavelength tuning in a well-controlled laser system is important for the study of cavity optomechanics.



*Figure 1.2.3. Schematic Diagram of a Fabry-Perot cavity with harmonically bound end mirror [11]*

### 1.3 Goal and Objectives

Therefore, our goal is to develop LabVIEW-based real-time control in terms of wavelength and power. We aim to achieve automatic scanning, both motor and piezo scan, which defined by

user-defined parameters. Most tunable lasers rely on the motion sensor in the cavity to estimate the wavelength. In our project, we aim to use a passive and low-cost interferometer to measure the wavelength in real time. Usually, the wavelength is measured by a device called wavemeters (or wavelength meter). It is a kind of interferometers with relatively high cost. Using a wavemeter is usually more precise than measuring a wavelength with a spectrometer. Our project developed a setup based on Mach-Zehnder interferometer to measure the wavelength of the tunable laser.

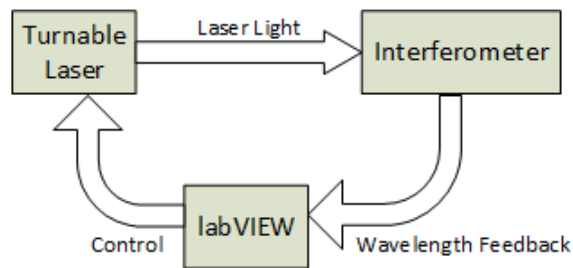


*Figure 1.3.1. System Schematic Diagram*

We formulated two objectives to fulfill our goal of developing the LabVIEW-based real-time control for the tunable laser source. The first objective was to develop the software control program of the tunable laser with LabVIEW codes. The development of the control software started with a clear definition of user operating procedure and functions. We developed and updated the software control program iteratively based on the advisor's demanding and suggestions. We analyzed the program execution and priority in real-time to achieve the maximum optimization and efficiency.

The second objective was to build an interferometer system to analyze the wavelength, transmission intensity and the physical properties of the interferometer. We searched and reviewed literature on the topic of interferometer principles and applications. Moreover, we presented the literature to the team for the purpose of sharing the knowledge on the interferometers and

practicing transferable skills, like the oral presentation. After discovering the best interferometer setup fitting our system requirement, we built the interferometer with the fiber materials purchased based on interference calculations. At the end of this project, we expected to find the length of different optical path in interferometer arms based on the spectra graph. Moreover, we expected to use the controlled tunable laser to test nanofabricated cavity optomechanical devices available in the WPI Optomechanics Lab.

## 2 Working Principles and Characterization Results of the Equipment

### 2.1 Fundamentals of Laser

Laser is an acronym for “light amplification by stimulated emission of radiation”. A laser is a device that emits light through a process of optical amplification based on the stimulated emission of electromagnetic radiation.

Stimulated Emission works as shown in Figure 2.1.1. If an electron is in an excited state, an incoming photon will interact with it, the electron would transit to a lower energy level, producing a second photon of the energy in the difference between levels.

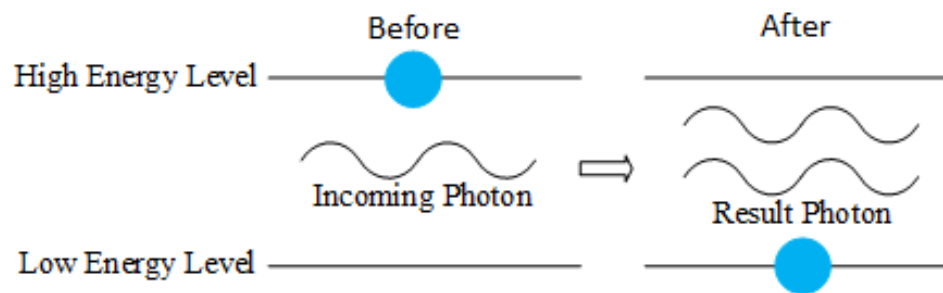


*Figure 2.1.1. Stimulated Emission Theory*

Optical cavities are major components of lasers, surrounding the gain medium and providing feedback of the laser light. Light restricted in the optical cavity reflects multiple times generating standing waves for certain resonance frequencies or wavelengths.

### 2.2 Equipment Overview

In the project, a LabVIEW program is used to control inputs to tunable laser, and the actual measurement is made in the interferometer. In LabVIEW program, we edit the original program

to add functions such as motor scan and piezo scan, and also visualized output and convenient input. To achieve better control to laser, structures such as case structure, event structure, and subroutine program are added and edited. Also, a Data Acquisition (DAQ) is applied to acquire and generate signal—voltage. With well controlled tunable laser, a Mach-Zehnder interferometer fiber setup is added to the laser output. The basic setup of Mach-Zehnder includes two 2x2 optical couplers, standard fibers with various length, and a photodetector.

A fiber optic coupler is a device widely used in optical fiber systems as shown in Figure 2.2.1. Specifically, a 2x2 fiber optic fiber has two input fibers and two output fibers. Light passed through the coupler with power distribution depending on the wavelength and polarization. A 2x2 optical fiber coupler with 50/50 split ratio is shown in below figure.



*Figure 2.2.1. 2x2 Optical Coupler [12]*

Fiber is widely used in communications technology. In our project, single mode fiber is used as optical paths, which are in between two optical couplers. The difference between two fibers will cause optical path length difference that is defined as  $\Delta nL$ . Symbol  $n$  represents the refractive index while symbol  $L$  represents the fiber length. These two fibers serve as optical cavities. Based on the equation  $2nL=N\lambda$ , where  $N$  is an integer, different fiber length will promise different wavelength and thus different power loss. Finally, the light power is measured by a photodetector.

A fiber cable is usually consisted of four parts, including core, cladding, buffer and jacket. The figure below shows the structure of a typical single-mode fiber. The core of the fiber is a cylinder of glass or plastic that runs along the fiber length. It is surrounded by a medium with a



lower index of refraction, typically a cladding of different glass. The buffer providing some functions as mechanical isolation, protection from physical damage and fiber identification. [13]

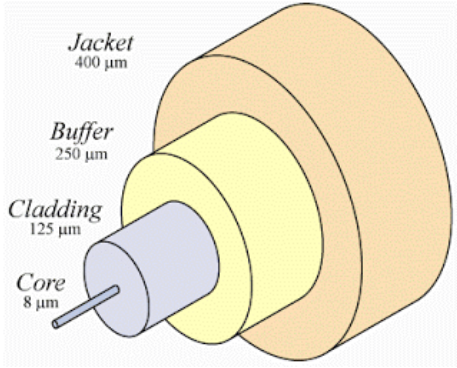


Figure 2.2.2. Cross Section of Optical Fiber [14]

The main difference between multimode fiber and single-mode fiber is the different core diameter. The multimode optical fiber typically 50 to 100 micrometer core diameter while the single mode optical fiber had 8 micrometer core diameter [15].

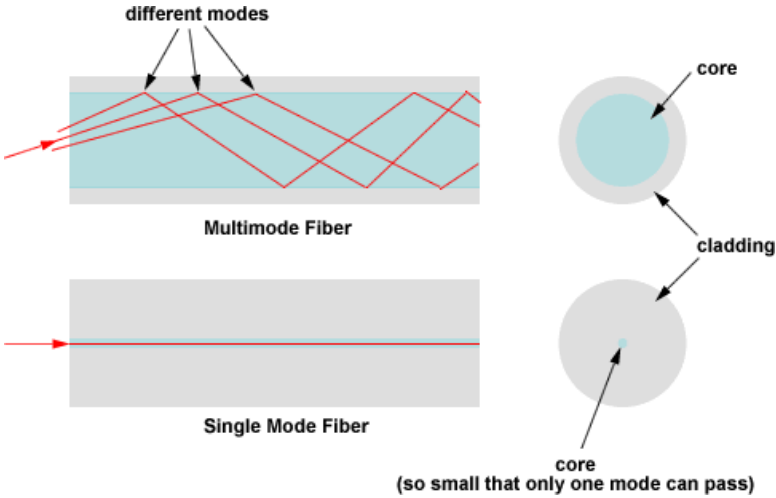


Figure 2.2.3. Internal Reflection of Optical Fiber [16]

Optical fiber is a useful tool to transmit light made by drawing glass or plastic. It is widely used in optic- communication. The advantage of optical fiber compare to metal wires in

communication is that: signal travel along in fiber has less amount of loss and immune to electromagnetic interference. A major type of optical fiber is single-mode fiber. It has a diameter between 7.5 to 9.5  $\mu\text{m}$ .

Optical Fiber Attenuator is the device to reduce the power of the laser signal in an optical fiber. We use attenuator before the photodetector to protect it from damage due to high power.

There are many types of optical attenuators; some attenuator works by absorbing the light, like a sunglasses absorbing part of the optical energy. The attenuator we choose works by reducing the contact area of two connected fiber. The power transmits the attenuator will be correlated with the contact area. We used a variable optical attenuator, which means the attenuator ratio can be adjusted by changing the contract area.

### 2.3 Fiber Optical Coupler

The optical coupler is a passive fiber optic device that can split light into multiple paths or combine multiple light beams into one. It is based on a quartz substrate of an integrated waveguide optical power distribution device, similar to a coaxial cable transmission system.

Before the experiment, the splitting ratio should is measured to make sure it is close to 50/50. Since if not, the interference signal after interferometer could obtain a high amount of error. For our experiment, we find the splitting ratio by measuring the optical intensity at each end of the coupler. We set the laser output power to be 10mW, and power we measured is 8.91mW, the decrement is due to fiber loss. The result is shown in Table 2.3.1.

Input Channel	Output Channel	Power (mW)	Split %
A	B	3.33	50.531
	C	3.26	49.469

Input Channel	Output Channel	Power (mW)	Split %
B	B	4.34	49.374
	C	4.45	50.626

Input Channel	Output Channel	Power (mW)	Split %
A	B	4.16	49.940
	C	4.17	50.060

Input Channel	Output Channel	Power (mW)	Split %
B	B	4.31	50.175
	C	4.28	49.825

Table 2.3.1. Coupler's Splitting Ratio

## 2.4 Photon Detector

The Photodetector is an active device that photons of light in term of voltage or current as shown in Figure 2.4.1. Its schematic diagram is shown in below. When a photon hit the metal electrode, electrons emit out from current flow through a wire. Therefore, a current or voltage can be measured with a multimeter. In principle, high power light carries more photons, and more electrons emit to from bigger current or voltage when the light hits the electrode.

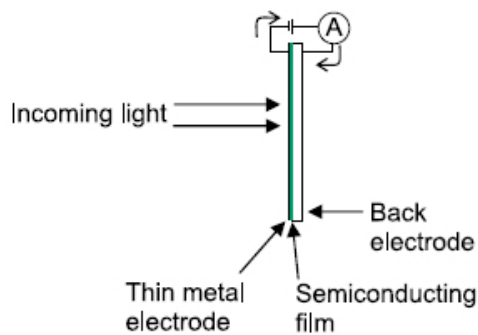


Figure 2.4.1. Photodetector Working Principle [17]

In our experiment, we used THORLABS InGaAs PDA20C Photodetector (Figure 2.4.2) to measure the transmission intensity.



Figure 2.4.2. THORLABS In Gas PDA20C Photodetector [18]

PDA20C has a wavelength range of 800-1700 nm, which include our laser source range (1270-1330 nm) well. Its responsivity behaves as shown in Figure 2.4.3. From Figure 2.4.4, we can find that at our laser source range (1270-1330 nm) the photodetector has a very high responsivity.

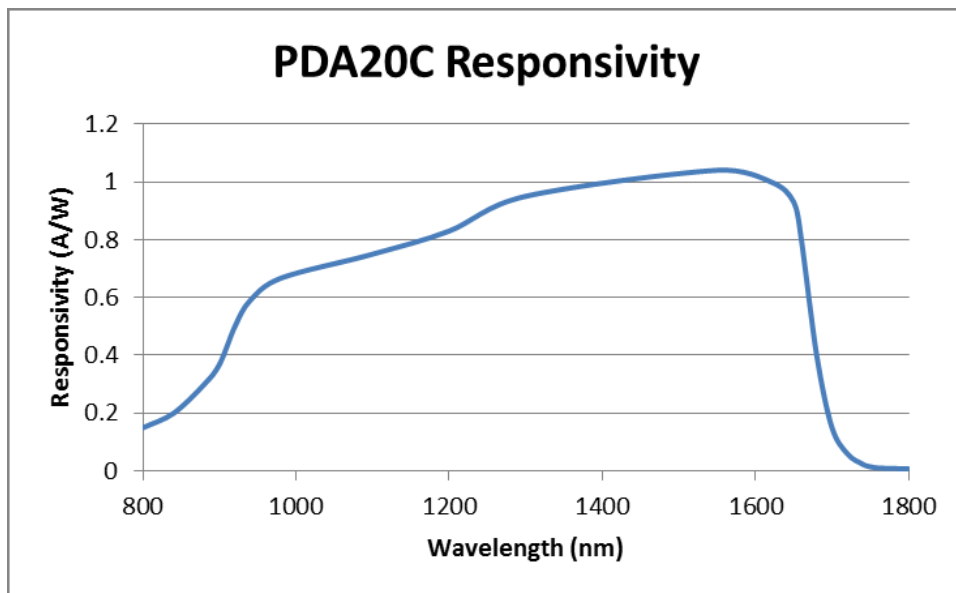


Figure 2.4.3. PDA20C Responsivity [18]

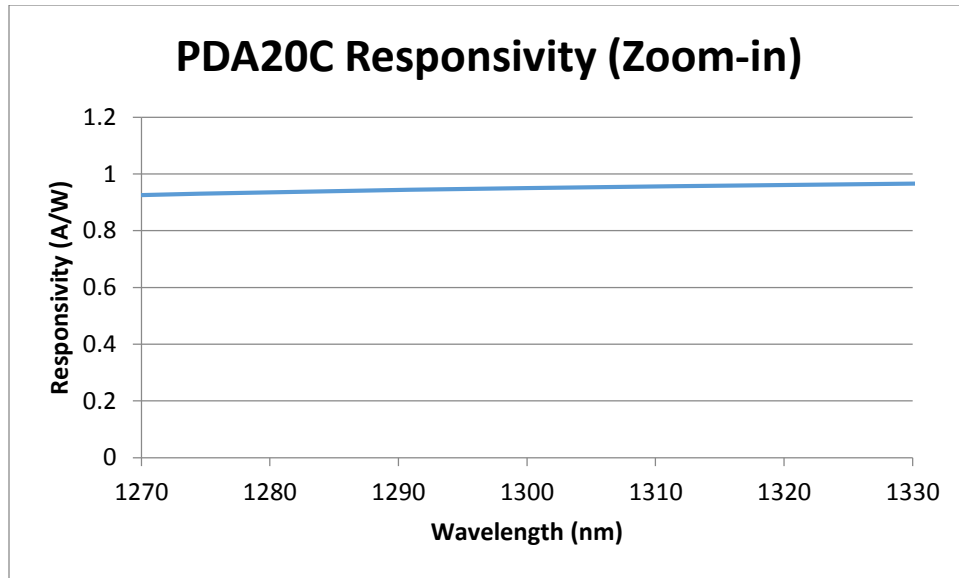


Figure 2.4.4. PDA20C Responsivity (Zoom-in) [18]

## 2.5 New Focus Laser Source

We choose TLB-6700 Velocity™ Widely Tunable Lasers to be our laser source system. This laser source is one of the most advanced laser source available. It consists of two parts: the laser head and the controller.

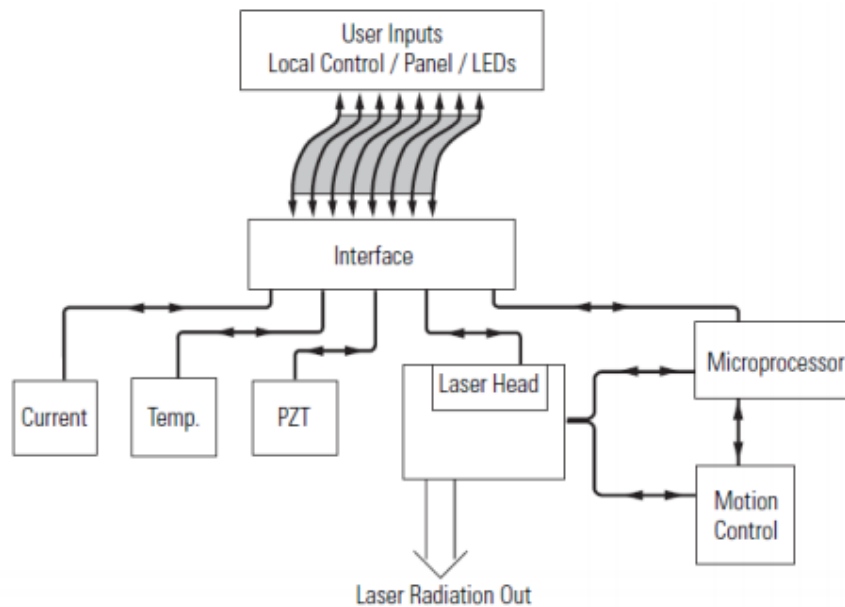
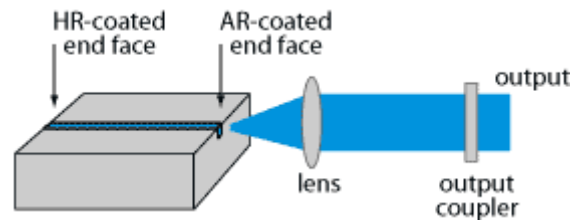


Figure 2.5.1. Controller Block Diagram [19]

An external cavity diode laser is a diode laser based on a laser diode chip that typically has anti-reflection coating on the one end, and the laser resonator as shown in Figure 2.5.2. The resonator usually involves a collimating lens and an external mirror as shown in the figure.



*Figure 2.5.2. Laser head [20]*

Tunable external-cavity diode lasers usually use a diffraction grating as the wavelength-selective element in the external resonator, they are called grating-stabilized diode lasers.

The diode laser is bonded to a temperature sensor and a thermoelectric cooling block that maintains a highly stable diode temperature. Moreover, a small fraction of the output beam is directed to a power monitor. The reading from this monitor displays on the front panel of the controller [20].

The Laser source in the project, Newport TLB-6700 Velocity™ Widely Tunable Lasers applies Littman-Metcalf setup. The Littman-Metcalf configuration includes a fixed grating orientation, and an additional mirror that reflects the first-order beam back to the laser diode. Rotating of that mirror causes tuning of the wavelength. A diode laser functions as the gain medium. The Laser source takes advantage of the broad gain bandwidths available in semiconductor diode lasers. In addition to being widely tunable, the laser source offers narrow linewidths using a design of laser cavity that began at the Massachusetts Institute of Technology.

The modified Littman-Metcalf laser cavity is shown in Figure 2.5.3. One end of the diode laser with a high-reflection coating and an extremely reflective tuning mirror together form the cavity. Starting from the diode, the beam in the cavity passes through a collimating lens and then strikes a diffraction grating at near grazing incidence. The beam is diffracted toward the tuning mirror that reflects the light back on itself for the reverse path. Part of the light from the diode is reflected, not diffracted, by the grating. This portion forms the output beam. The wavelength in the front panel comes from the signal generated by the angle sensor [19].

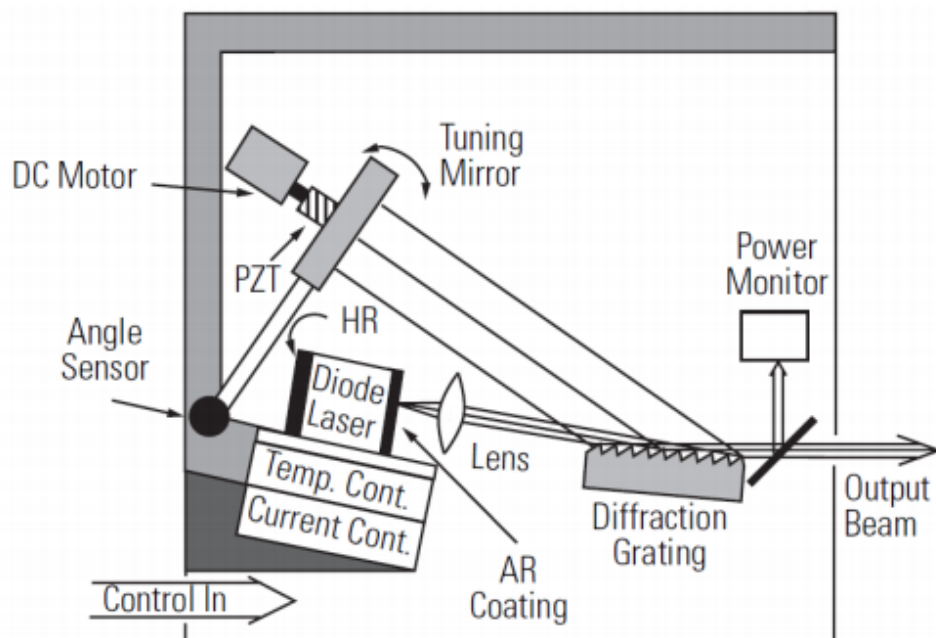
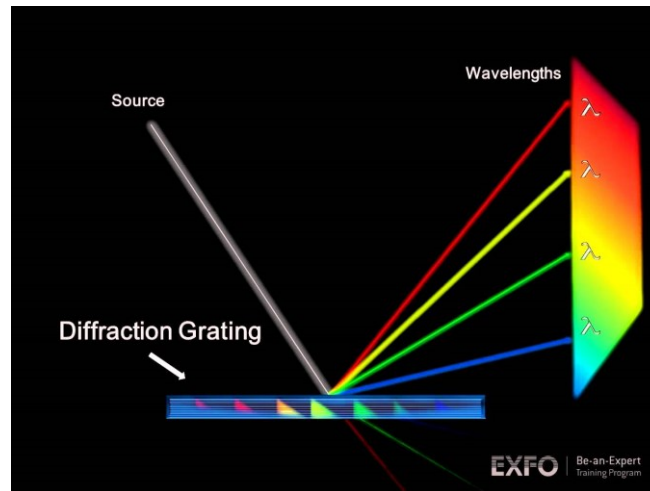


Figure 2.5.3. New Focus Laser Cavity Diagram [19]

The diffraction grating is an optical component with a periodic structure, which splits the light into several beams emitting in different directions as shown in Figure 2.5.4. In the laser head, it functions as a narrow spectral filter. Its passband is only a few gigahertz wide. The high wavelength selectivity results because many lines of the grating are illuminated by the grazing incidence beam and because the beam is diffracted by the grating twice in each round trip through

the cavity. The grating spectral filter is narrow enough to force the laser to operate on only a single longitudinal mode [19].



*Figure 2.5.4. Diffraction-Grating Theory [21]*

Different wavelengths diffract off the grating at different angles as shown in fig. above. However, only one wavelength leaves the grating in a direction that is exactly perpendicular to the surface of the tuning mirror closing the resonant laser cavity. It follows that we can tune the laser by changing the angle of the tuning mirror. The tuning mirror is mounted on a stiff arm. An angle sensor near the pivot point of the arm provides data for wavelength readout. The other end of the arm is moved by a DC motor driven screw and a piezoelectric transducer (PZT) [19]. Piezoelectric motors make use of the inverse piezoelectric effect whereby the material produces to produce a linear motion. The mechanical motor is consisted with gears. Different from the mechanical motor, Piezo motor's resolution is not limited by the mechanical constraints like the dimension of gear teeth. Moreover, it does not generate vibration because there is no internal physical contact involved. Therefore, the piezo motor can achieve a better resolution and accuracy. So PZT motor is ideal for fine adjustment for distance [22].



The DC motor makes coarse wavelength changes while the PZT is used for micron scale movements, which correspond to sub-angstrom wavelength tuning precision. There is one critical innovation that allows the laser source to tune continuously without mode hops. In order to maintain resonance in the same mode as we tune the laser, the number of waves in the cavity must be kept constant (even though the wavelength of the light in the cavity is changing) [19][23].

As shown in Figure 2.5.1, the controller provides a stable, low-noise power source for the diode laser. It could set the temperature in the laser head, as well as control wavelength scanning and provide readouts of all relevant laser parameters.

Conceptually, the circuitry inside the controller is built in two layers: analog and digital. . The analog layer incorporates low-noise design for temperature, current, and fine wavelength tuning. The digital layer includes all the readouts and circuits to set operating points and scan parameters [19].

The relationship of piezo scan voltage and actual piezo voltage were explored. Therefore, we can combine two figures to obtain desired information. The first figure indicates the relationship between wavelength and actual piezo. The second figure indicates the relationship between laser power intensity and piezo scan voltage; DAQ box measured both through BNC cables. The process was to change piezo scan voltage and then recorded piezo scan voltage and corresponding real piezo voltage from the front panel of the LabVIEW program. The results show a linear relationship with corresponding sets of piezo scan voltage and real piezo voltage values: - 3V and 0V, 0V and 60V, 3V and 120V. Therefore, we convert piezo scan voltages to real piezo voltages by mathematical equations.

## 2.6 Optical Interferometers

The interferometer is an optical device that utilizes the effect of interference. The incoming light will usually be split into an amount number of beams, after traveled different length of the path, the beams would combine together. Based on the principle of superposition of waves as shown in Figure 2.6.1, if the phase difference between the waves is a multiple of  $2\pi$ , constructive interference occurs; and if the phase difference is an odd multiple of  $\pi$ , destructive interference occurs.

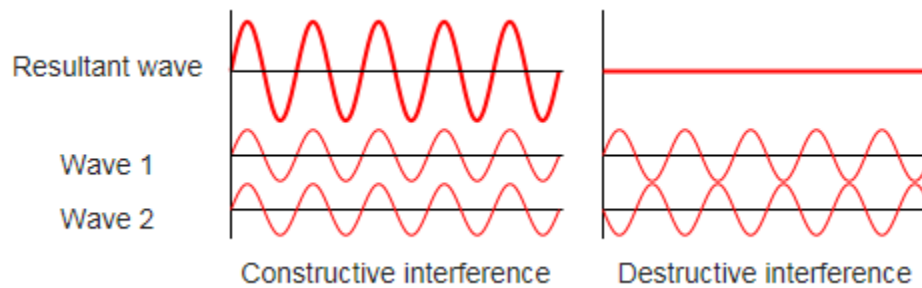


Figure 2.6.1. Principle of Superposition of Waves [24]

The interference of laser could give us a spectral graph similar to Figure 2.6.2, we are able to find the parameters like wavelength or refractive index or path difference based on Equation 5.5 by looking at the wavelength value at adjacent peak in the plot.

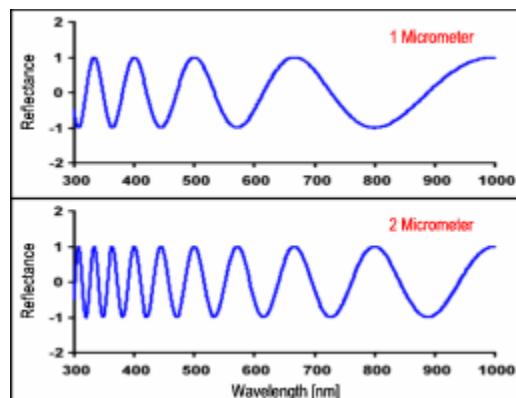


Figure 2.6.2. Examples of Interference Spectral Plot [25]

In our research, three types of interferometers are studied. They are Mach-Zehnder, Michelson, and Fabry–Pérot Interferometers. We can sort these three interferometers into two categories: two-beam interferometers and multiple beam interferometers.

#### 2.6.1 Working Principles for Two Beam Interferometers

Two beam interferometers usually start with a light beam and then split it into two separate beams. People usually refer two beams as a reference beam and a sensing beam. Then the beams recombined, and interference happened based on the optical path length difference in two arms.

#### 2.6.2 Two Beam Interferometers: Michelson Interferometers

The Michelson Interferometer is one of the common interferometer invented by Albert Abraham Michelson. The basic working principle of the interferometer is use splitter to separate and then combine signals. For Michelson interferometer, its classic setup includes one half-passive mirror and two standard mirrors. The schematic diagram of this type of interferometer is shown in Figure 2.6.3.

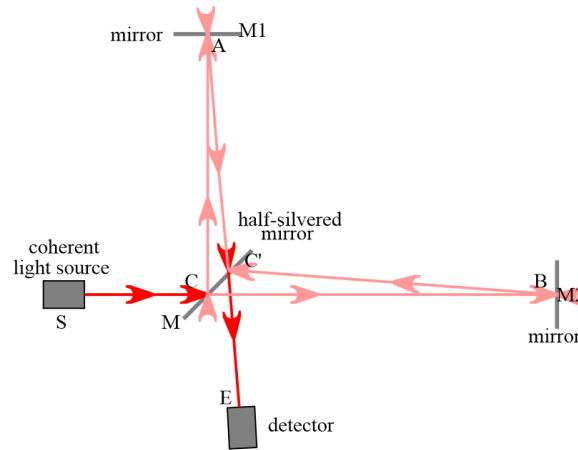


*Figure 2.6.3. Michelson Interferometer Setup and Path of light in the interferometer [26]*

Light comes from a light source (S) then passes through a half-silvered mirror (C). By passing mirror C, the light source is split, half of the light reflects towards a standard mirror (M1) and half passes through to mirror (M2). After reaching two standard, both half-light will be reflected back to pass through mirror C again. The reflected light from M1 (Shown at A) has half-light passing through mirror C again. The reflected light from M2 (Shown at B) has half-light reflected by mirror C. Then they meet while traveling to a detector.

Since in our project, more precise measurement is required, the fiber setup is applied. With the same working concept, a coupler, usually 2x2 coupler, is used to replace traditional half-silvered mirror to split and combine signals. A 2x2 coupler is directional independent, and it has four connectors, two serves as inputs and two serves as outputs. Since lights can travel together without affecting each other, the single coupler can be used to split and combine light. Shown in below figure, Light comes from its sources (LCS) and then is divided into two parts by passing through the coupler. At reference fiber arm, it is coated with silver, which reflect light back to the coupler. At sensing fiber arm, a movable mirror is putted in front of fiber arms end, which reflects

light back to coupler but with time delay and power decay. Then the reflected lights are combined and detected by a photodetector (PD).

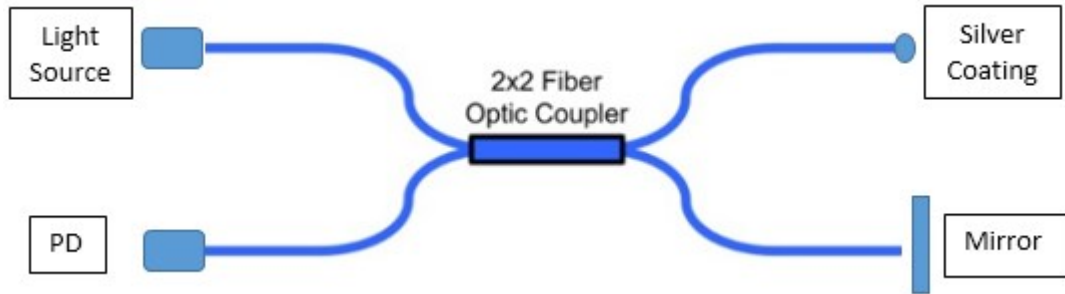


Figure 2.6.4. Michelson Interferometer Fiber Setup Schematic Diagram

### 2.6.3 Two Beam Interferometers: Mach-Zehnder Interferometers

The Mach-Zehnder interferometer is often used to determine the relative phase shift between two collimated beams derived by splitting light beam from one single light source. The phase shift between two beams is usually caused by the changing in the optical length of one beam. The device is named after two physicists Ludwig Mach and Ludwig Zehnder.

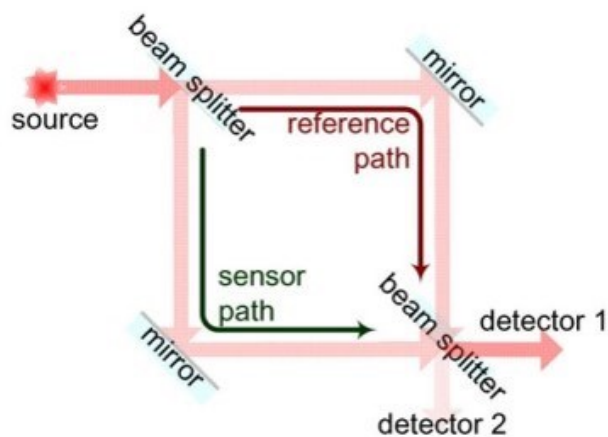


Figure 2.6.5. Mach-Zehnder Interferometer Working Principle [27]

A typical Mach-Zehnder interferometer is composed of a light source, two half-silvered mirrors, two standard flat mirrors and two detectors. First, a collimated beam is split by the half-silvered mirror, and two resulting beams are generated. We call them the sensing beam and the reference beam. Flat mirrors reflect the two resulting beams. After passing the second half-silvered mirror, the two beams enter two photodetectors.

Since the optical path of sample path and reference path is different, a certain amount of phase shift occurs between two beams at the location of detections. The optical path difference is usually caused by the difference in physical lengths two beams traveled or the difference in refractive index of the medium two beams traveled, like air, glass, and fiber.

Compares to the standard interferometer setup, fiber setup has the benefits of high precision and low setup difficulty. The fiber setup for the Mach-Zehnder interferometer is composed of several fibers and two couplers. The first coupler is functioned as a beam splitter and the second coupler is functioned as a re-combiner. The incoming beam is split into two resulting beam after passing through the coupler. Then the two beams travel different optical path in the two separate fibers and meet at the second coupler. After passing the second coupler, two beams enter the diode via the fiber. In the fiber setup, standard single-mode fiber is usually utilized.

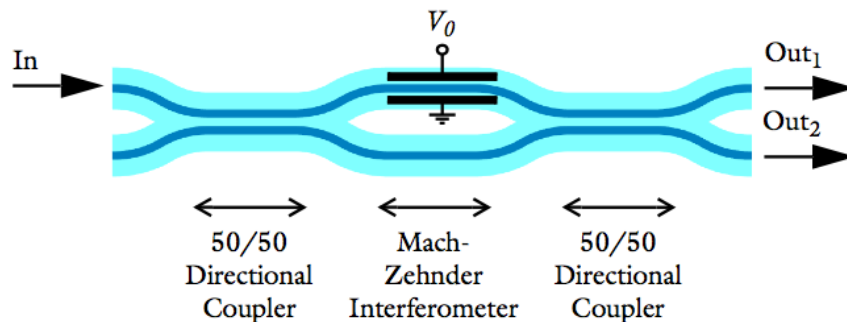
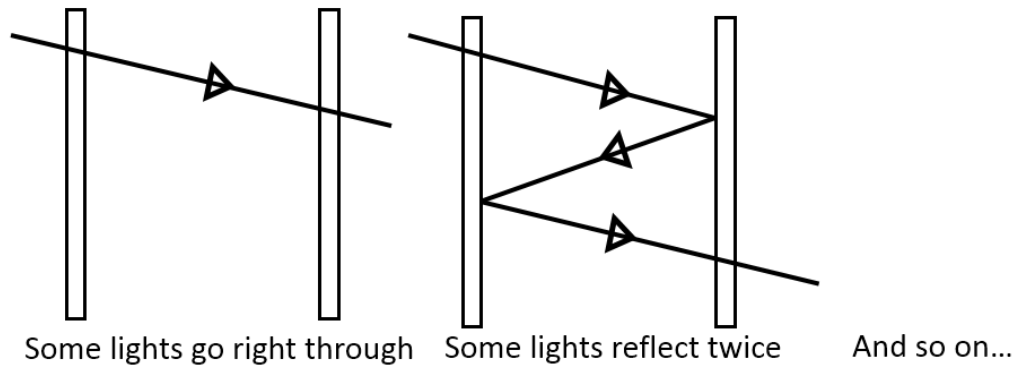


Figure 2.6.6. Mach-Zehnder Interferometer Fiber Setup Schematic Diagram [28]

#### 2.6.4 Multiple Beam Interferometers: Fabry-Pérot Interferometers

Fabry-Pérot interferometer is also commonly used. It consists of two highly reflecting mirrors and is often used as a high-resolution optical spectrometer. Part of the light is transmitted once the light reaches the second surface, resulting in multiple offset beams that can interfere with each other.



*Figure 2.6.7. Fabry- Pérot Interferometer Working Principle*

Because the Fabry-Pérot interferometer has a higher resolution than others, it is easier to observe the fringes produced by two extremely closely spaced spectral lines.

Classical setup for Fabry-Pérot interferometer is shown in Figure 2.6.8. The incident beam enters with the incident angle into the optical cavity that consists of two high reflective mirrors. The laser beam reflects back and forth to divide into numerous transmitted beams. The divided laser beams will then be focused by focusing lens and received by the detector.

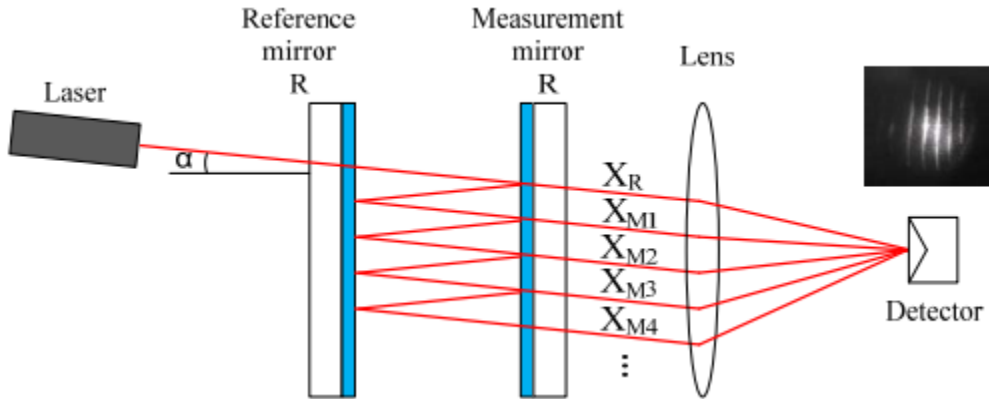


Figure 2.6.8. Schematic Diagram of Fabry- Pérot Interferometer Classical Setup [29]

The fiber setup for Fabry-Pérot interferometer typically consists of two fiber on each end and connected with the extrinsic material, which means the index number of center material is different from the fiber. Fabry-Pérot interferometer is than M-Z and Michelson to set up because there is no coupler involved. However, the hardness for creating a fiber Fabry-Pérot interferometer is that two refractive surface has to be as flat as possible.

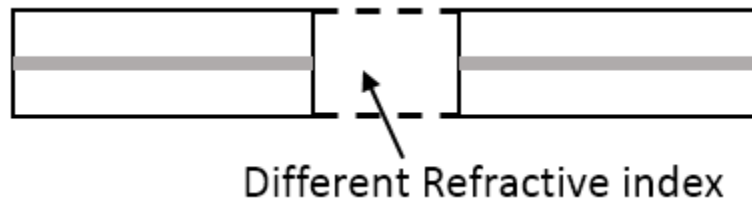


Figure 2.6.9. Fabry- Pérot Interferometer Fiber Setup

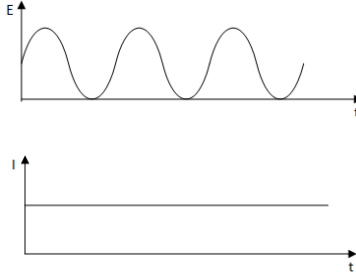
### 2.6.5 Calculation of Interference

The interference between the two different arms of the interferometer is given as a function of intensities of two arms  $I_1, I_2$ , and the phase shift  $\phi$  between two arms.

$$I_{\text{total}} = I_1 + I_2 + 2\sqrt{I_1 I_2} \cos(\Delta\phi)$$

Equation 2.1





Intensity is measured in the unit of  $\text{J}/\text{m}^2\text{s} = \text{W}/\text{m}^2$ . The electric field is measured in the unit of  $\text{V}/\text{m}$ .

$$E = E_0 e^{i\omega t}, \text{ where } \omega \text{ is the angular frequency, } \omega = 2\pi f$$

*Equation 2.2*

The relationship between intensity  $I$  and electric field  $E$  is shown as below.

$$I = \frac{1}{2} E E^* = \frac{1}{2} |E|^2 = \frac{1}{2} E_0^2$$

*Equation 2.3*

For the convenience of the derivation, we assume  $I \sim |E|^2$ .

$$E_1 = E_{01} e^{i\omega_1 t}$$

$$E_2 = E_{02} e^{i\omega_2 t}$$

$$E_{\text{total}} = E_{01} e^{i\omega_1 t} + E_{02} e^{i\omega_2 t}$$

$$I = E_{\text{total}} E_{\text{total}}^*$$

*Equation 2.4*

Assume  $\omega_1 = \omega_2$

$$I = (E_{01} e^{i\omega_1 t} + E_{02} e^{i\omega_2 t})(E_{01} e^{-i\omega_1 t} + E_{02} e^{-i\omega_2 t}) = I_1 + I_2 + \sqrt{I_1 I_2} (e^{i(\omega_1 - \omega_2)t} + e^{i(\omega_2 - \omega_1)t})$$

*Equation 2.5*

Since  $e^{ix} = \cos(x) + i\sin(x)$

$$\begin{aligned}
& e^{i(\omega_1 - \omega_2)t} + e^{i(\omega_2 - \omega_1)t} \\
& = \cos((\omega_1 - \omega_2)t) + i\sin((\omega_1 - \omega_2)t) + \cos((\omega_2 - \omega_1)t) \\
& \quad + i\sin((\omega_2 - \omega_1)t) = 2 \cos((\omega_1 - \omega_2)t)
\end{aligned}$$

*Equation 2.6*

Then we have the following equation

$$I = I_1 + I_2 + 2\sqrt{I_1 I_2} \cos(\omega_1 - \omega_2) t$$

*Equation 2.7*

Since  $\phi = \omega t$

$$I = I_1 + I_2 + 2\sqrt{I_1 I_2} \cos(\Delta\phi)$$

*Equation 2.8*

$$\Delta\phi = \frac{2\pi}{\lambda_0} \Delta(nL), \text{ where } nL \text{ is optical path length}$$

*Equation 2.9*

$$\Delta\phi = \frac{2\pi}{\lambda_0} (n_1 L_1 - n_2 L_2), \text{ where } n \text{ is refractive index, and } L \text{ is physical fiber length}$$

*Equation 2.10*

In the case of Michelson interferometer, the refractive index of the sensing arm is the same as that of the reference arm. However, the physical fiber length of the sensing arm is different from that of the reference arm. We can derive the previous equation into following.

$$\Delta\phi = \frac{2\pi}{\lambda_0} n\Delta L$$

*Equation 2.11*

$$I = I_1 + I_2 + 2\sqrt{I_1 I_2} \cos\left(\frac{2\pi}{\lambda_0} n\Delta L\right)$$

*Equation 2.12*

In the case of Mach-Zehnder interferometer, the physical fiber length of the sensing arm is the same as that of the reference arm. However, the refractive index of the sensing arm is different from that of the reference arm. We can derive the previous equation into following.

$$\Delta\phi = \frac{2\pi}{\lambda_0} L\Delta n$$

Equation 2.13

$$I = I_1 + I_2 + 2\sqrt{I_1 I_2} \cos\left(\frac{2\pi}{\lambda_0} L\Delta n\right)$$

Equation 2.14

### 2.6.6 Calculation of interference for Fabry–Pérot Interferometers

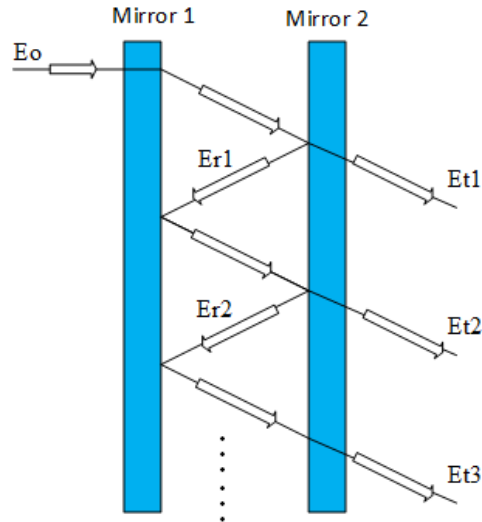


Figure 2.6.10. Schematic Diagram of Fabry–Pérot Interferometer Working Principle

From the Figure 2.6.10, we can find the first order E based on the transmit rate and reflection rate. Thus, we can obtain the second order, the third order, and the Kth order.

$$E(t) = E_o e^{j\omega t}$$

$$E_1(t) = E_o e^{j\frac{Ln}{c}\omega t}$$

Equation 2.15

$$E_2(t) = E_0 e^{j \frac{3Ln}{c} \omega r t}$$

Equation 2.16

$$E_3(t) = E_0 e^{j \frac{5Ln}{c} \omega r^2 t}$$

Equation 2.17

$$E_k(t) = E_0 e^{j \frac{(2k-1)Ln}{c} \omega r^{k-1} t}$$

Equation 2.18

We sum these orders together and get the following equations.

$$\sum_{k=1}^{\infty} E_k = \frac{E_0 e^{j \frac{Ln}{c} \omega t}}{e^{j \frac{2Ln}{c} \omega} (r - 1)} e^{j \frac{2Ln}{c} \omega r}$$

Equation 2.19

$$I_{\text{total}} = |E_{\text{total}}|^2 = \frac{\text{constant}}{1 - 2\cos\Delta\phi}$$

Equation 2.20

## 2.7 Fourier Transform

In the research, we want the plot with wavelength as the x-axis, and intensity as the y-axis, but we can only get two separate plot: wavelength vs. time and intensity wavelength vs. time from the measurement. Therefore we want combine two plots into one single plot, so we need Fourier Transform.

The Fourier transform decomposes a function of time into the frequencies that make it up. The Fourier transform of a function of time itself is a complex-valued function of frequency, whose absolute value represents the amount of that frequency present in the original function, and whose complex argument is a phase offset of the basic sinusoid at that frequency. [30]

$$f(\xi) = \int_{-\infty}^{\infty} f(x) e^{-2\pi i x \xi} dx, \text{ For any real number } \xi.$$

Equation 2.21

When the independent variable  $x$  represents time, the transform variable  $\xi$  represents frequency.

$$f(x) = \int_{-\infty}^{\infty} f(\xi) e^{-2\pi i \xi x} d\xi$$

Equation 2.22

For any real number  $x$ .

$$E_1 = E_{0_1} * e^{i*\omega_1*t}$$

Equation 2.23

$$E_2 = E_{0_2} * e^{i*\omega_2*t}$$

Equation 2.24

$$E_{\text{total}} = E_{0_1} * e^{i*\omega_1*t} + E_{0_2} * e^{i*\omega_2*t}$$

Equation 2.25

$$\begin{aligned} \text{Intensity} &= E_{\text{total}} * E_{\text{total}}^* \\ &= (E_{0_1} * e^{i*\omega_1*t} + E_{0_2} * e^{i*\omega_2*t}) * (E_{0_1} * e^{i*\omega_1*t} + E_{0_2} * e^{i*\omega_2*t}) \\ &= I_{\text{clad}} + I_{\text{core}} + \sqrt{I_{\text{clad}} * I_{\text{core}}} * \cos(e^{i*(\omega_1-\omega_2)*t} + e^{i*(\omega_2-\omega_1)*t}) \\ &= I_{\text{clad}} + I_{\text{core}} + \sqrt{I_{\text{clad}} * I_{\text{core}}} * \cos((\omega_1 - \omega_2) t) \end{aligned}$$

Equation 2.26

$$\Delta(\omega * t) = \Delta\varphi = \frac{2 * \pi}{\lambda} * \Delta(n * L)$$

Equation 2.27

$$I_{\text{total}} = I_{\text{clad}} + I_{\text{core}} + \sqrt{I_{\text{clad}} * I_{\text{core}}} * \cos(\Delta\varphi)$$

Equation 2.28

$$I_{\text{total}} = I_{\text{clad}} + I_{\text{core}} + \sqrt{I_{\text{clad}} * I_{\text{core}}} * \cos\left(\frac{2 * \pi}{\lambda} * n * \Delta L\right)$$

Equation 2.29

## 2.8 Wavelength Calculation based on Adjacent Peaks of the Spectrum

Starting with the two-beam optical interference equation:

$$I = I_1 + I_2 + 2\sqrt{I_1 I_2} \cos\left(\frac{4\pi}{\lambda_0} L \Delta n\right)$$

*Equation 2.30*

Where,  $I$  is the intensity of the interference signal;  $I_1$  and  $I_2$  are the reflections at the cavity end faces, respectively is the cavity length;  $n$  is the refractive index of the medium filling the cavity;  $\lambda_0$  is the optical wavelength in vacuum. According to equation above, the interference signal reaches its minimum ( $I_{\min}$ ) when the phase of the cosine term becomes an odd number of  $\pi$ . That is

$$I = I_{\min}, \text{ when } \frac{4\pi n * L}{\lambda_v} = (2m + 1)\pi$$

*Equation 2.31*

Where  $m$  is an integer and  $\lambda_v$  is the center wavelength of the specific interference valley.

The two adjacent interference minimums have a phase difference of  $2\pi$ . Therefore the optical length of the cavity can be calculated by:

$$L * n = \frac{1}{2} * \frac{\lambda_{v1} * \lambda_{v2}}{\lambda_{v2} - \lambda_{v1}}$$

*Equation 2.32*

Where  $\lambda_{v1}$  and  $\lambda_{v2}$  are the center wavelengths of two adjacent valleys in the interference spectrum [31].

### 3 Experimental System Setup

As we mentioned at the beginning of the paper, our project is consisted of multiple parts, including the tunable laser, DAQ, LabVIEW control, interferometer, attenuator, and photodetector. Now we are going to explain our experiment setup. We connected the computer with the tunable laser using a USB cable for controlling. We connected the tunable laser with the DAQ using two BNC cables for data feedback. We connected the laser output to one end of the coupler and split the laser equally into two beams with different length. The two beams meet at another coupler. Two coupler and two arms with various length form a Mach-Zehnder interferometer. Therefore, then the intensity of the optical interference signal will be detected by the photodetector. An attenuator is used before photodetector to protect it from damage by high energy.

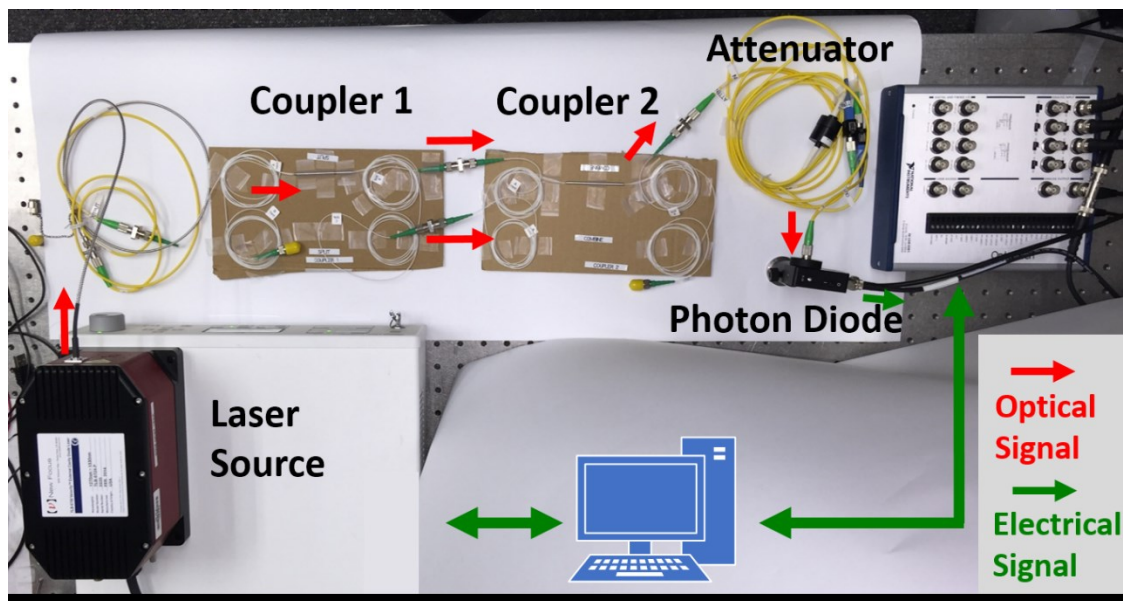


Figure 2.8.1. Actual System Setup

The controlled optical signal will start from the laser head of laser source system, and then the signal will be split into two beams by the first optical coupler. Two beams will travel in optical fibers with different lengths and

recombined by the second optical coupler. Then the combined optical signal will be attenuated and then detected by the photodetector. The signal generated by photodetector will then transmitted to a DAQ box through BNC cable.

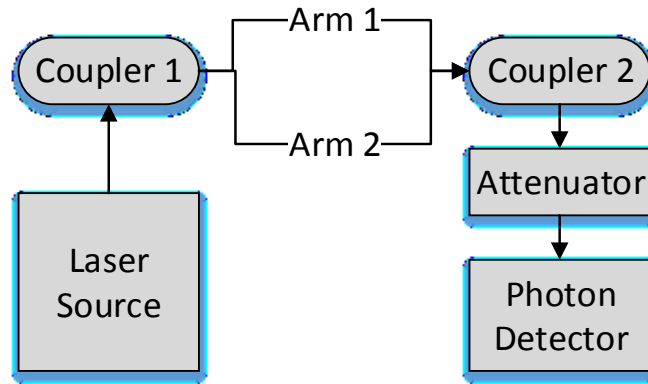


Figure 2.8.2. Schematic Diagram of System Setup

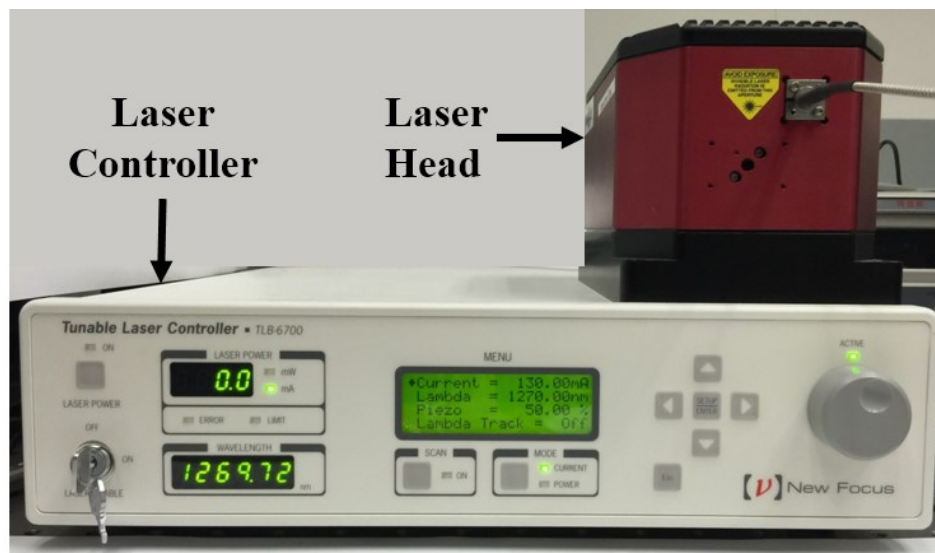
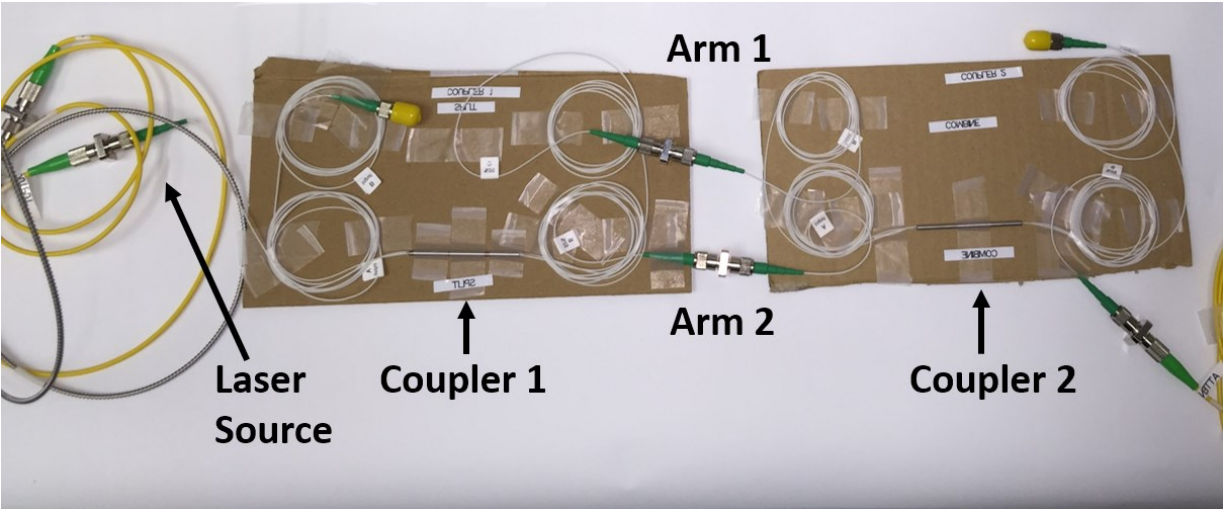


Figure 2.8.3. Laser Source System

The Mach Zehnder interferometer is assembled as shown in *Figure 2.8.4*, the laser was split into two beams at coupler 1. After traveled from arm 1 and arm 2, two beams met at coupler 2 where interference happened. The interferenced light beam then transmitted to the photodetector. This interferometer is low cost and easy to assemble but obtain a high accuracy.





*Figure 2.8.4. Mach Zehnder Interferometer Setup*

To find the best length difference to generate the interference pattern, we first try to connect two couplers with fibers of different lengths, but we only have access to 1 meter and 3 meter long fibers. Therefore, the difference in optical path's length is much larger than desired value. Therefore, we connect the two couplers directly with their arms to achieve desired optical path difference.

## 4 Development of Software Control of the Tunable Laser with LabVIEW

### Codes

#### 4.1 Flowchart of Laser Feedback Control

In our project, one of the most important tasks was to implement the home-made software control of the tunable laser. We formulated the program in three parallel while loops that would run with different CPU cores. To make sure the smoothness of the loop executions, we eliminated all the dependent elements between parallel loops, like the input of the loop, came from the output from the other loop. With independent running loops, the loops were able to run simultaneously. We initially had all the functions in one giant loop, then we organized the functions and ranked them in the order of priorities and function categories. In the following flowchart, we demonstrated our control program's workflow and dependencies.

This flowchart was consisted of three separate substructures. On top of the flowchart, the substructure showed the workflow of all the USB command control of the tunable laser using the information from the front panel. This loop mainly dealt with the user's input and preference. The major components we checked in the loop were the piezo stage and the motor stage in the tunable laser. With flexible controls of the piezo stage and the motor stage, the tunable laser can perform fine scanning and coarse scanning as the user wanted. On the bottom left of the flowchart, the substructure showed the workflow of collecting the motor stage and piezo stage feedback from the tunable laser via USB commands. Finally, in the bottom right of the flowchart, the substructure showed the external control of the piezo, and data sampling of wavelength as well as laser intensity using the DAQ. Those three loops had their clear tasks and worked together to make the program functional and optimal.

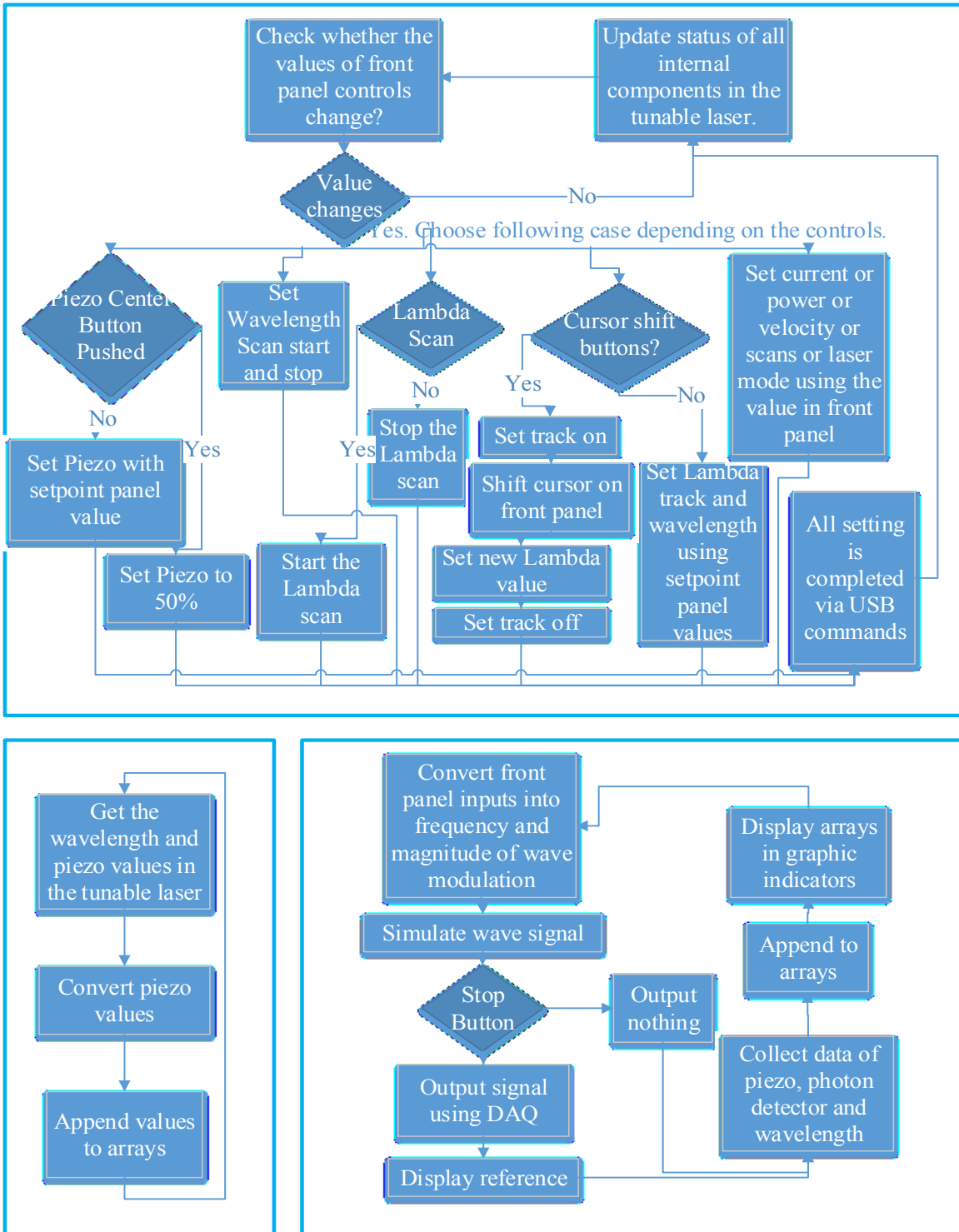


Figure 4.1.1. Detailed System Flow Chart

## 4.2 Front Panel of Laser Feedback Control

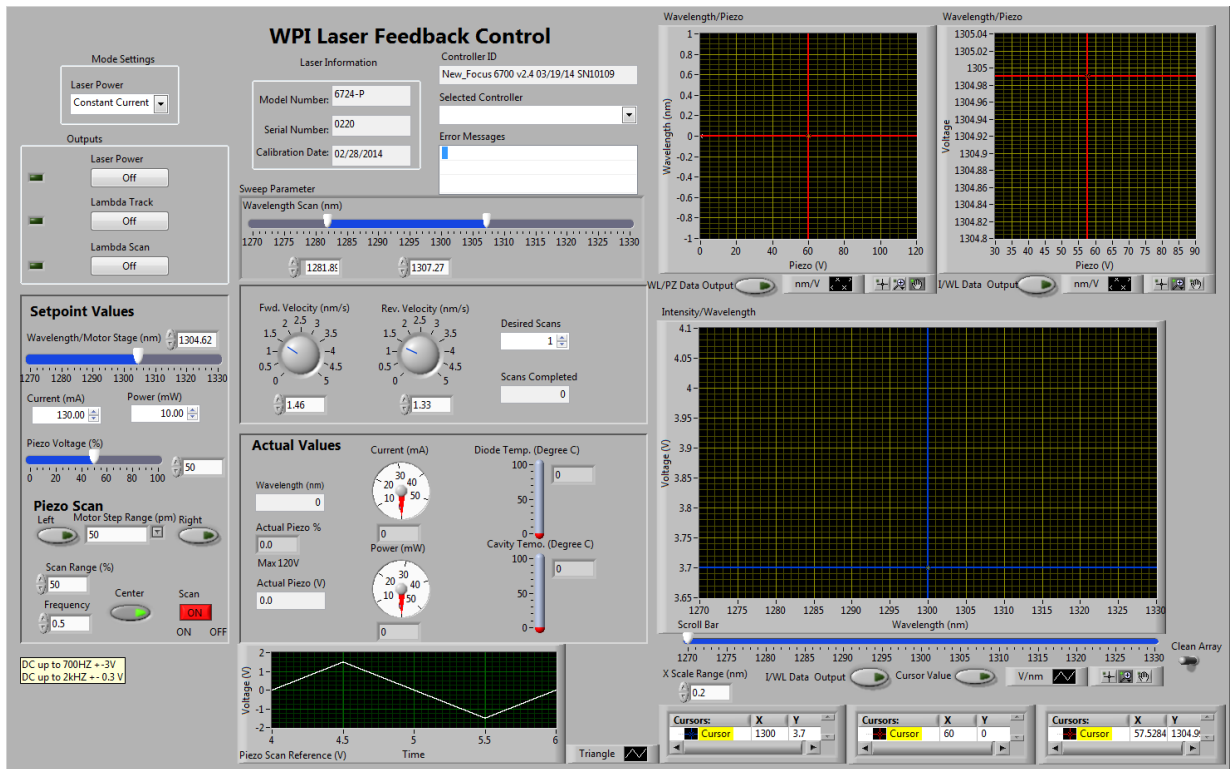


Figure 4.2.1. LabVIEW Program Front View

We write a LabVIEW program to control the laser and measure wavelength. There are mainly four modules in this program: Setup Values Module, Piezo Scan Module, Wavelength Scan, and Numerical and Graphical Indicator. To obtain all desired function, we use many different structures such as While loop, Case Structure, Event Structure, Stacked Sequence Structure, For Loop and Formula Node.

### While Loop



Repeats the code within its subdiagram until a specific condition occurs. A While Loop always executes at least one time.

*Figure 4.2.2. While Loop*

In our program, all functions are mainly running in several While Loops. By organizing these while loops, the entire program is capable of running at fast speed. Therefore, the user can use different functions at the same time and make an adjustment while the program is running.

### Case Structure

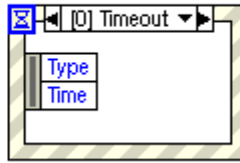


Contains one or more subdiagrams, or cases, exactly one of which executes when the structure executes. The value wired to the selector terminal determines which case to execute.

*Figure 4.2.3. Case Structure*

The case structure is widely used in our program so that the embedded subprograms can be selected, usually by Boolean button, to execute or stop.

### Event Structure

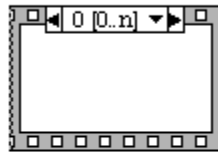


Waits until an event occurs, then executes the appropriate case to handle that event. The Event structure has one or more subdiagrams, or event cases, exactly one of which executes when the structure executes to handle an event. This structure can time out while waiting for notification of an event. Wire a value to the Timeout terminal at the top left of the Event structure to specify the number of milliseconds the Event structure waits for an event. The default is -1, which indicates never to time out.

*Figure 4.2.4. Event Structure*

Event Structure is another critical structure, which allow us to run embedded subprograms when satisfactory is achieved such as value change, key and mouse action and time.

### Stacked Sequence Structure [Stacked Sequence]



Consists of one or more subdiagrams, or frames, that execute sequentially. Right-click the structure border to add and delete frames or to create sequence locals to pass data between frames. Use the Stacked Sequence structure to ensure a subdiagram executes before or after another subdiagram.

*Figure 4.2.5. Stacked Sequence Structure*

Stacked Sequence Structure is used to run subprograms in certain desired sequence. In Stacked Sequence Structure, each subprogram will run in sequence starting from number 0 to any integer number depends on the number of subprograms.

Also, the signal generation and acquisition are achieved by DAQ assistant. Therefore, we can generate needed voltage signal, in other words, waves such as sine wave, saw tooth wave and triangle wave. These generated waves can be set up with certain frequency and magnitude. The piezo scan will be processed with generated voltage signal.

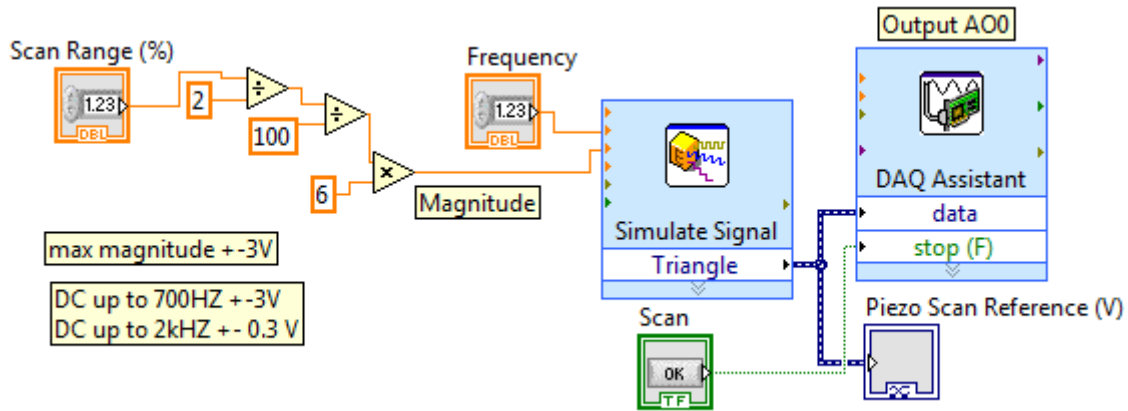


Figure 4.2.6. LabVIEW Subprogram of Wave Generation

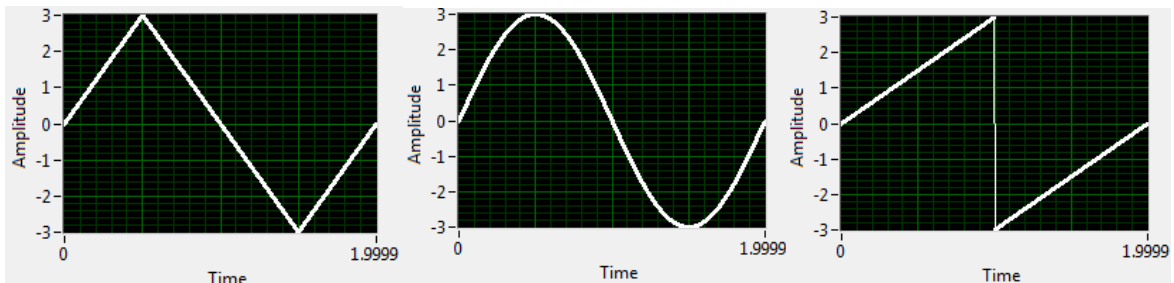


Figure 4.2.7. Generated Waveform (Triangle Wave, Sine Wave and Saw-tooth Wave)

The second DAQ assistant is used to acquire voltage signals such as wavelength voltage signal, piezo scan voltage signal and photodiode voltage. Thus, with these obtained voltage signals, the relation between wavelength and piezo voltage, and intensity and wavelength can be explored when data is plotted. In addition, the multiple signal can be separated and processed to satisfy users needs.

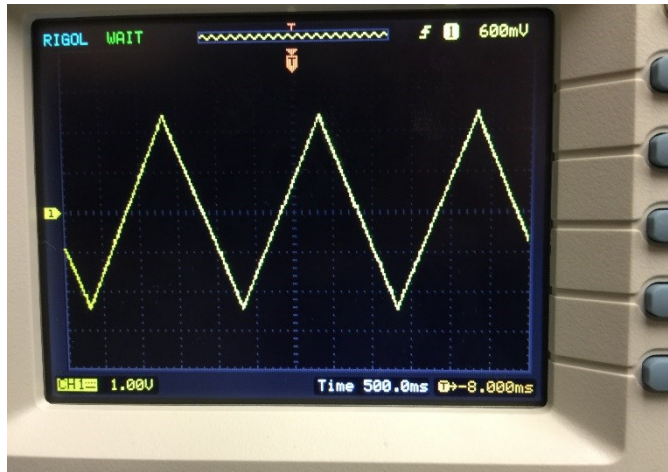


Figure 4.2.8. Signal produced from DAQ box, controlled by LabVIEW, measured by an oscilloscope.

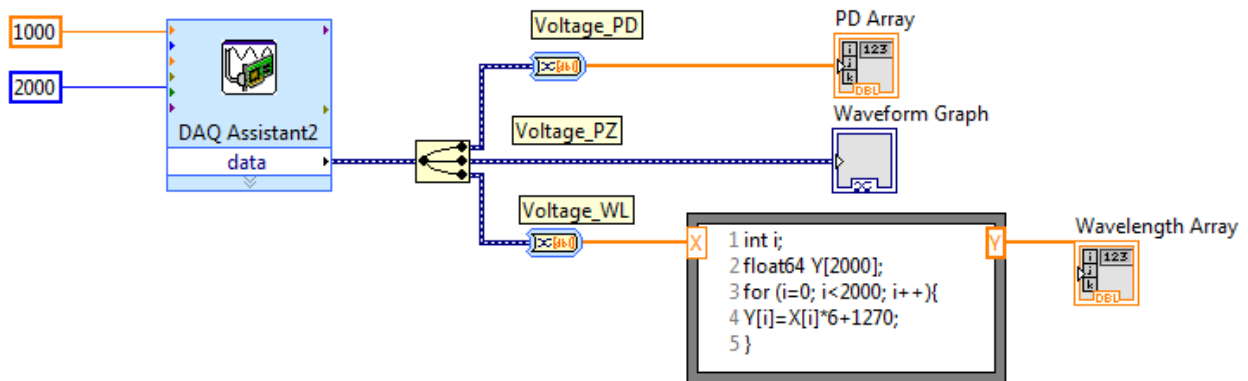
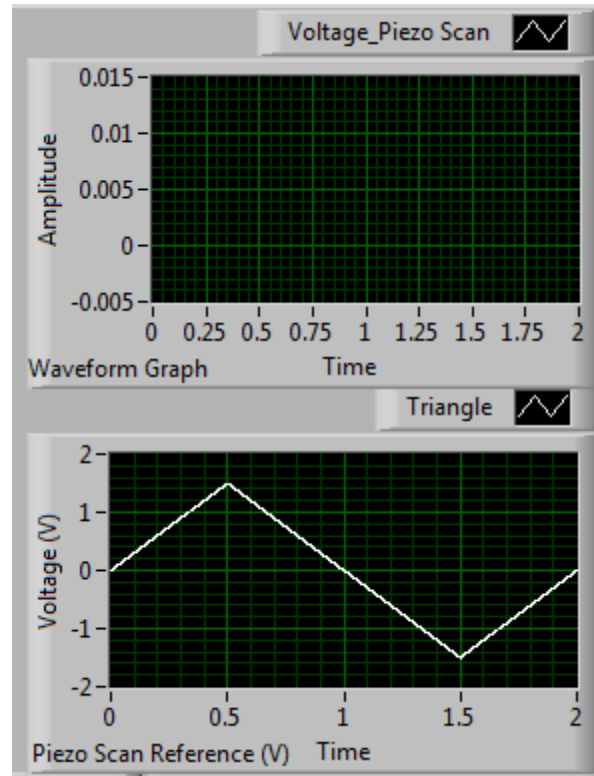


Figure 4.2.9. LabVIEW Subprogram of Signal Acquisitions

For exploring the relations between signals, different plot graphs are used to display clearly data such as wave chart form graph and XY graph. For wave chart form graph, the user can only input data for y-axis element, in other words, single scalar data or a one-dimensional array. X axis elements are defined as time or index number by default.





*Figure 4.2.10. Measurement of Generated Signal and Reference of Generated Signal*

For XY graph, the user needs to define x and corresponding y elements thus data are plotted in the form of points. In addition, some convenient functions are added to graph such as cursor values, zoom in/out, and output data value to excel file.

### 4.3 Back-end of Laser Feedback Control

Our first while loop is the major part of the whole LabVIEW program. It had all the control functions for the tunable laser. In the while loop, we used event structures to organize all the controls. Specific event case was triggered under specific situation, usually caused by value change of a front panel control. In the following figure, an outline of the event cases was showed. The

case zero was the timeout case, which ran after other cases were timeout. Other cases would run once their corresponding criteria were triggered.

- [0] Timeout
- ✓ [1] "Right", "Left", "Cursor Value", "I/WL Data Output", "WL/PZ Data Output": Value Change
- [2] "Lambda Track": Value Change
- [3] "Wavelength/Motor Stage (nm)": Value Change
- [4] "Current\_Set (mA)": Value Change
- [5] "Power\_Set (mW)": Value Change
- [6] "Piezo Voltage (%)", "Center": Value Change
- [7] "Sweep Parameter.Wavelength Scan (nm)": Value Change
- [8] "Scroll Bar": Value Change
- [9] "Fwd. Velocity (nm/s)": Value Change
- [10] "Rev. Velocity (nm/s)": Value Change
- [11] "Desired Scans": Value Change
- [12] "Laser Power Mode": Value Change
- [13] "Laser Power": Value Change
- [14] "Lambda Scan": Value Change
- [15] Application Instance Close?
- [16] Panel Close?
- [17] "Selected Controller": Value Change

Figure 4.3.1. Event Structure Drop Down Menu

The following figure showed the timeout case. In this case, the program communicated with the tunable laser and updated the status of laser components to the front panel indicators.

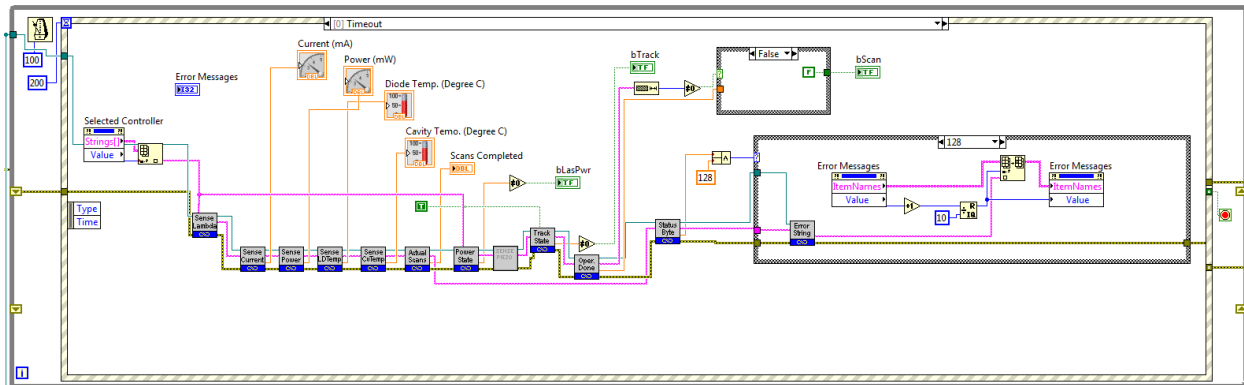


Figure 4.3.2. Timeout Event in Event Structure

One of the most complex case is the first event case, which used five front panel controls including left shift button, right shift button, cursor value and two data output buttons.

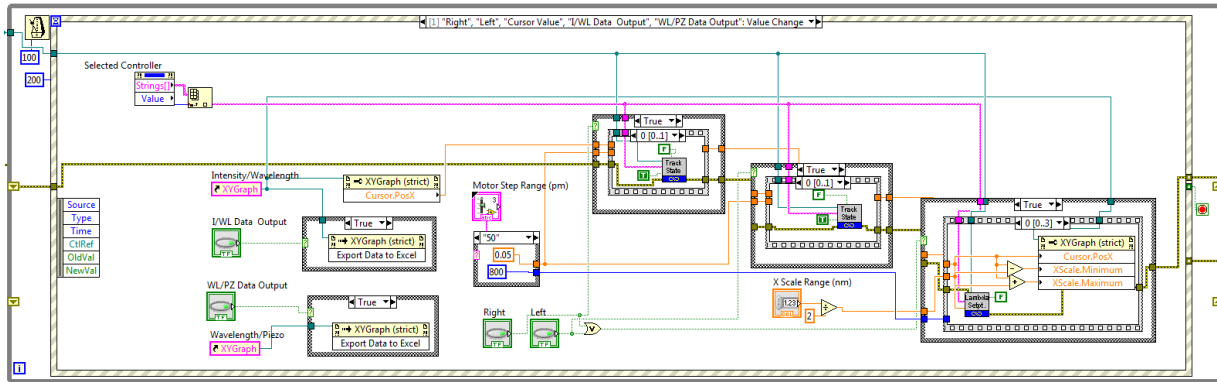


Figure 4.3.3. Wavelength Shift and Cursor Operation Event Case

In the case, two data buttons control whether the graph data should be exported or not.

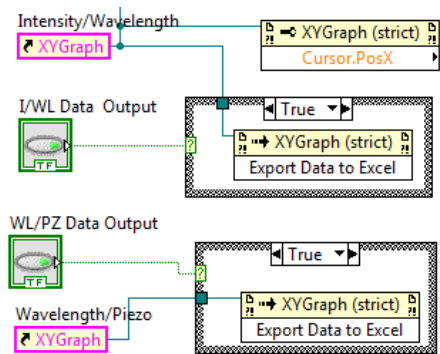


Figure 4.3.4. Graph Data Output

On the right side of the case, both left shift button and right shift button control three case structures. Whenever the user clicks the left of right shift button, the lambda track will turn on, the wavelength will be set to the value after shifting, and the lambda track will turn off. If the user moves the cursor around and clicks the cursor value button, the wavelength will be set to the cursor position. Since only one of the three buttons will be clicked simultaneously, we wrote the three

case structures in three situations. The first situation is that the left button was clicked, and the first case will be true, the second case will be false, and the third case will be true.

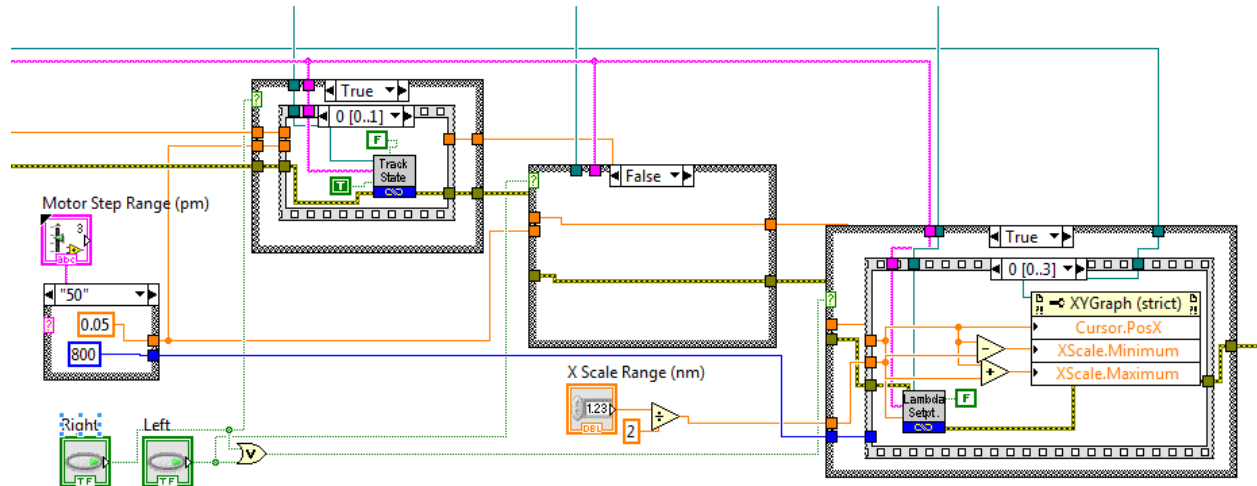


Figure 4.3.5. Left Shift Situation

In this situation, the lambda track will be turned on, and then the wavelength set point will be the cursor value plus the shift increment value. Then in the third case structure, the wavelength set point will be set, and the cursor position will be updated. The range of the x scale will be set so that the cursor is always at the center. Then a certain time will be delay to wait the motor stage moving to the new position. After that, the lambda track is turned off, and the user have the choice to auto scale once.

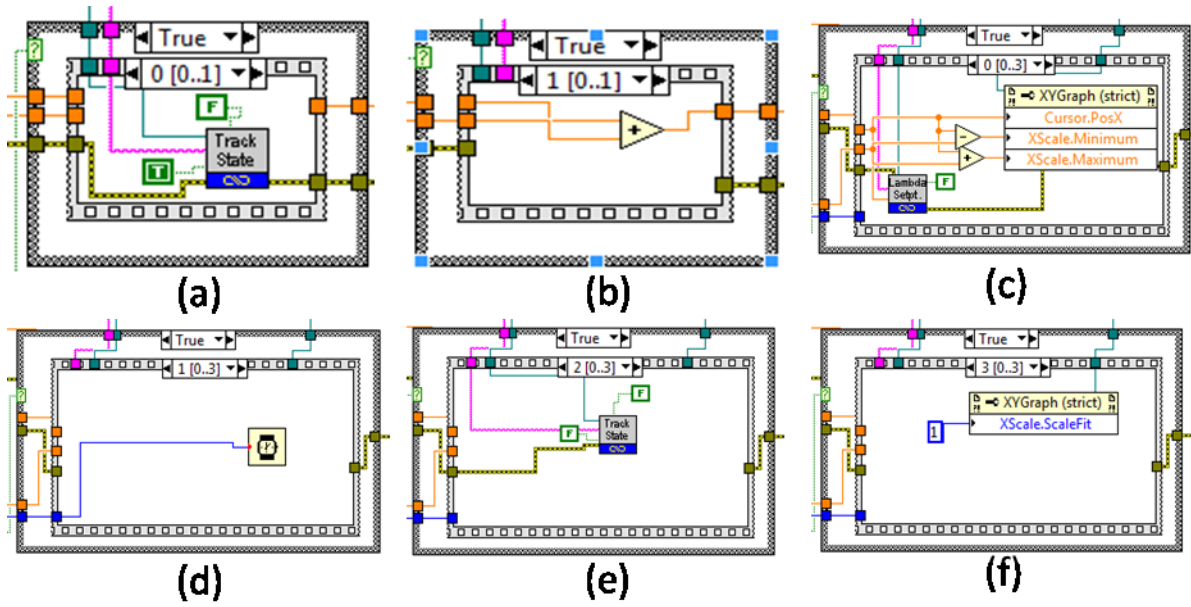


Figure 4.3.6. Detail Cases in the Sequence Structures

Similar to the previous situation, the second situation will happen when the right button is clicked. Almost all the procedure are the same; the only difference is that the new wavelength set value will be the wavelength minus the shift decrement value.

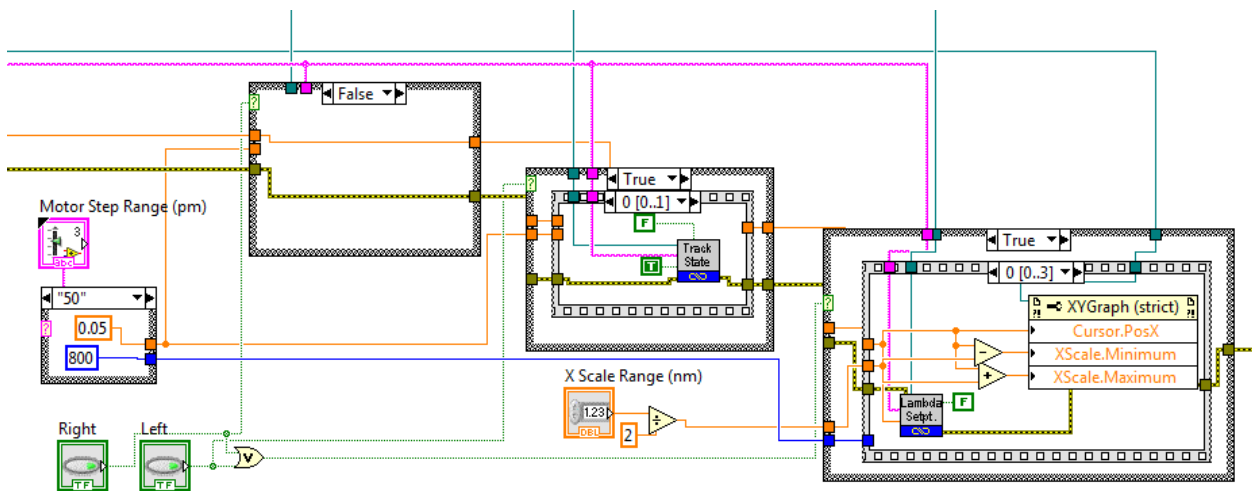


Figure 4.3.7. Right Shift Situation

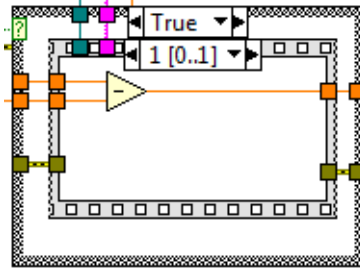


Figure 4.3.8. Detail Case in Right Shift Wavelength Calculation

In the third situation, only the cursor value button is clicked. So three case structures are all false. In this situation, the cursor will be pass to the lambda set-point without any modification and the lambda track will be turned on or off depending on the status of cursor value button. At last, the user could auto scale the graph by changing the scale-fit to 1.

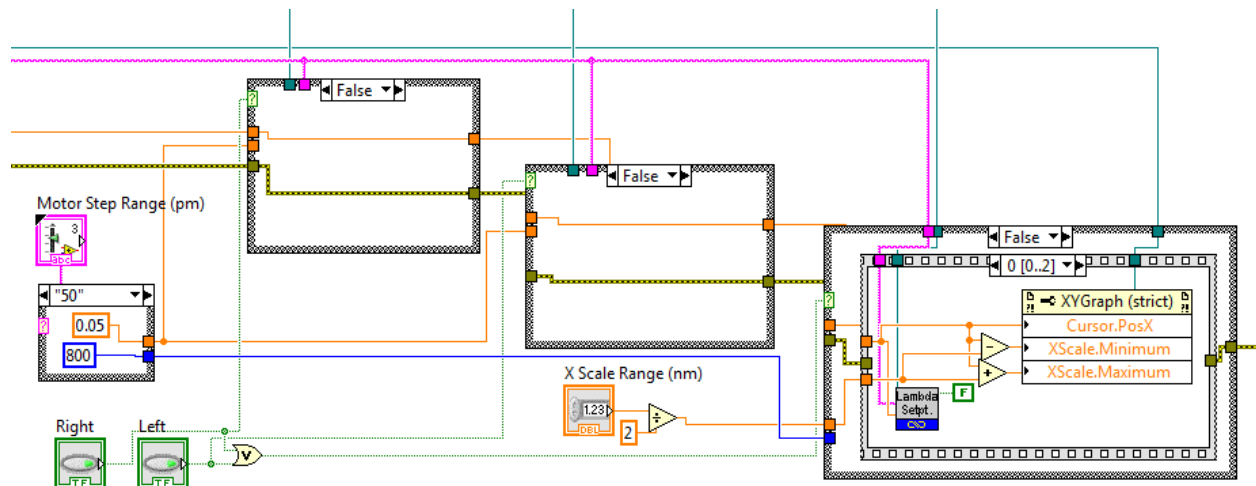


Figure 4.3.9. Cursor Operation Situation

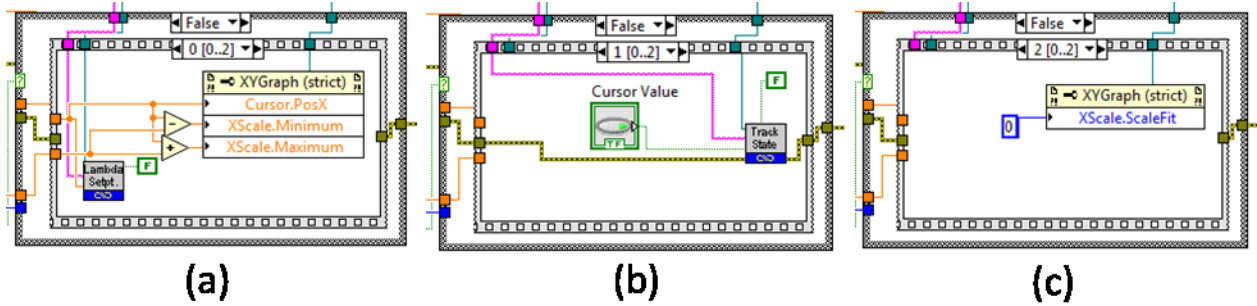


Figure 4.3.10. Details of Sequence Structure in Cursor Operation Situation

The following event shows that the USB commands will be sent when the sweep parameter changes its setting. For other events in the drop-down menu, the change of the front panel control will change the corresponding tunable laser setting via USB commands. Here, we are not going to list all the events.

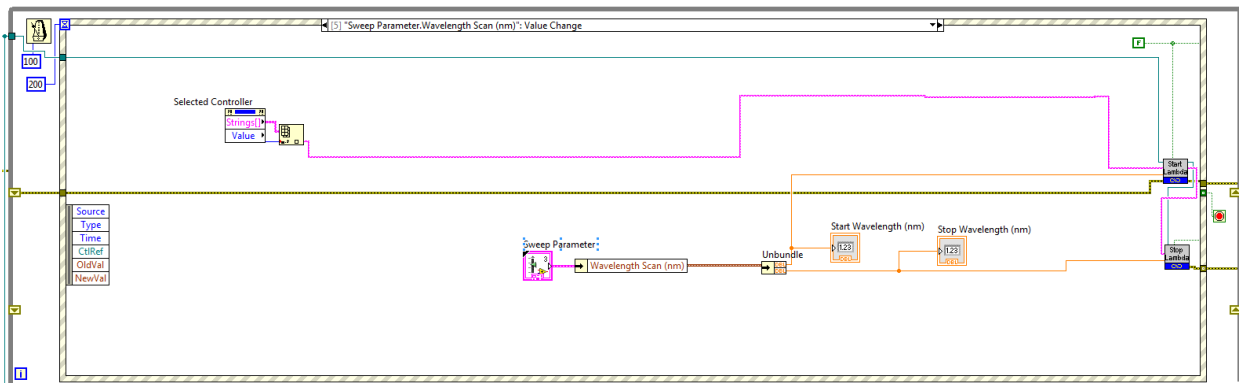


Figure 4.3.11. Details of the Second While Loop

As we mentioned in the flowchart of the software control for the tunable laser, our second while loop was in the charge of collecting the feedback data from the tunable laser using USB communications. The LabVIEW program of this loop was showed in the following figure. The for loop was used for appending the data of wavelength and piezo to the arrays. The loop number

determined the size of the array. At the same time, there were three indicators showing the real-time feedback of the wavelength, piezo voltage, and piezo percentage.

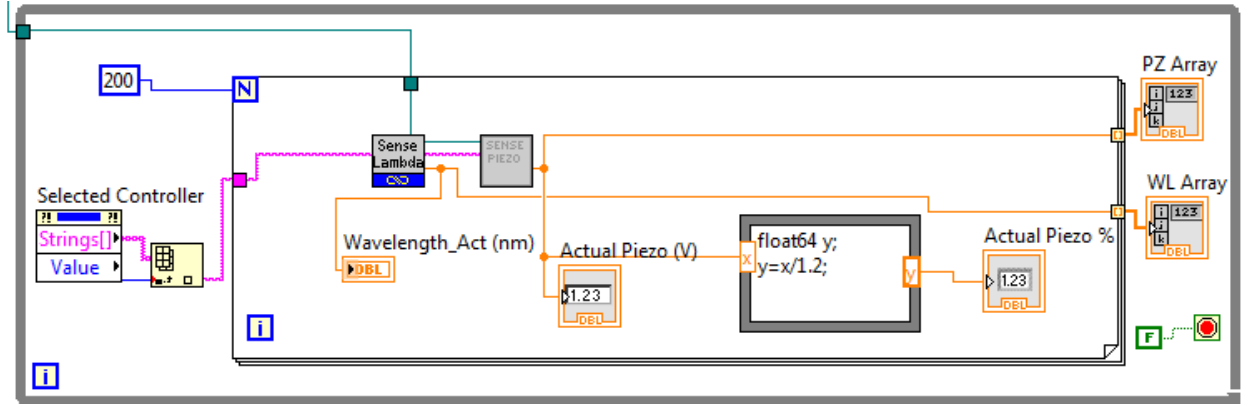


Figure 4.3.12. Details of the Third While Loop

In the third loop, we had a sequence structure inside the while loop. In the first sequence, we used the scan range input from the front panel to calculate the corresponding magnitude of the wave signal. Based on the manual of the tunable laser, the piezo modulation range is -3v to +3v corresponding to the range percentage of 0% to 100%. We used calculated magnitude and frequency to set the simulated signal and output it using DAQ Assistant.

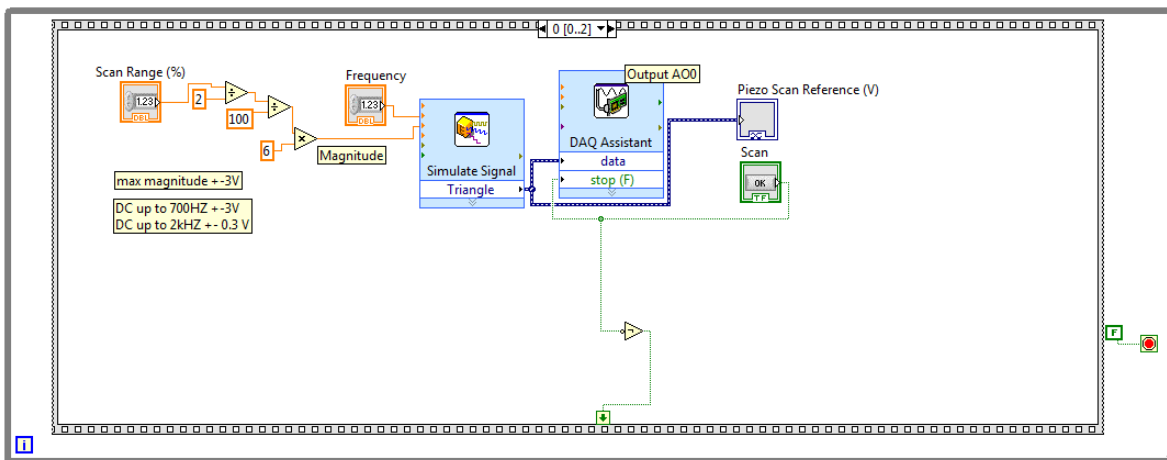


Figure 4.3.13. Wave Generation



In the second sequence, we set up the DAQ assistant to collect the data of voltage of photodetector, voltage of the piezo modulation and the voltage of the wavelength. Then we used a formula node to convert the voltage data to wavelength value based on the equation  $V = 10 * (\lambda_{\text{actual}} - \lambda_{\text{min}}) / (\lambda_{\text{max}} - \lambda_{\text{min}})$ , where  $\lambda_{\text{max}} = 1330\text{nm}$  and  $\lambda_{\text{min}} = 1270\text{nm}$ .

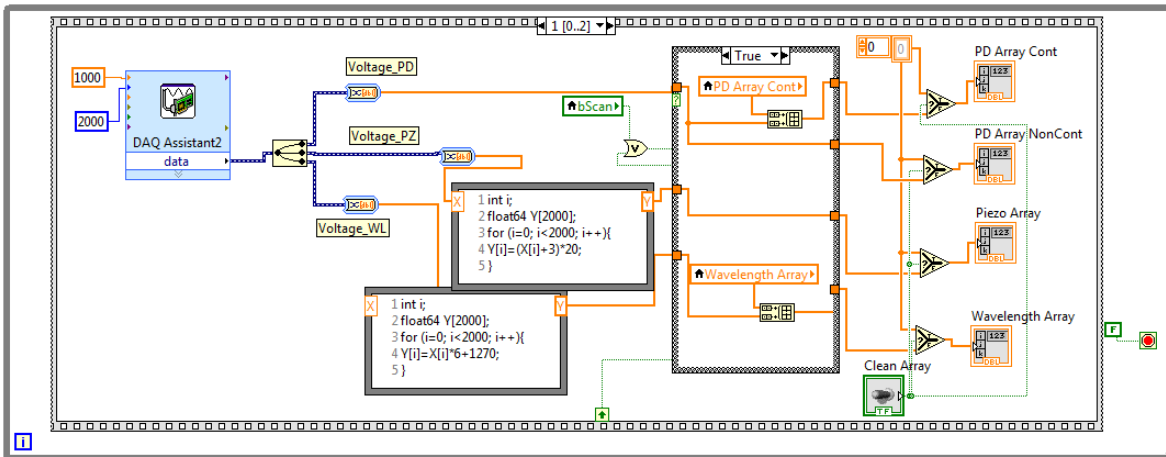


Figure 4.3.14. Data Acquisition

In the last sequence, we displayed two necessary graphs in terms of piezo vs. wavelength and photon intensity vs. wavelength.

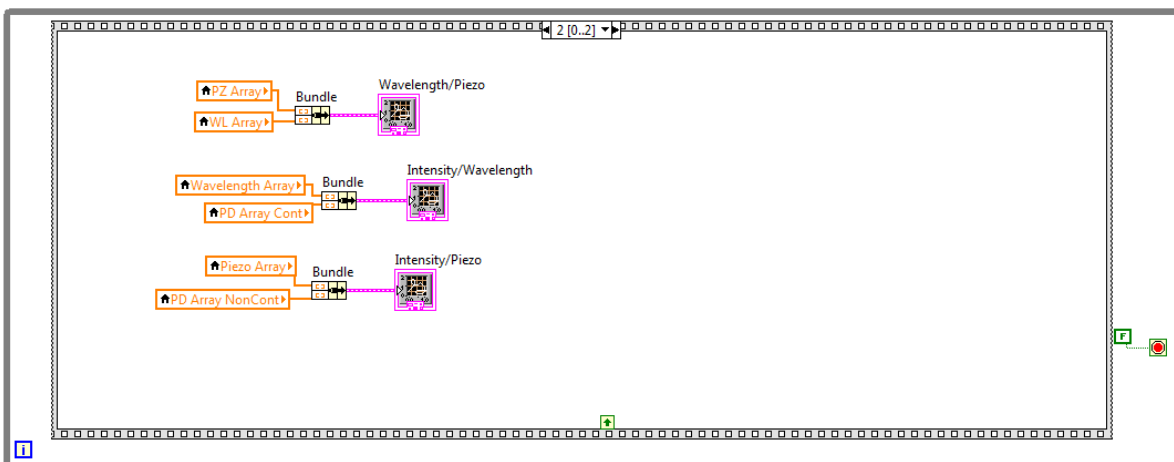


Figure 4.3.15. Data Displays

#### 4.4 USB communication syntax and protocols

One of the major components of our project is to implement the LabVIEW program to control the tunable laser. The tunable laser is connected to the computer via USB cable, so it is essential to understand the communication protocol. The USB communication of the tunable laser has a standard formatting and syntax. By sending the proper command, we can set the functions of laser and get the status of the laser. Here, we summarize some important syntax and command that we frequently use in the LabVIEW program. The following figure shows the front panel of USB communication subroutine.

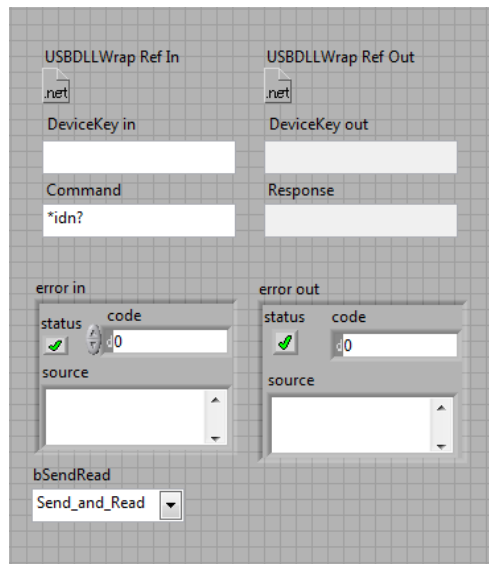


Figure 4.4.1. Front Panel of USB Communication Subroutine

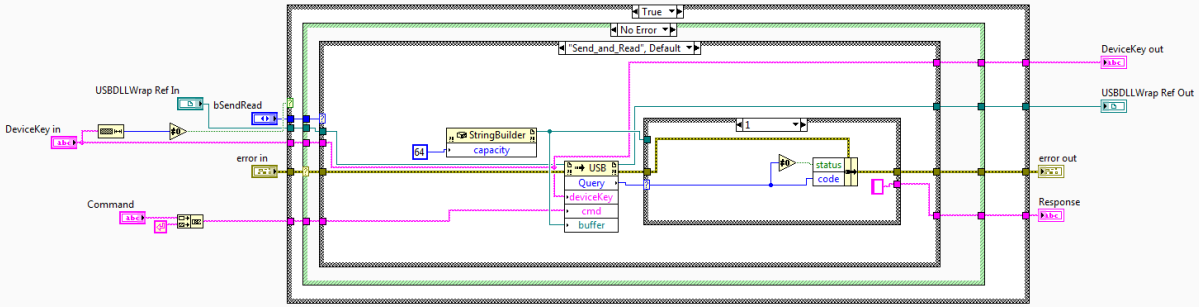


Figure 4.4.2. Back Panel of USB Communication Subroutine

By sending the command that begins with “SENSE:”, we can get the feedback of any components status in the tunable laser, like diode current, power, temperature, wavelength, piezo voltage. To get the feedback of a property of a component, we send the command “SENSE: Property: Component”. For example, we send “SENSE: VOLTage: PIEZO” to get the feedback of the piezo stage that functioned as a fine tuning for wavelength control.

Understanding how to detect the status of the laser component is not enough, we need to know how to set the value for those parts, like diode, piezoelectric stage, and motor stage. The command formatting is similar to sensing; we send the command that begins with “SOURCE:” and follows by “Property: Component”. For example, we send “SOURCE: CURRENT: DIODE” to set the diode current set point.

The following figures show some examples of commands in the format of LabVIEW subroutine based on the usage of the basic USB subroutine.

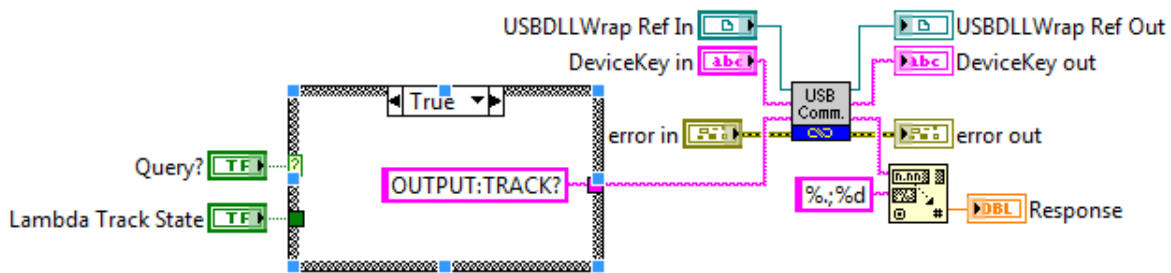


Figure 4.4.3. USB Command for Lambda Track

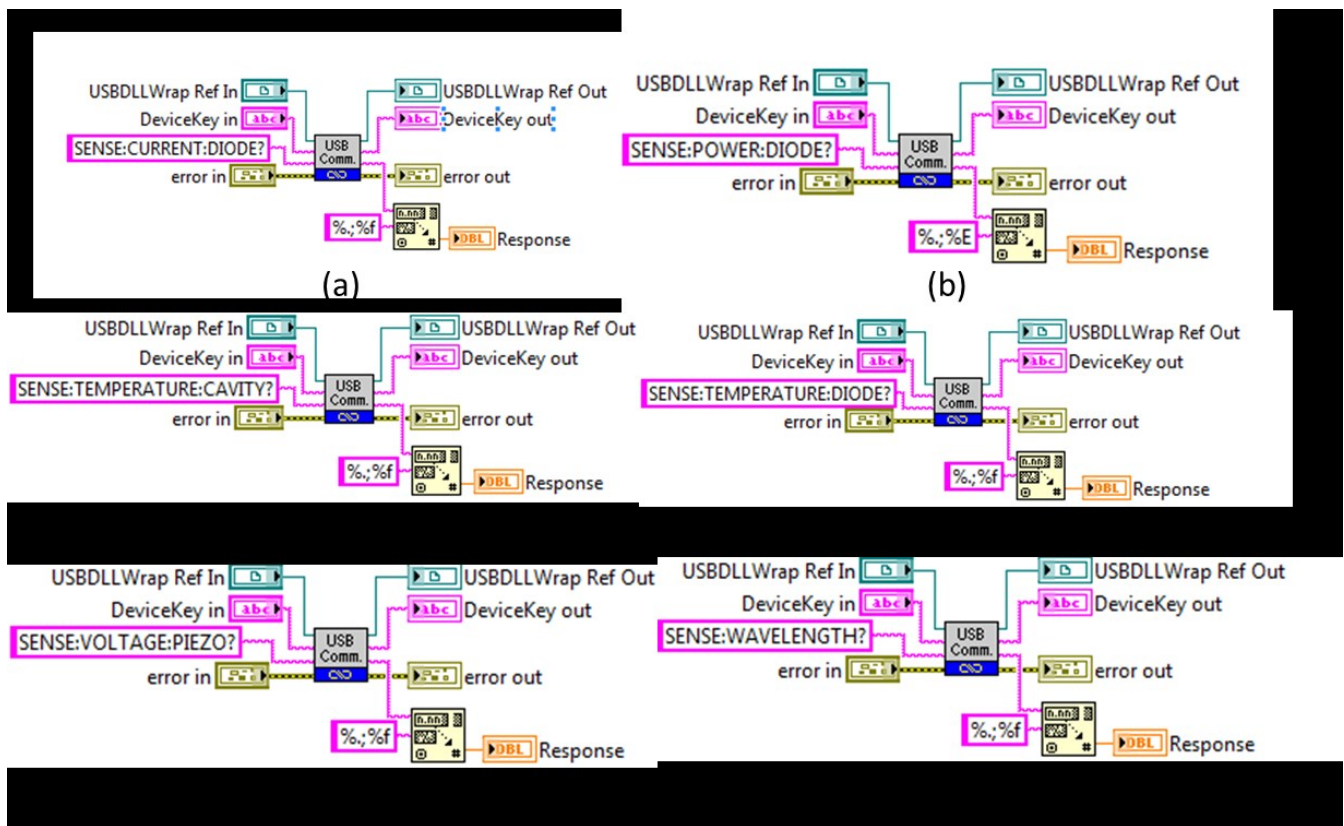


Figure 4.4.4. USB Command for (a) Current Sensing. (b) Power Sensing. (c) Cavity Temperature Sensing. (d) Diode Temperature Sensing. (e) Piezo Voltage Sensing. (f) Wavelength Sensing.

## 5 Operating Protocol and Results of Tunable Laser Control

### 5.1 Physical Connections of the System

Before the experiment, the Laser Controller should be connected as shown in Figure 5.1.1. The Laser Control port should be connected to the laser head. The Frequency Modulation port should be connected to DAQ box output channel by a BNC wire. The Wavelength Output should be connected to one of the DAQ box input channel also by a BNC wire.

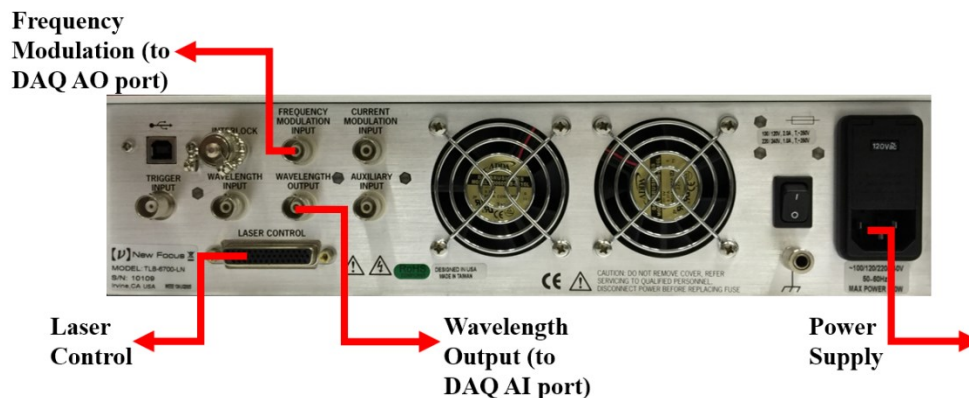


Figure 5.1.1. Physical Connection of the Laser Controller

The Photodetector should be connected to another channel of DAQ Input channel with a BNC wire. The user should make sure the channel information in DAQ Assistant in back panel corresponds to the channel connected to DAQ box.

### 5.2 Procedure of LabVIEW Control of Tunable Laser

To get a precise measurement, we default laser mode settings as constant current. In order to get an optimal real-time measurement, default current value is set at 130 mA. The laser power will undulate with various wavelength output within a tiny range. All buttons, especially laser power, lambda track, and lambda scan, are set with default off status to protect hardware including

tunable laser controller, laser head and photodetector, and to protect users not to be injured by high power laser. Piezo Scan range is set as 50%, which is in the range of -1.5V and 1.5V. Also, Piezo scan frequency is set at 0.5 Hz as the minimum value. The motor wavelength scan, has forward scan speed 1nm/s and reverse scan 1nm/s with desired scan number as 1.

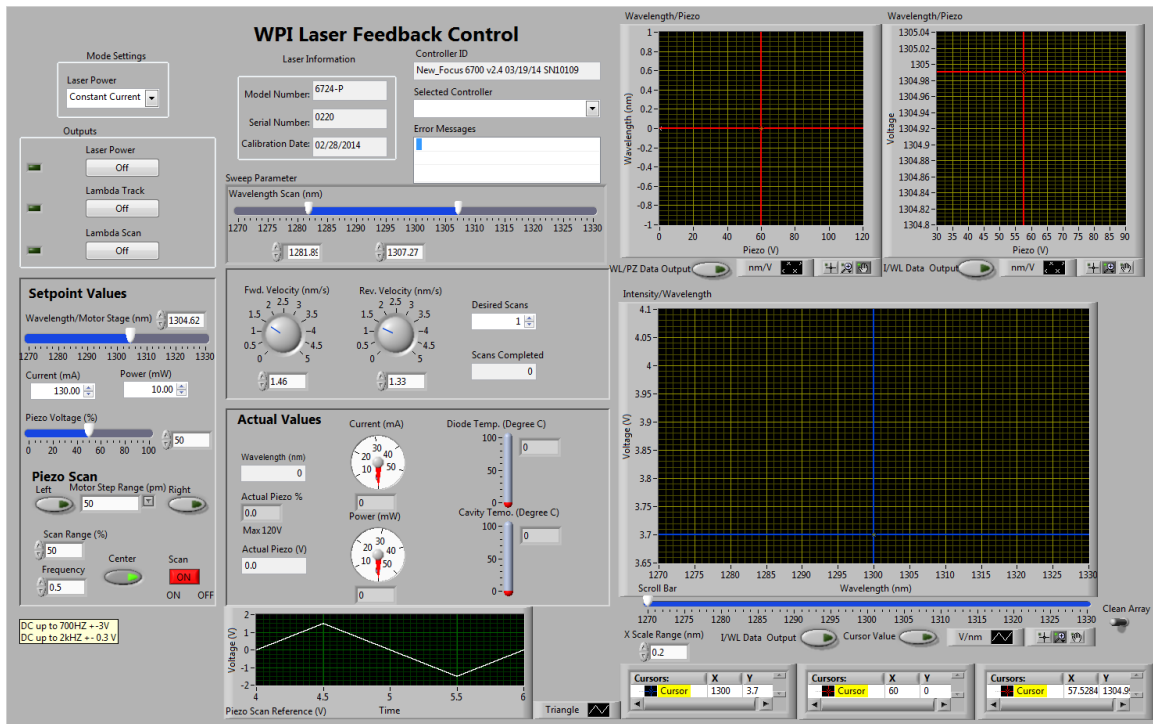


Figure 5.2.1. Front Panel Screen Capture

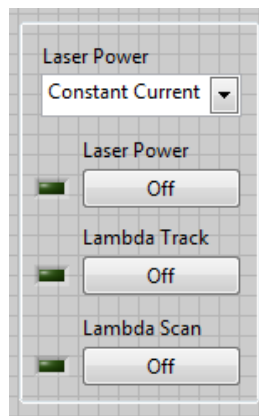


Figure 5.2.2. Laser Power Mode and Control Buttons Panel

The figure shown above are laser power mode selection, and three main buttons controlling laser power output, motor movement, and motor scan respectively. In addition, lambda track button controls motor motion inside laser head to control cavity length, and then control wavelength.

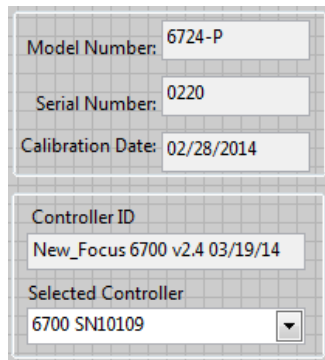


Figure 5.2.3. Basic Information Panel

The figure above shows basic laser information and connecting status. The basic information includes the model number, serial number, and calibration date. The connecting status shows in lower part in terms of connected controller and selected controller drop-down menu listing all used devices.

Before starting our program, the user must choose power mode as constant power or constant current. These two parameters are related to each other, in other word, one parameter changes with the other. Next, the user needs to define a value for current in mA. For our project, we choose 130 mA.

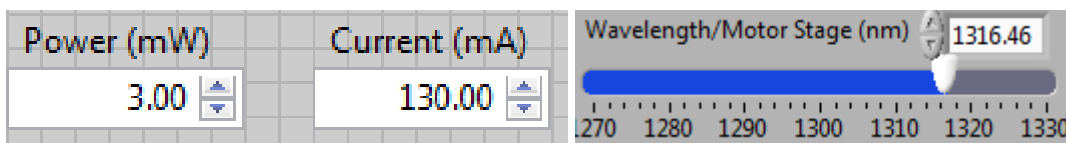


Figure 5.2.4. Power, Current and Wavelength Setting Panel

The wavelength/motor stage bar is the input wavelength value controlled by moving the motor inside the laser head.

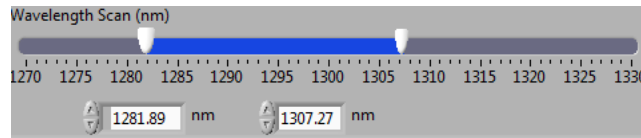


Figure 5.2.5. Wavelength Scan Range Setting Panel

Wavelength scan function allows the user to choose start and stop wavelength scan value.

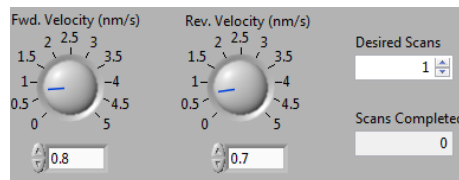


Figure 5.2.6. Wavelength Scan Velocity and Number Setting Panel

Then, the user needs to define scan speed for both forward scan and reverse scan, and scan repeating numbers.

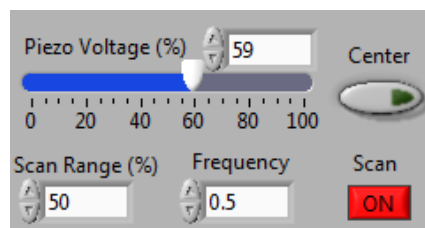


Figure 5.2.7. Piezo Modulation Setting Panel

Shown in the above figure, piezo voltage scrolling bar controls piezo voltage in term of percentage. Center button inputs piezo voltage value as 50 %. Next, before starting a piezo scan by clicking scan button, the user must define scan range and frequency, in which the generated triangle waves' magnitude and frequency are defined correspondingly.



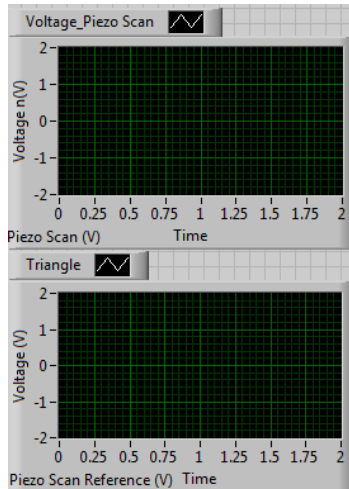


Figure 5.2.8. Piezo Scan Reference and Feedback Graphs

In the figure above, there are two separate plots graphically indicating generated wave (piezo scan). The upper plot shows measured voltage verse time. The lower plot shows generating voltage verse time. Therefore, we have confidence that the generated wave satisfies our needs.

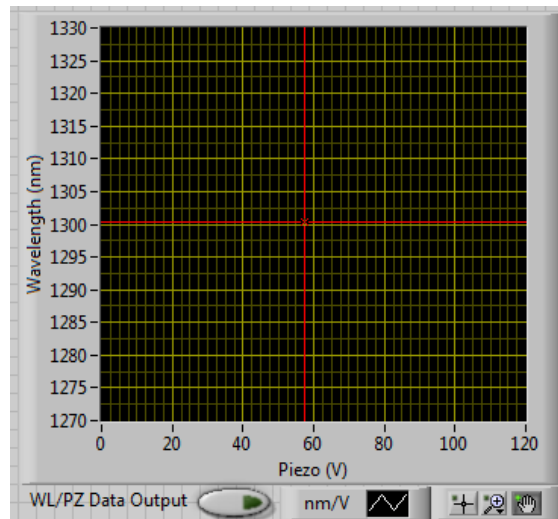
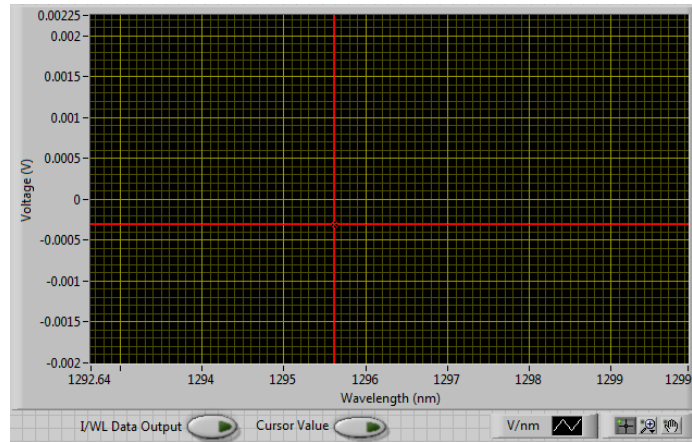


Figure 5.2.9. Wavelength Vs Piezo Graph

The figure above plots 2D data of wavelength and Piezo voltage. The red cross cursor is able to help the user to find corresponding values on horizontal and vertical axes. The data output

button will output the data on the graph as Excel file. Also, in right lower corner, functions such as move cursor, zoom in and move graph are added for users' convenience.



*Figure 5.2.10. Voltage Vs Wavelength Graph*

Similar to wavelength verse piezo figure, above figure plots data with Intensity in term of the voltage measured by photodetector and wavelength. Also, we add data output and some convenient functions to optimize user's experience. Cursor value button allows the user to input selected wavelength.

### 5.3 Calculation of $\Delta L$

To find the change in length, we first find the range by measuring the wavelength at when piezo motor equals to 0% and 100%.

	0% PZT (nm)	100% PZT (nm)	Range (nm)
test 1	1270.00	1270.29	0.29
test 2	1300.00	1300.27	0.27
test 3	1329.74	1330.00	0.26

*Table 5.3.1. Measurement of Full Piezo Scan Range*

$$\text{Range}_\lambda = \lambda_{100\% \text{ PZT}} - \lambda_{0\% \text{ PZT}}$$

Equation 5.1

We are looking for a peak number between 2 and 10 peaks. So we could get a clear measurement and have a better accuracy. We calculated the  $\Delta\lambda$ ,  $\lambda_1$ ,  $\lambda_2$  for 2 peaks and 10 peaks situation based on the follow equations:

$$\Delta\lambda = \frac{\text{Range}_\lambda}{\#\text{Peak}}$$

Equation 5.2

$$\lambda_1 = \lambda_{0\% \text{ PZT}} + \frac{\Delta\lambda}{2}$$

Equation 5.3

$$\lambda_2 = \lambda_1 + \Delta\lambda$$

Equation 5.4

2 PEAKs			10 PEAKs		
$\lambda_1$ (nm)	$\lambda_2$ (nm)	$\Delta \lambda$ (nm)	$\lambda_1$ (nm)	$\lambda_2$ (nm)	$\Delta \lambda$ (nm)
1270.073	1270.218	0.145	1270.015	1270.044	0.029
1300.068	1300.203	0.135	1300.014	1300.041	0.027
1329.805	1329.935	0.13	1329.753	1329.779	0.026

Table 5.3.2. The Calculation of Wavelength

Then we calculated the  $\Delta L$  based on equation

$$\Delta L = \frac{\lambda_1 \lambda_2}{n * \Delta\lambda}$$

Equation 5.5

The effective group index of refraction of the fiber we used in the research (Corning© SMF-28™ single-mode optical fiber) is 1.4677 at 1310 nm [32].

$\Delta L$ for 2 Peaks (mm)	$\Delta L$ for 10 peaks (mm)
7.58	37.90
8.53	42.65
9.27	46.34

Table 5.3.3. The Result for Peaks Length Difference Calculation

#### 5.4 Spectral Measurement Results of Laser Control of Motor Scan with LabVIEW

We disabled the piezo scan and scanned the entire wavelength tuning range using motor stage scanning. From the result figures, we could not find obvious interference spectrums. Then we ran the piezo scan at three different wavelength positions: 1280nm, 1300nm, and 1320nm. With piezo scanning, we observed interference pattern, and we found adjunct peaks and conducted further interference calculations.

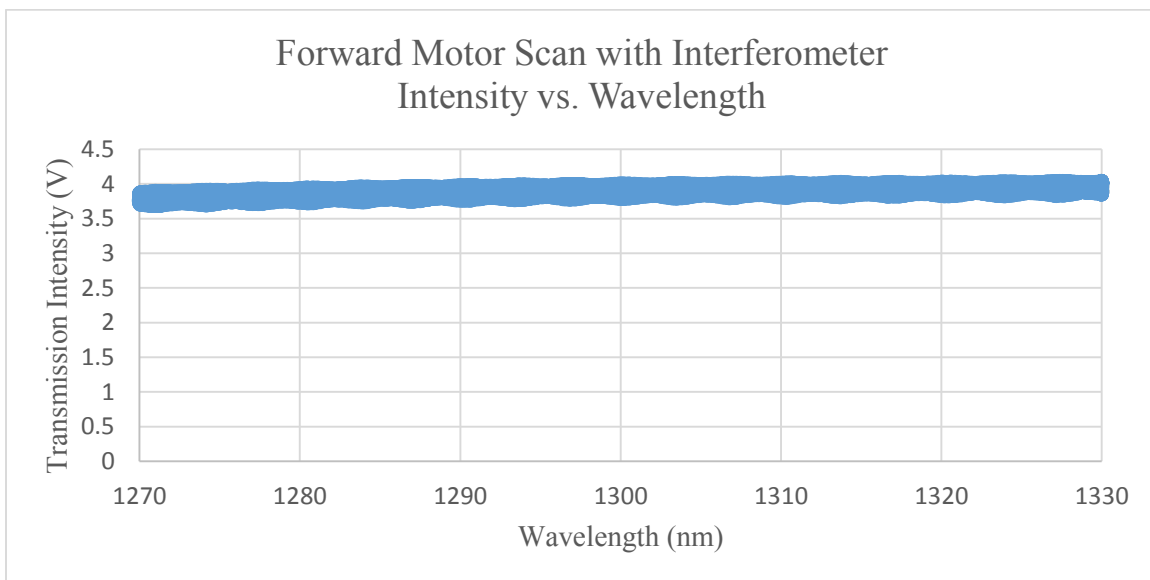


Figure 5.4.1. Forward Motor Scan with Interferometer Intensity vs. Wavelength

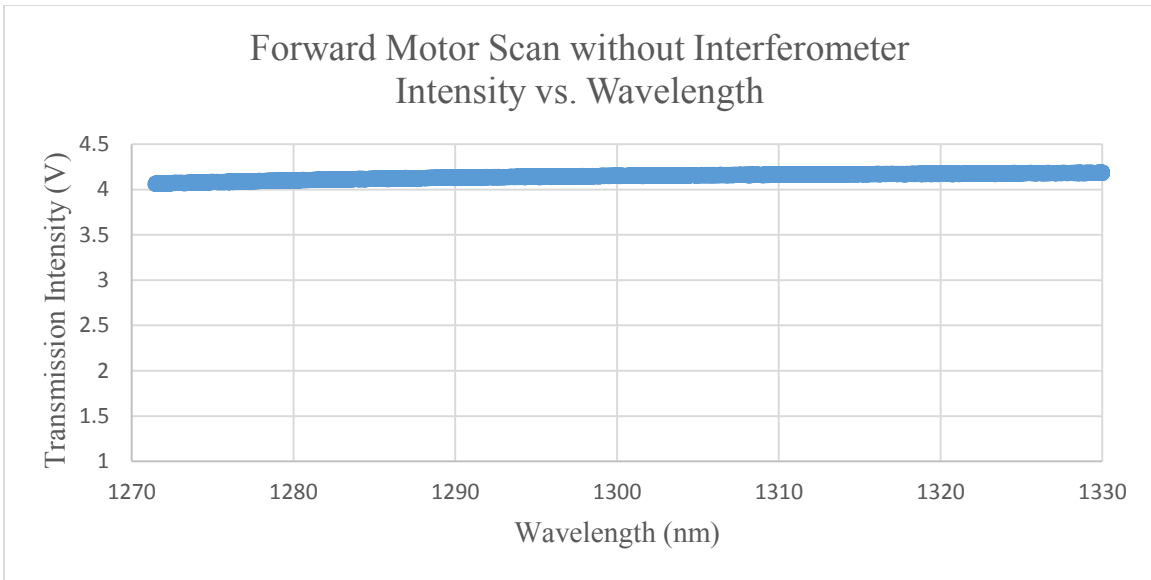


Figure 5.4.2. Forward Motor Scan without Interferometer Intensity vs. Wavelength

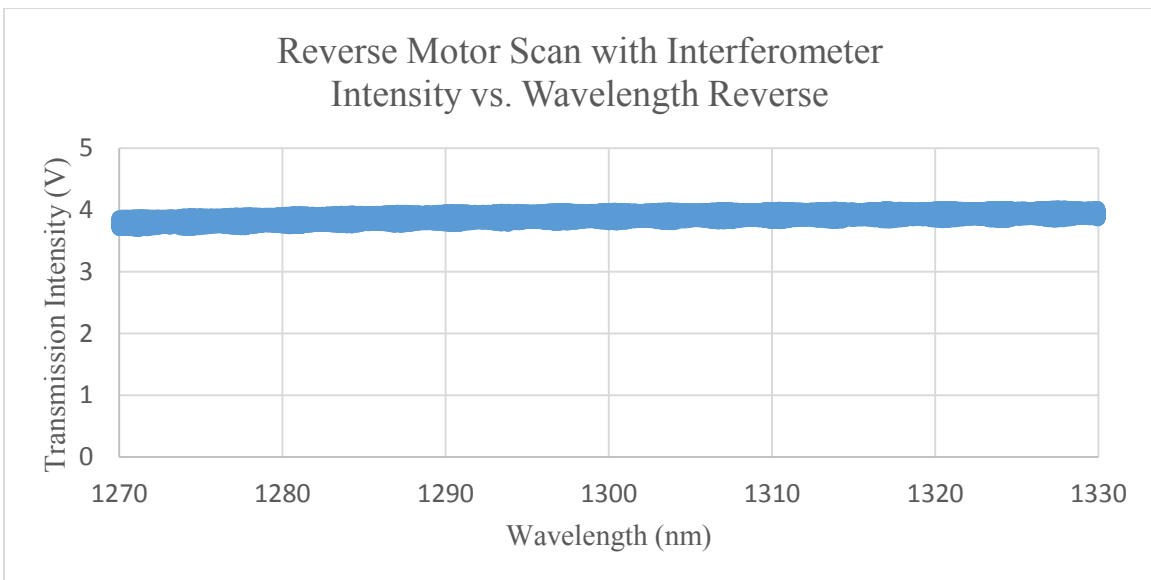
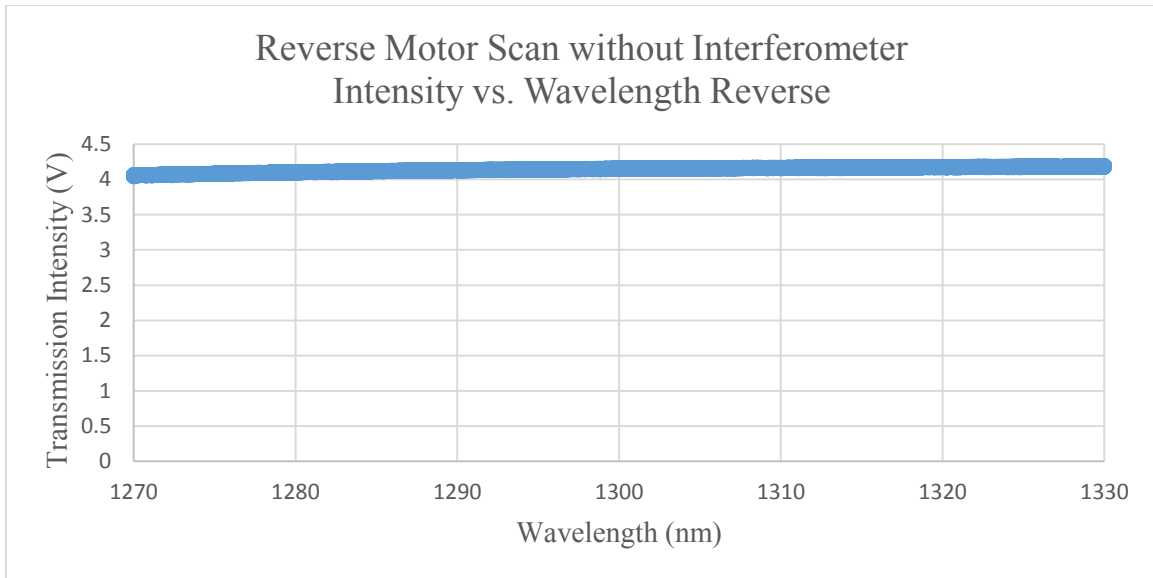


Figure 5.4.3. Reverse Motor Scan with Interferometer Intensity vs. Wavelength



*Figure 5.4.4. Reverse Motor Scan without Interferometer -Intensity vs. Wavelength*

In Figure 5.4.1 and Figure 5.4.3 above, we can see the wide range motor scan could not give any detail information about interference pattern. This might be caused by fiber energy lost, temperature fluctuation, and other environmental influences. So we use the piezoelectric motor to scan a much finer range (0.3 nm) to see the properties of the interference pattern.

Compare the motor scan result with interferometer to the one without from figures above, we can find that without the interferometer, there will be less fiber loss, so the transmission intensity is slightly higher, but there is no interference mode, and this would be clearer in the piezoelectric scan measurement after.

Because in the piezo scan plot, the laser intensity data comes from BNC channel, and piezo voltage data comes from USB channel of the laser system, they obtain different sampling frequency. Therefore, we are not able to combine these two information together in the spectra graph. However, we are able to plot the graph of wavelength vs. piezo voltage. And the wavelength vs. piezo voltage has a linear relationship, we are able to find the equation of the trend line in the

graph. And use this equation to find the corresponding wavelength in intensity vs. piezo voltage graph.

We took measurements of piezo scan at three wavelengths (1280nm, 1300nm and 1320nm) the result as shown in figures below.

### 5.5 Spectral Measurement Results of Laser Control of Piezo Scan at 1280nm with LabVIEW

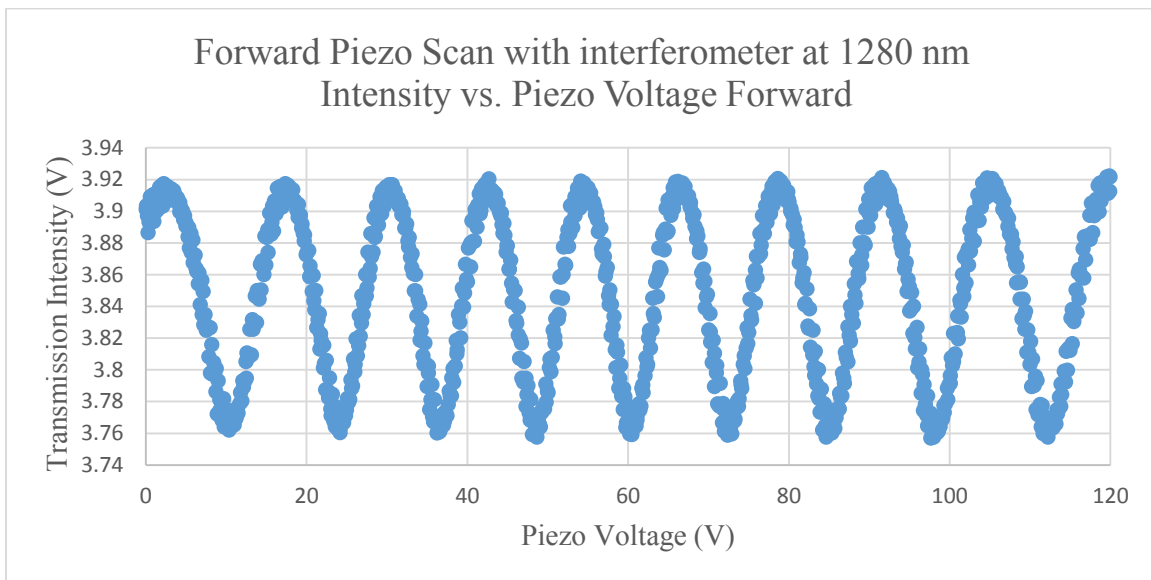
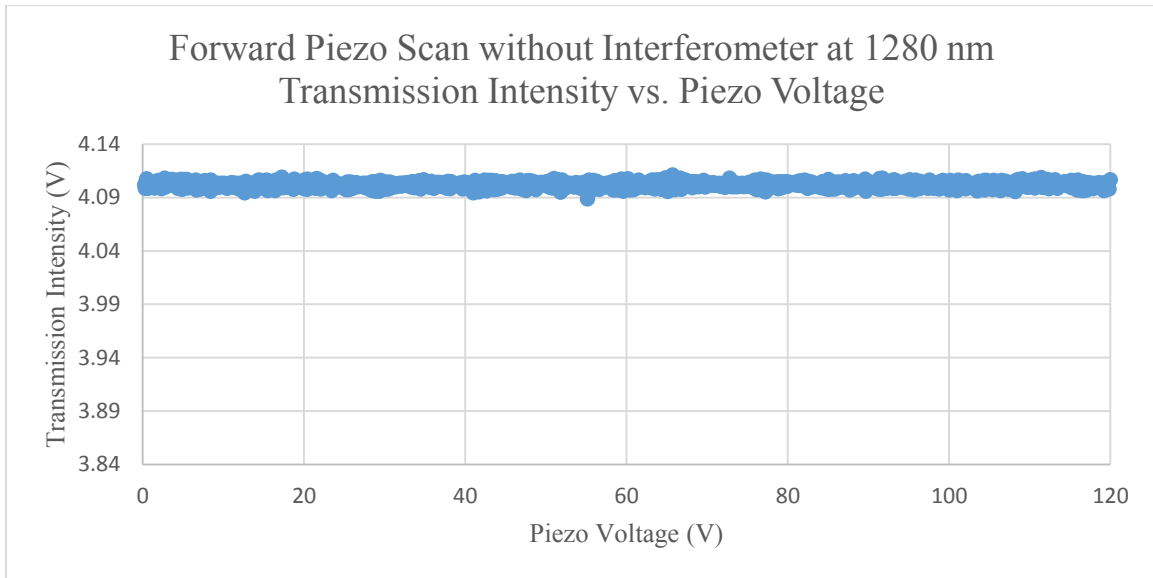


Figure 5.5.1. Forward Piezo Scan - Intensity vs. Piezo Voltage at Wavelength 1280 nm



*Figure 5.5.2. Forward Piezo Scan without Interferometer at Wavelength 1280 nm - Transmission Intensity vs. Piezo Voltage*

Compare between the Piezo Scan with and without the interferometer as shown in Figure 5.5.1 and Figure 5.5.2, we can clearly see that the transmission intensity of the measurement without interferometer is at 4.1V no matter what Piezo Voltage is. In the other word, there is no optical mode we are looking for. This proves the necessary of the interferometer. Without the interferometer, we can't find the optical mode, therefore we can't find the change in optical length based on wavelength.



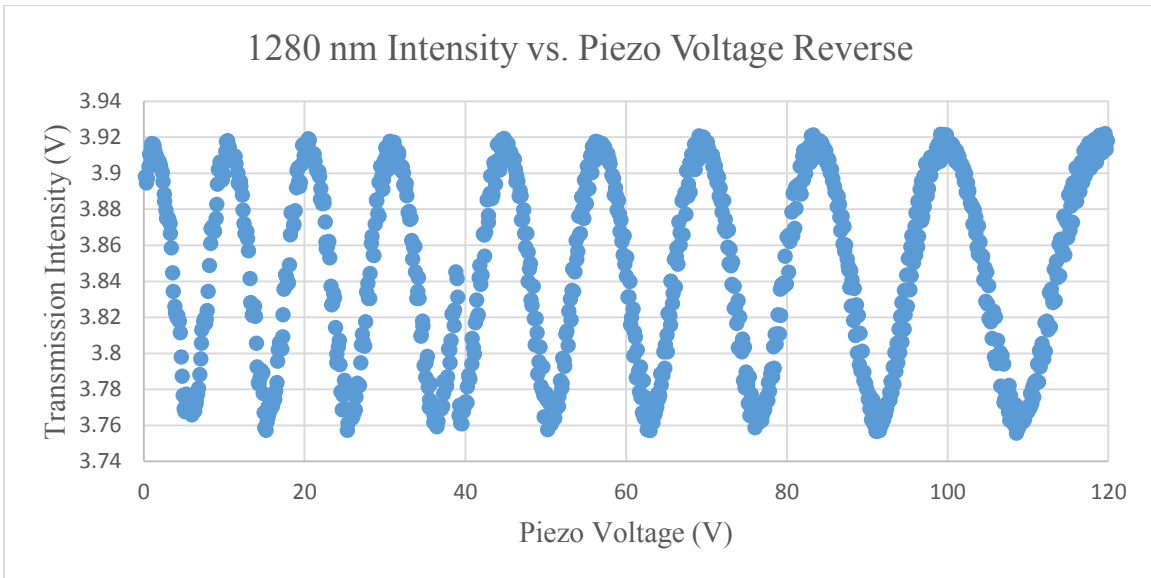


Figure 5.5.3. Reverse Piezo Scan Intensity vs. Piezo Voltage at Wavelength 1280nm

Figure 5.5.1 and Figure 5.5.3 show the interference patterns while the piezo was scanning around 1280nm. The peak of the spectra shows the additive interference and the bottom show the subtractive interference. In these two graphs, we are interested in the wavelength of the peak and the gap between two adjunct peaks.

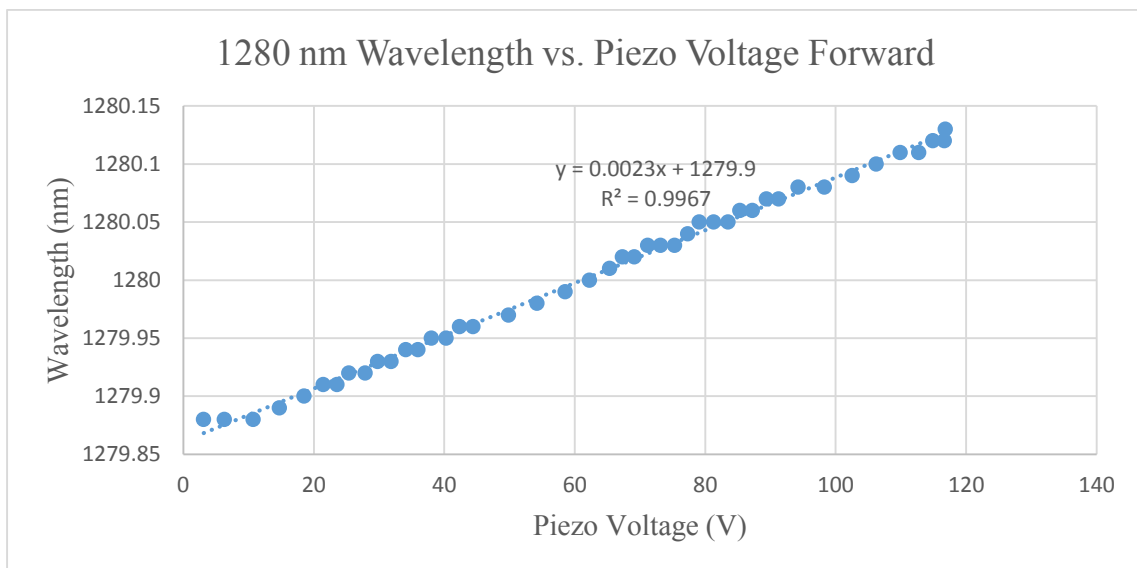


Figure 5.5.4. Forward Piezo Scan Wavelength vs. Piezo Voltage at Wavelength 1280 nm

$$y = 0.0023x + 1279.9$$

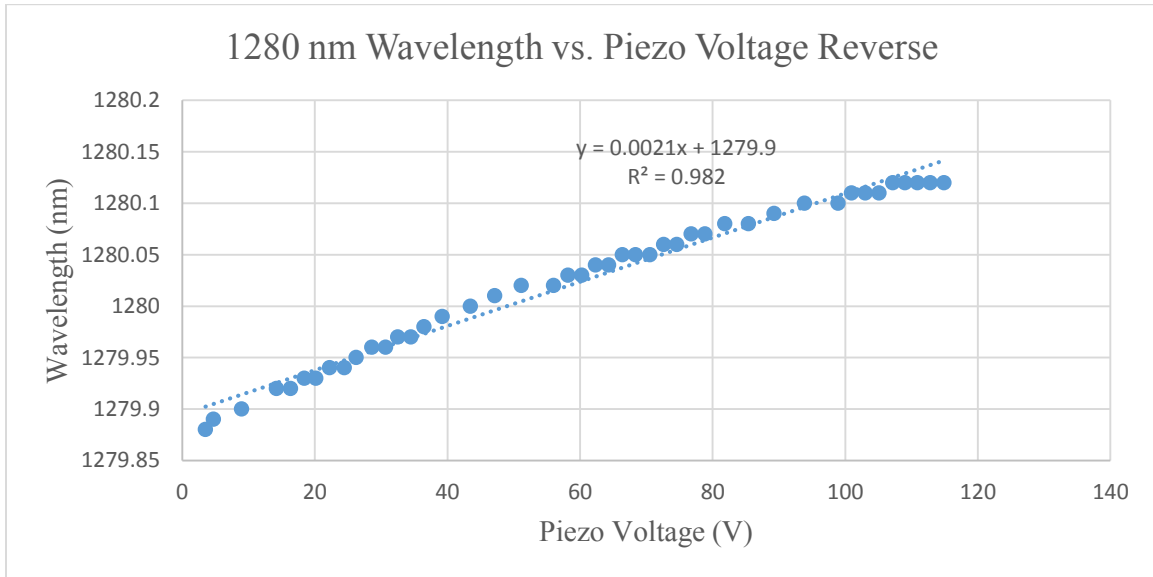


Figure 5.5.5. Reverse Piezo Scan Wavelength vs. Piezo Voltage at Wavelength 1280 nm

$$y = 0.0021x + 1279.9$$

Figure 5.5.4 and Figure 5.5.5 demonstrate the linear relationship between the wavelength of the laser and piezo scanning voltage. We found the linear equations for further data conversion and  $R^2$  for goodness-of-fit reference.

## 5.6 Spectral Measurement Results of Laser Control of Piezo Scan at 1300nm with LabVIEW

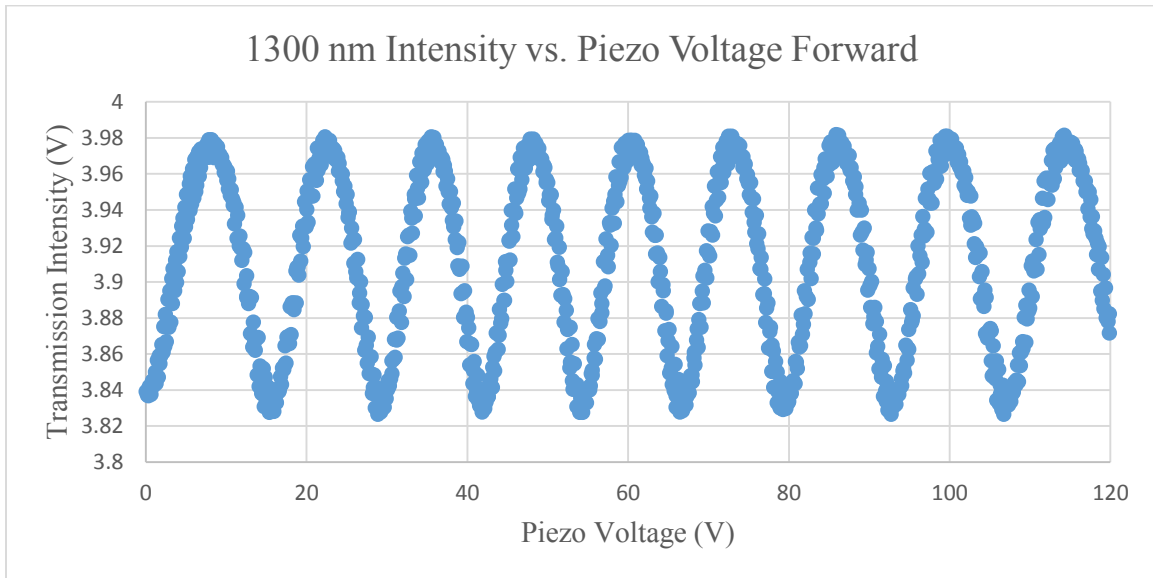


Table 5.6.1. Forward Piezo Scan Intensity vs. Piezo Voltage at Wavelength 1300 nm

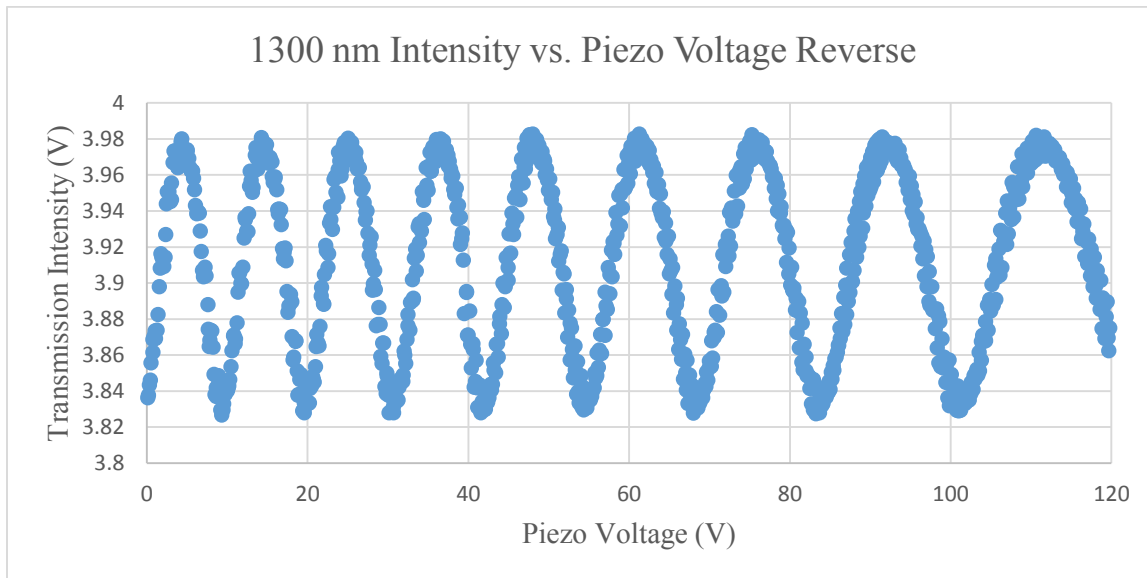


Table 5.6.2. Forward Piezo Scan Intensity vs. Piezo Voltage at Wavelength 1300 nm

Table 5.6.1 and Table 5.6.2 show the interference patterns while the piezo was scanning around 1300nm. The peak of the spectra shows the additive interference and the bottom show the

subtractive interference. In these two graphs, we are interested in the wavelength of the peak and the gap between two adjunct peaks.

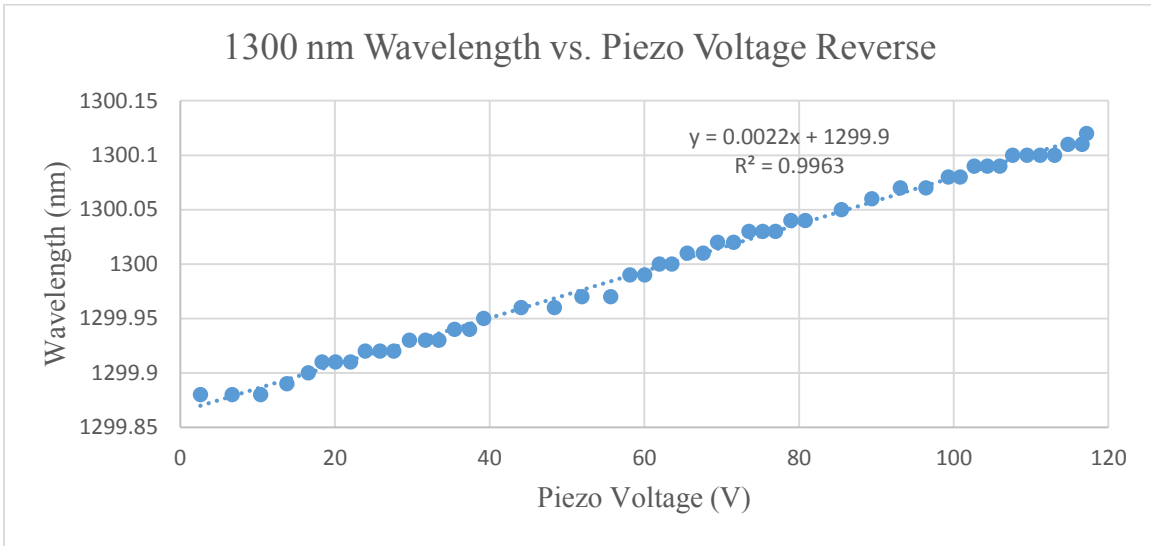


Figure 5.6.1. Forward Piezo Scan Wavelength vs. Piezo Voltage at Wavelength 1300 nm

$$y = 0.0022x + 1299.9$$

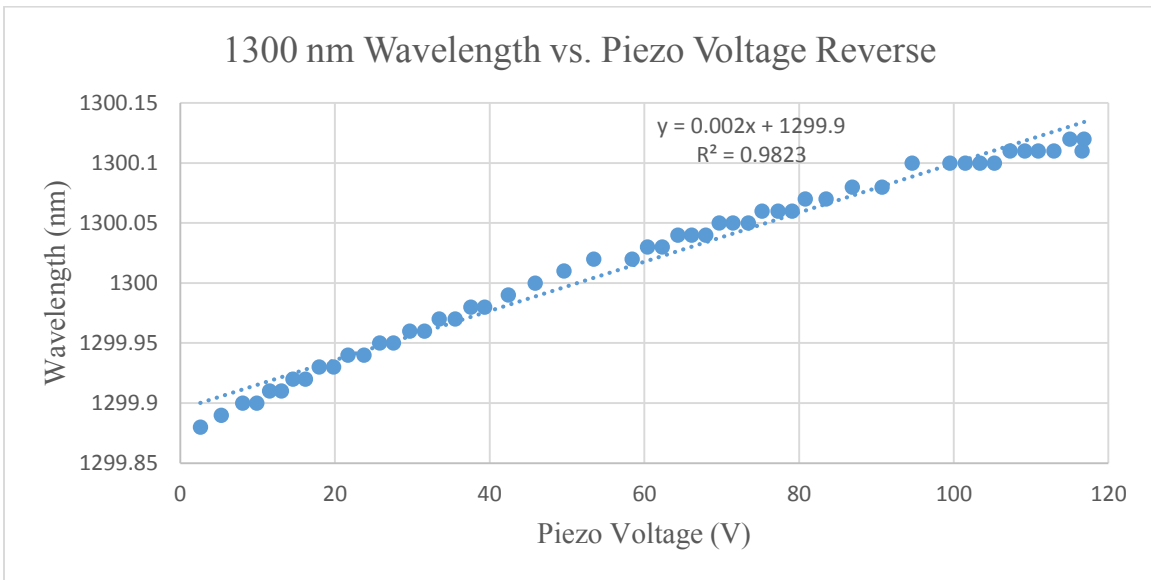
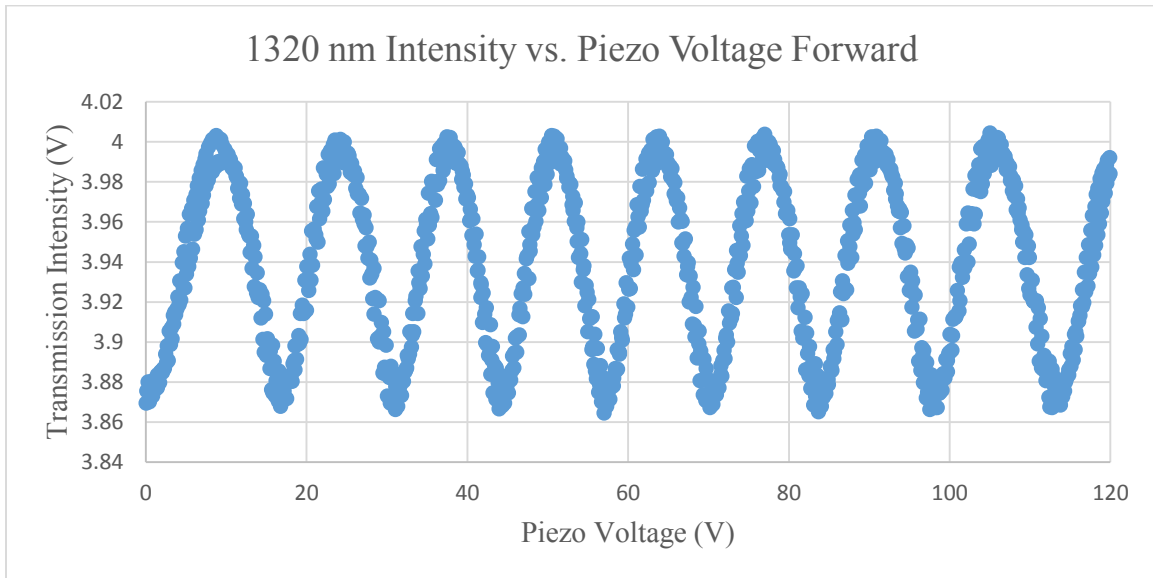


Figure 5.6.2. Reverse Piezo Scan Wavelength vs. Piezo Voltage at Wavelength 1330 nm

$$y = 0.002x + 1299.9$$

## 5.7 Spectral Measurement Results of Laser Control of Piezo Scan at 1320nm with LabVIEW



*Figure 5.7.1. Forward Piezo Scan Intensity vs. Piezo Voltage at Wavelength 1320 nm*

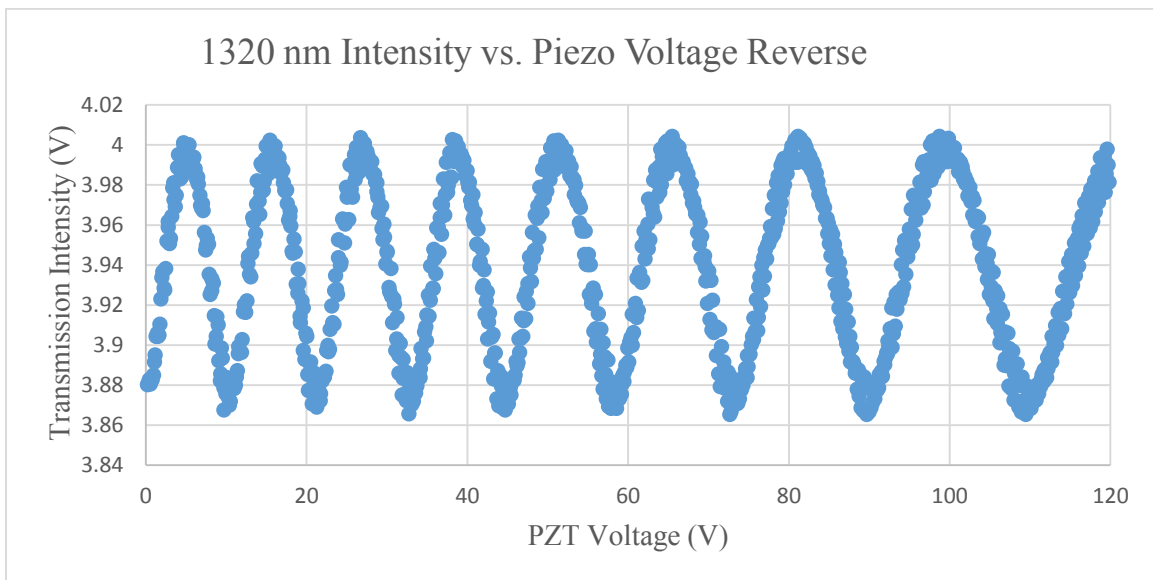


*Figure 5.7.2. Reverse Piezo Scan Intensity vs. Piezo Voltage at Wavelength 1320 nm*

Figure 5.7.1 and Figure 5.7.2 show the interference patterns while the piezo was scanning around 1280nm. The peak of the spectra shows the additive interference and the bottom show the

subtractive interference. In these two graphs, we are interested in the wavelength of the peak and the gap between two adjunct peaks.

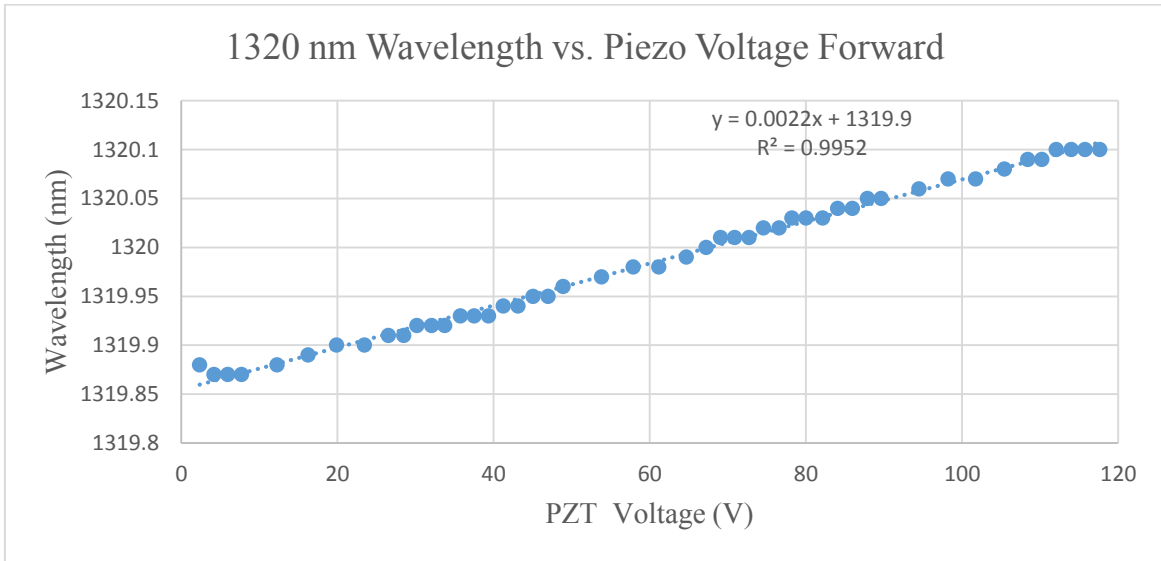


Figure 5.7.3. Forward Piezo Scan Wavelength vs. Piezo Voltage at Wavelength 1320 nm

$$y = 0.0022x + 1319.9$$

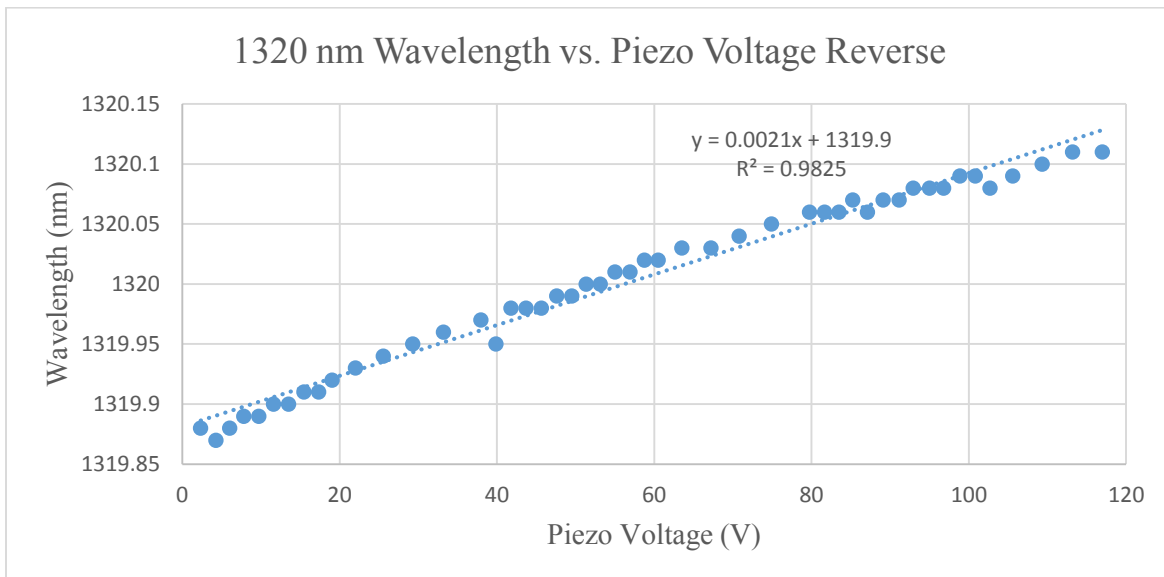


Figure 5.7.4. Reverse Piezo Scan - Wavelength vs. Piezo Voltage at Wavelength 1320 nm

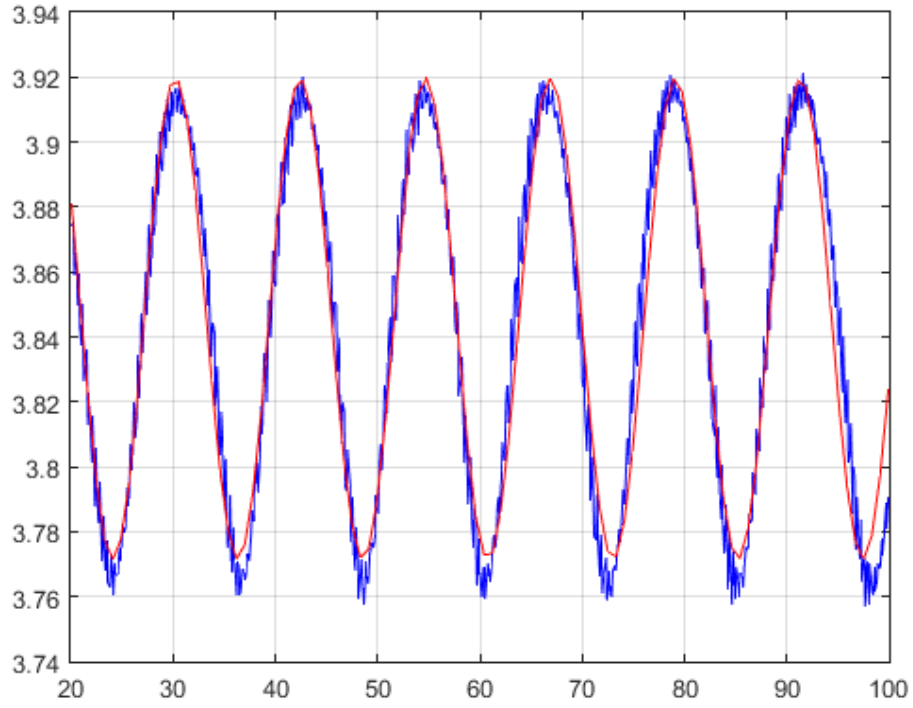
$$y = 0.0021x + 1319.9$$

Figure 5.7.3 and Figure 5.7.4 demonstrate the linear relationship between the wavelength of the laser and piezo scanning voltage. We found the linear equations for further data conversion and  $R^2$  for goodness-of-fit reference.

From the results, we can observe the interference pattern clearly. Therefore, we can find the length difference of two arms of the interferometer using the interference data from the graphs.

### 5.8 Curve Fitting to Determine the Optical Path Difference

As mentioned above, to find the length difference, we plot the MATLAB sinusoidal wave fitting (code is shown in Appendix A) for the Intensity vs. Piezo Voltage Plot as shown in figures below. Then we find the peaks, and put the Piezo Voltage peak values into the formulas we get from Wavelength vs. Piezo Plot. Therefore we can get the wavelength for the optical mode, and then we can calculate the length difference based on Equation 5.5.



*Figure 5.8.1. Sine Wave Fitting for Forward Piezo Scan at Wavelength 1280nm*

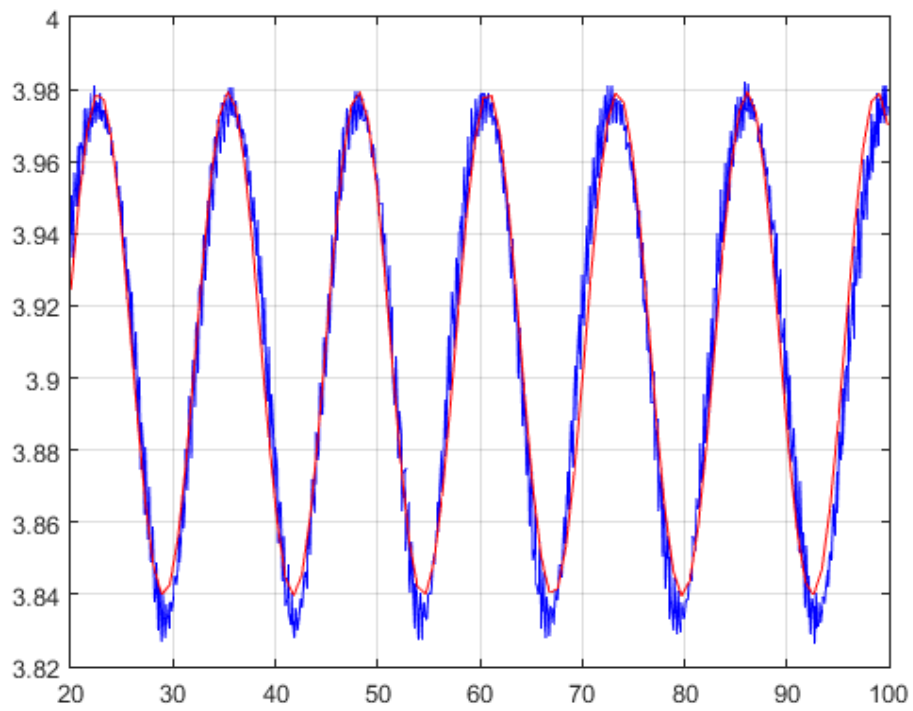


*Figure 5.8.2. Sin Wave Fitting for Forward Piezo Scan at Wavelength 1300nm*



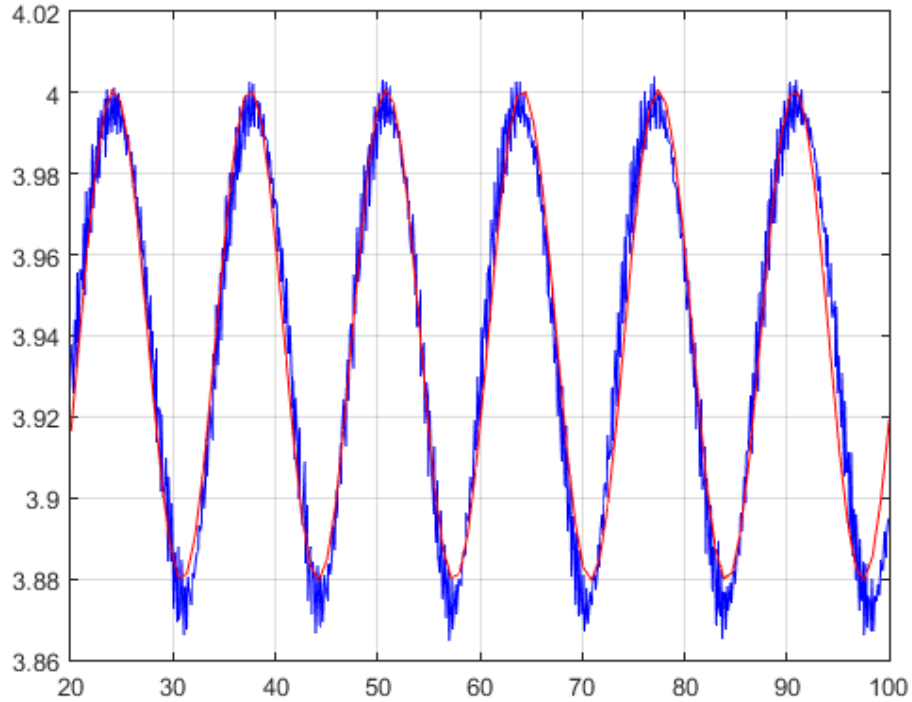


Figure 5.8.3. Sine Wave Fitting for Forward Piezo Scan at Wavelength 1320nm

We fit the result of the measurement using sin wave by finding four key parameters define a sin wave, amplitude, period, phase, and offset. We found the positions of peaks on fitted sin wave and converted them from piezo voltages into corresponding wavelengths.

	Amplitude	Period	Phase	Offset
1280nm	0.0741	12.222	-0.8181	3.8456
1300nm	0.0699	12.6802	-1.8395	3.9095
1320nm	-0.0606	13.3124	-14.6128	3.9402

Table 5.8.1. Fitted Sine Waves Data Sheet at Various Wavelength

		Peak 1	Peak 2	Peak 3	Peak 4	Peak 5	Peak 6
Forward 1280nm	PZT Voltage (V)	30.5638	42.6611	54.7583	66.8556	78.9529	91.0502
	Wavelength(nm)	1279.9703	1279.9981	1280.0259	1280.0538	1280.0816	1280.1094
Forward 1300nm	PZT Voltage (V)	22.4257	35.3336	48.2416	61.1495	73.2506	86.1585
	Wavelength(nm)	1299.9493	1299.9777	1300.0061	1300.0345	1300.0612	1300.0895
Forward 1320nm	PZT Voltage (V)	24.0639	37.7968	50.7219	64.4548	77.3799	91.1128
	Wavelength(nm)	1319.9529	1319.9832	1320.0116	1320.0418	1320.0702	1320.1004

Table 5.8.2. Forward Scan Peaks Data Sheet at Various Wavelength

Then we calculated the delta L based on the wavelengths at the adjunct peaks of the spectra graphs.

		<b>Peak 1,2</b>	<b>Peak 2,3</b>	<b>Peak 3,4</b>	<b>Peak 4,5</b>	<b>Peak 5,6</b>
Forward 1280nm	delta L in cm	4.011951	4.012159	4.0123	4.012474	4.012649
Forward 1300nm	delta L in cm	4.054588	4.054734	4.054943	4.325475	4.055286
Forward 1320nm	delta L in cm	3.929204	4.174959	3.929553	4.17533	3.929903
average of delta L (cm)					4.049701	
standard deviation delta L (cm)					0.102609	
					2.533752	%

Table 5.8.3. Calculations of Delta L

We used the Equation 5.5 to find  $\Delta L$ .

$$\Delta L = \frac{\lambda_1 \lambda_2}{n * \Delta \lambda}, \text{ where } n = 1.4677 \text{ and } \Delta \lambda = |\lambda_2 - \lambda_1|$$

Based on the method mentioned above. We find the length difference for each group, and the average of the length difference is 4.0497 cm, with standard deviation of 0.1026 cm.

## 5.9 Spectral Measurement Results of Disk Resonator with LabVIEW

At the end of this project, we had the opportunity to test our LabVIEW-based control program with the disk resonator available in the WPI Optomechanics Lab as shown in Figure 5.9.1. A disk resonator is a disk-shaped device that performs resonance or resonant behavior, in other words, the disk resonator oscillates at certain resonant wavelengths. In the test, we ran the full range motor scanning with the disk resonator to measure the spectrum of the transmission intensity versus the wavelength as shown in Figure 5.9.2.

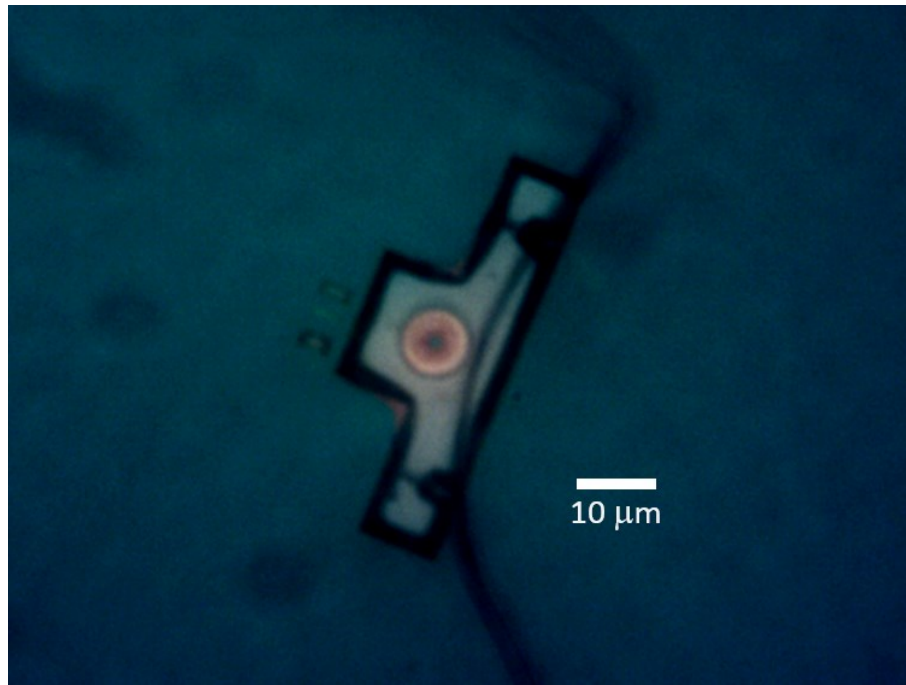
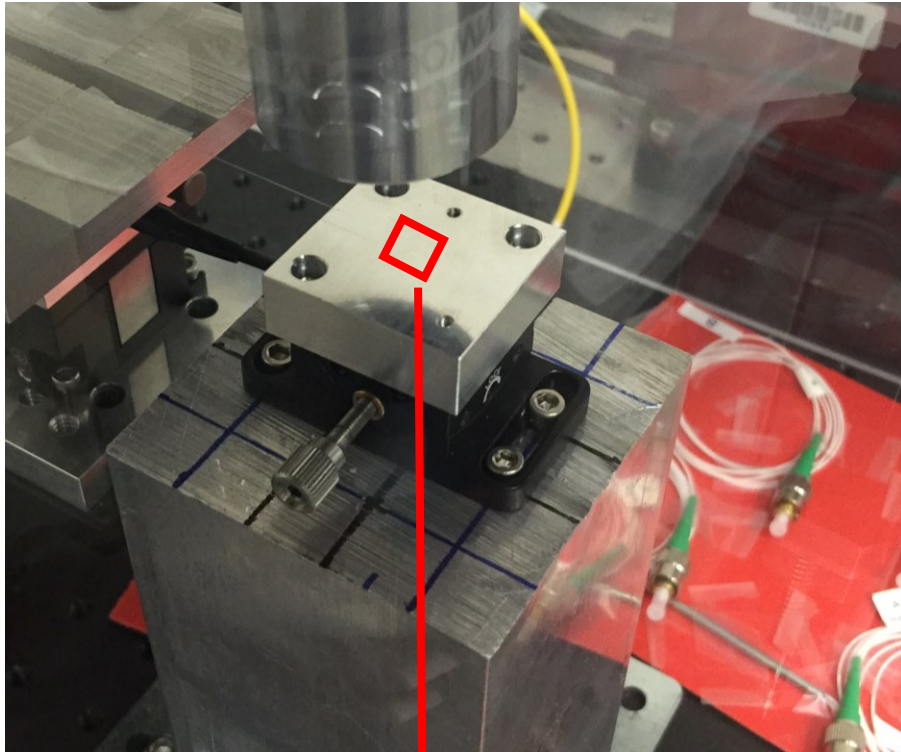


*Figure 5.9.1. Nanophotonic Device (Disk Resonator) in WPI Optomechanics Lab*

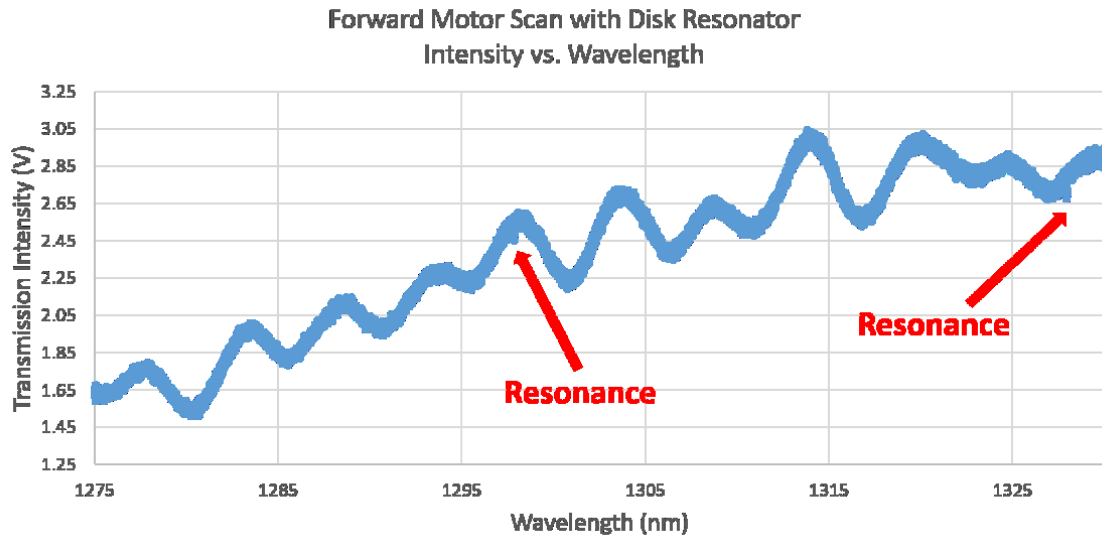


Figure 5.9.2. Forward Motor Scan with Disk Resonator Intensity vs. Wavelength

To find the exact wavelength of resonance, we did the piezo scan at the most obvious resonance wavelength, 1328nm. The results are shown in Figure 5.9.3 and Figure 5.9.4.

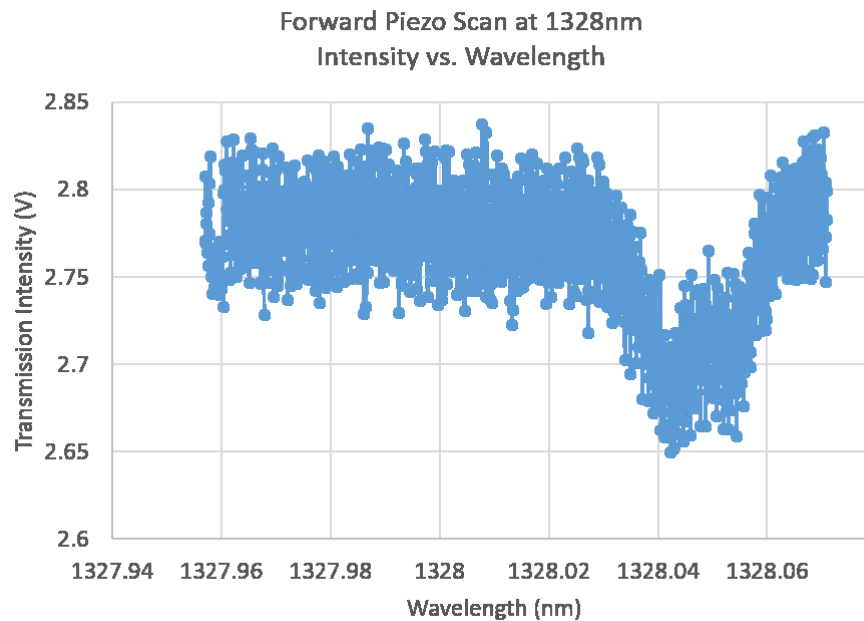
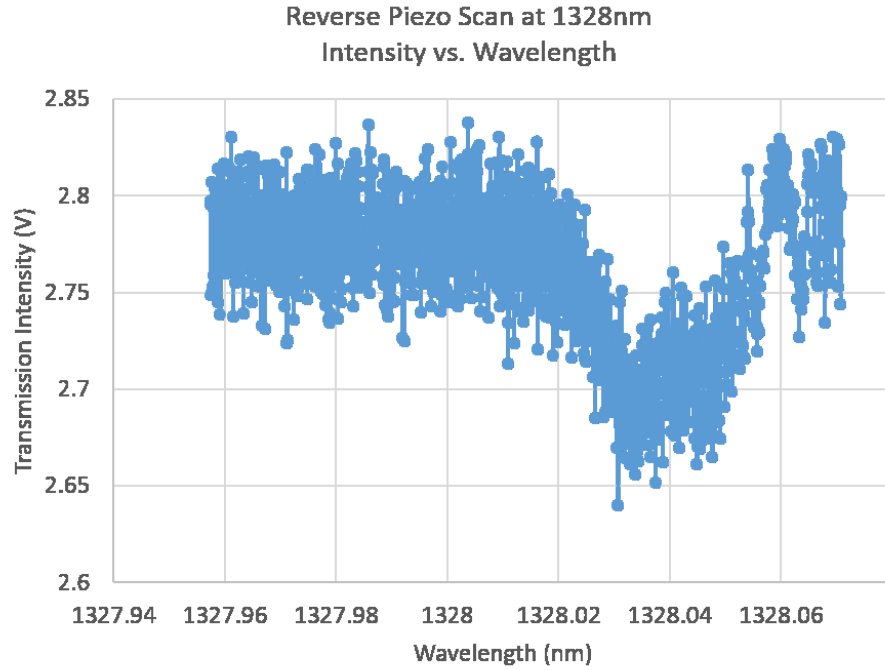


Figure 5.9.3. Forward Piezo Scan at 1286nm Intensity vs. Wavelength



*Figure 5.9.4. Backward Piezo Scan at 1286nm Intensity vs. Wavelength*

We did curve fitting for the forward piezo scan result and found the center frequency as well as bandwidth in frequency. Then we calculated the optical quality factor by dividing the center frequency by the bandwidth as shown in Figure 5.9.5. Finally, we got center frequency of  $2.259 * 10^{11} \text{ Hz}$ , bandwidth of  $3.91 * 10^6 \text{ Hz}$ , and optical quality factor of  $0.578 * 10^5$ .

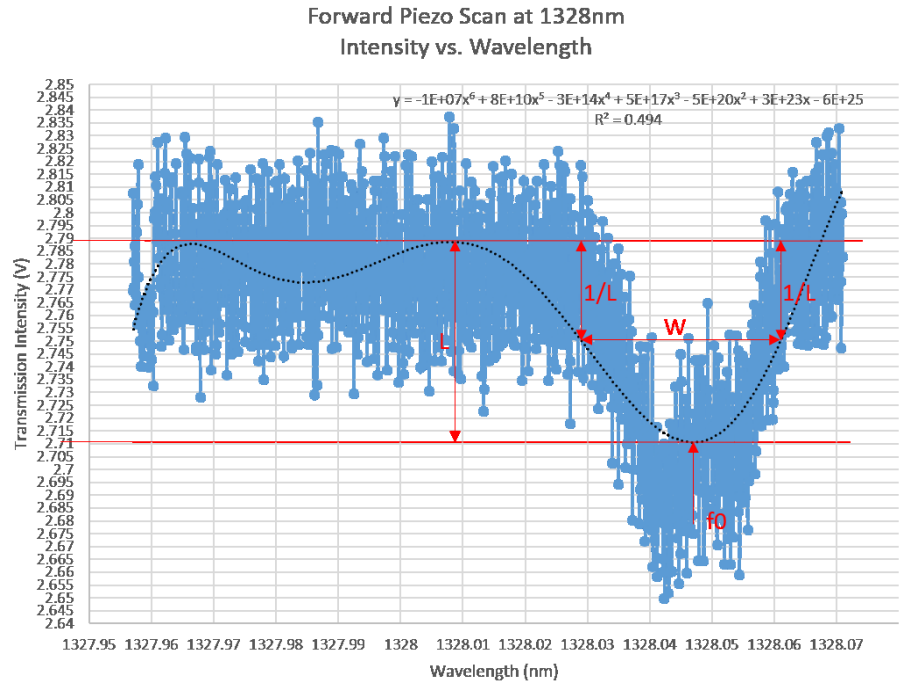


Figure 5.9.5. *Q* factor calculation (*W* is the bandwidth and *f*0 is the center frequency)

This testing proves that our LabVIEW-based control program is advanced and functional enough to find the spectrum that is detailed enough to analyze the peaks or troughs. In the future research in the field of cavity optomechanics, this control program could be utilized to analyze the detail spectrum and behavior of the optical devices.

## 6 Error Analysis

In this chapter, we used the propagation of error theory to find the error percentage of the delta lambda. Propagation of error is the effect of errors of variables on the error of a function based on them. Absolute error is shown as  $\Delta x$ , and relative error is shown as  $(\Delta x)/x$  in percentage. Normally, the error on a quantity  $\Delta x$  is given as the standard deviation,  $\sigma$ . In our calculations, we used the following formulas to calculate the standard deviations.

$$\text{For } f = aA, \sigma_f = a\sigma_A$$

$$\text{For } f = aA + bB, \sigma_f = \sqrt{a^2\sigma_A^2 + b^2\sigma_B^2 + 2ab\sigma_{AB}}$$

$$\text{For } f = AB, \sigma_f = |f| \sqrt{\left(\frac{\sigma_A}{A}\right)^2 + \left(\frac{\sigma_B}{B}\right)^2 + 2\frac{\sigma_{AB}}{AB}}$$

$$\text{For } f = \frac{A}{B}, \sigma_f = |f| \sqrt{\left(\frac{\sigma_A}{A}\right)^2 + \left(\frac{\sigma_B}{B}\right)^2 - 2\frac{\sigma_{AB}}{AB}}$$

As we mentioned in the previous chapters, results from interferometer can be analyzed using the following equation. In this chapter, we would like to find the error of the delta lambda using the known variables.

$$\Delta\lambda = \frac{\lambda_1\lambda_2}{n\Delta L}$$

If X and Y are independent, then their covariance  $\sigma_{XY}$  is zero. Since we did not find any information of the error of refractive index, we assume  $n_{eff}$  has zero uncertainty. In the first step, we let  $f_1 = \lambda_1\lambda_2$ . So the error of  $f_1$  can be found using the following equation.

$$\sigma_{f_1} = \sqrt{f_1^2 * \left[ \left(\frac{\sigma_{\lambda_1}}{\lambda_1}\right)^2 + \left(\frac{\sigma_{\lambda_2}}{\lambda_2}\right)^2 + 2\frac{\sigma_{\lambda_1\lambda_2}}{\lambda_1\lambda_2} \right]}, \text{ where } \sigma_{\lambda_1\lambda_2} = 0$$

In the second step, we let  $f_2 = n\Delta L$ . So the error of  $f_2$  can be found using the following equation.

$$\sigma_{f_2} = n\sigma_{\Delta L}$$

In the third step, we let  $f_3 = \frac{\lambda_1\lambda_2}{n\Delta L} = \frac{f_1}{f_2}$ . So the error of  $f_3$  can be found using the following equation.

$$\sigma_{f_3} = \sqrt{f_3^2 * \left[ \left( \frac{\sigma_{f_1}}{f_1} \right)^2 + \left( \frac{\sigma_{f_2}}{f_2} \right)^2 - 2 \frac{\sigma_{f_1 f_2}}{f_1 f_2} \right]}, \text{ where } \sigma_{f_1 f_2} = 0$$

The following table shows the standard deviation of lambda, n, delta L, the standard deviation of delta L and the error rate of delta L.

$\sigma$ of $\lambda$ (nm)	n	$\Delta L$ (nm)	$\sigma$ of $\Delta L$ (nm)	$\sigma$ of $\Delta L$ (%)
0.1	1.4677	40497010	1026090	2.533742615

*Table 5.9.1. Error of delta L*

The following table shows the calculation results of the three error analysis steps mentioned above.



Measurements			Error of $\Delta\lambda$				
$\lambda_1$ (nm)	$\lambda_2$ (nm)	$\Delta\lambda$ (nm)	$\sigma$ of ( $\lambda_1*\lambda_2$ ) (nm <sup>2</sup> )	$\sigma$ of ( $n* \Delta L$ ) (nm)	$\sigma$ of $\Delta\lambda$ (nm)	( $\sigma$ of $\Delta\lambda$ )/ ( $\Delta\lambda$ ) (%)	
1279.9 7	1279.9 98	0.0278	181.0171015	1505992.29	3.1247E- 06	0.011239938	%
1279.9 98	1280.0 26	0.0278	181.0210331	1505992.29	3.12464E- 06	0.011239702	%
1280.0 26	1280.0 54	0.0279	181.0249716	1505992.29	3.13581E- 06	0.011239465	%
1280.0 54	1280.0 82	0.0278	181.0289102	1505992.29	3.12451E- 06	0.011239229	%
1280.0 82	1280.1 09	0.0278	181.0328417	1505992.29	3.12444E- 06	0.011238993	%
1299.9 49	1299.9 78	0.0284	183.8426012	1505992.29	3.14475E- 06	0.011073062	%
1299.9 78	1300.0 06	0.0284	183.8466176	1505992.29	3.14468E- 06	0.011072829	%
1300.0 06	1300.0 35	0.0284	183.850634	1505992.29	3.14462E- 06	0.011072595	%
1300.0 35	1300.0 61	0.0267	183.8545301	1505992.29	2.95632E- 06	0.011072369	%
1300.0 61	1300.0 9	0.0283	183.8584192	1505992.29	3.13342E- 06	0.011072143	%
1319.9 53	1319.9 83	0.0303	186.6716718	1505992.29	3.30607E- 06	0.010911124	%
1319.9 83	1320.0 12	0.0284	186.6758225	1505992.29	3.09869E- 06	0.01091089	%
1320.0 12	1320.0 42	0.0302	186.6799662	1505992.29	3.29502E- 06	0.010910657	%
1320.0 42	1320.0 7	0.0284	186.6841098	1505992.29	3.09856E- 06	0.010910423	%
1320.0 7	1320.1	0.0302	186.6882535	1505992.29	3.29488E- 06	0.01091019	%
				Average	3.15007E- 06	0.011074241	%

Table 5.9.2. Error Analysis of Delta L

Based on our calculations, we can see our standard deviation of delta lambda is  $3.15 * 10^{-6}$ , which is equivalent to an error rate of 0.011%. Furthermore, when we have a gas cell that can provide an absolute peak in our spectrum with a wavelength accuracy of 0.1pm, we can do further analysis regarding the absolute error of lambda measurement. Since we knew the error for the difference between lambda 1 and lambda 2, where lambda 2 is the peak of the gas cell and

lambda 1 is the signal from our device, we can come up with the absolute error for lambda 1 measurement of 0.1pm.

$$\lambda_1 = \lambda_2 + \Delta\lambda$$

$$\sigma_{\lambda_1} = \sqrt{\sigma_{\lambda_2}^2 + \sigma_{\Delta\lambda}^2 + 2\sigma_{\lambda_2\Delta\lambda}, \sigma_{\lambda_2\Delta\lambda} = 0}$$

$$\sigma_{\lambda_1} = \sqrt{0.0001nm^2 + (3.15 * 10^{-6}nm)^2} = 0.00010005nm = 0.10005pm$$

## 7 Conclusion

In our project, three common type interferometer, Michelson interferometer, Mach-Zehnder interferometer and Fabry-Perot interferometer were compared in classic setup and fiber setup. Based on fully understanding of tunable laser and tunable laser controller, we wrote an advanced LabVIEW program to control tunable laser and built Mach-Zehnder interferometer with fiber setup for precise wavelength measurement. The LabVIEW program has function including wavelength (motor) scan, piezo voltage scan, and data plotting, etc. The Data Acquisition Box (DAQ box) was used for generating signals and collected data. The fiber setup interferometer was built with two 2x2 optical coupler used for splitting and combining signals, and patch cables with different length (optical path length). Attenuators and photodetector were used to measure laser power intensity without damaging our device. With the fully functioning system, we processed wavelength (motor) scan from minimum wavelength value of 1270 nm to a maximum value of 1330 nm. Followed with piezo scans, we measured three sets of data at 1280 nm, 1300 nm and 1320nm respectively. Finally, we calculated optical path length difference, which is 4.0244 cm, with standard deviation of 0.5503 cm.

From this MQP project, we researched basic knowledge of cavity optomechanics and laser working principle, classic and fiber interferometers. We also practiced hands-on skills with fiber, optical coupler and electrical instruments for measurements, and improved the LabVIEW developing skills. The finished LabVIEW program allows users to control laser and visualize data. The measured optical path difference datasheet and wavelength calculation equation can benefit users to conduct more precise wavelength measurement in the future.

## Bibliography

1. Wikipedia,. (2015). Littrow prism. Retrieved 28 August 2015, from [https://en.wikipedia.org/wiki/Littrow\\_prism](https://en.wikipedia.org/wiki/Littrow_prism)
2. CVI, Melles (2010). "CVI Melles Griot : Introduction to Laser Technology" in CVI Melles Griot : Introduction to Laser Technology, (p.<http://www.cvimellesgriot.com/Products/Documents/TechnicalGuide/Laser>).
3. Web.stanford.edu,. (2015). Stanford: Advanced Optical Ceramics Laboratory. Retrieved 28 August 2015, from <http://web.stanford.edu/group/scintillators/ceramicprocessing.html>
4. Wikipedia,. (2015). Tunable laser. Retrieved 21 August 2015, from [https://en.wikipedia.org/wiki/Tunable\\_laser](https://en.wikipedia.org/wiki/Tunable_laser)
5. Fain, B.; Milonni, P. W. (1987). "Classical stimulated emission". *Journal of the Optical Society of America B* 4: 78. doi:10.1364/JOSAB.4.000078
6. Hawthorn, C. J., Weber, K. P., & Scholten, R. E. (2001). Littrow configuration tunable external cavity diode laser with fixed direction output beam. *Review of scientific instruments*, 72(12), 4477-4479.
7. Minh, T. P., Hucl, V., Čížek, M., Mikel, B., Hrabina, J., Řeřucha, Š., ... & Lazar, J. (2015, June). Narrow-linewidth tunable laser working at 633 nm suitable for industrial interferometry. In *SPIE Optical Metrology* (pp. 95254N-95254N). International Society for Optics and Photonics.
8. Miao, H., Srinivasan, K., & Aksyuk, V. (2012). A microelectromechanically controlled cavity optomechanical sensing system. *New Journal of Physics*, 14(7), 075015.
9. Davanco, M., Ates, S., Liu, Y., & Srinivasan, K. (2014). Si<sub>3</sub>N<sub>4</sub> optomechanical crystals in the resolved-sideband regime. *Applied Physics Letters*, 104(4), 041101.
10. Neuhaus, L., Kuhn, A. G., Zerkani, S., Teissier, J., García-Sánchez, D., Deléglise, S., ... & Heidmann, A. (2013, May). Fabry-Perot Cavity Optomechanics with Ultrahigh Mechanical-Q-Factor Quartz Micropillars at Cryogenic Temperature. In *International Quantum Electronics Conference* (p. IA\_7\_4). Optical Society of America.
11. Kippenberg, T. J., & Vahala, K. J. (2007). Cavity opto-mechanics. *Optics Express*, 15(25), 17172-17205.
12. Fiber Instrument. (2015). Retrieved from FIS 1x2 SM Dual Window 1310/1550nm WDM 50/50 ratio 900um: <http://www.fiberinstrumentsales.com/assemblies/couplers-splitters-wdm-s-plc-s/fis-1x2-sm-dual-window-1310-1550nm-wdm-50-50-ratio-900um.html>
13. Wikipedia,. (2015). Core (optical fiber). Retrieved 21 August 2015, from [https://en.wikipedia.org/wiki/Core\\_\(optical\\_fiber\)](https://en.wikipedia.org/wiki/Core_(optical_fiber))
14. Ostrower, J. (2011, March 22). Boeing weighs narrowbody options. Retrieved from WinnCad Elements Blog: <http://winncad.blogspot.com/2011/03/boeing-weighs-narrowbody-options.html>

15. Wikipedia,. (2015). Multi-mode optical fiber. Retrieved 21 August 2015, from [https://en.wikipedia.org/wiki/Multi-mode\\_optical\\_fiber#Comparison\\_with\\_single-mode\\_fiber](https://en.wikipedia.org/wiki/Multi-mode_optical_fiber#Comparison_with_single-mode_fiber)
16. Fiberoptics4sale.com,. (2015). Optical Fiber Tutorial - Optic Fiber - Communication Fiber. Retrieved 21 August 2015, from <http://www.fiberoptics4sale.com/Merchant2/optical-fiber.php>
17. Spie.org,. (2015). Photon Detectors. Retrieved 21 August 2015, from <http://spie.org/x32386.xml>
18. Thorlabs.com. (2015). Thorlabs - PDA20C InGaAs Fixed Gain Detector, 800-1700 nm, 5 MHz BW, 3.14 mm<sup>2</sup>, 120 VAC. Retrieved 2 September 2015, from <http://www.thorlabs.com/thorproduct.cfm?partnumber=PDA20C>
19. Newport.com,. (2015). TLB-6700\_\_User\_Manual\_Rev\_D. Retrieved 21 August 2015, from [http://assets.newport.com/webDocuments-EN/images/TLB-6700\\_\\_User\\_Manual\\_Rev\\_D.pdf](http://assets.newport.com/webDocuments-EN/images/TLB-6700__User_Manual_Rev_D.pdf)
20. Paschotta, D. (2015). Encyclopedia of Laser Physics and Technology - external-cavity diode lasers, ECDL. Rp-photonics.com. Retrieved 21 August 2015, from [http://www.rp-photonics.com/external\\_cavity\\_diode\\_lasers.html](http://www.rp-photonics.com/external_cavity_diode_lasers.html)
21. Exfo.com,. (2015). Animated Glossary | Fiber Optics | EXFO. Retrieved 21 August 2015, from <http://www.exfo.com/support/services/instrument-services/be-expert-training-program/animated-optical-glossary>
22. Brown, W. J., & Williams, A. L. (1948). U.S. Patent No. 2,439,499. Washington, DC: U.S. Patent and Trademark Office.
23. Littman, M. G., & Metcalf, H. J. (1978). Spectrally narrow pulsed dye laser without beam expander. *Applied Optics*, 17(14), 2224-2227.
24. Wikipedia,. (2015). Interference (wave propagation). Retrieved 28 August 2015, from [https://en.wikipedia.org/wiki/Interference\\_\(wave\\_propagation\)](https://en.wikipedia.org/wiki/Interference_(wave_propagation))
25. Applied-spectroscopy.com,. (2015). Film Thickness Measurement and Film Thickness Gauge, Coating Thickness Gage. Retrieved 28 August 2015, from <http://www.applied-spectroscopy.com/ftm.htm>
26. Wikipedia,. (2015). Michelson interferometer. Retrieved 2 September 2015, from [https://en.wikipedia.org/wiki/Michelson\\_interferometer](https://en.wikipedia.org/wiki/Michelson_interferometer)
27. Spie.org,. (2006). Photonic crystals reduce the size of optical sensors. Retrieved 2 September 2015, from <http://spie.org/x8577.xml#fig1>
28. COMSOL Blog,. (2014). Optimizing Mach-Zehnder Modulator Designs with COMSOL Software. Retrieved 2 September 2015, from <https://www.comsol.com/blogs/optimizing-mach-zehnder-modulator-designs-comsol-software/>
29. Wang, Yung-Cheng, Lih-Horng Shyu, and Chung-Ping Chang. "The comparison of environmental effects on Michelson and Fabry-Perot interferometers utilized for the displacement measurement." *Sensors* 10.4 (2010): 2577-2586.

30. Wikipedia,. (2015). Fourier transform. Retrieved 21 August 2015, from [http://en.wikipedia.org/wiki/Fourier\\_transform](http://en.wikipedia.org/wiki/Fourier_transform)
31. Wei, Tao, et al. "Temperature-insensitive miniaturized fiber inline Fabry-Perot interferometer for highly sensitive refractive index measurement." *Optics Express* 16.8 (2008): 5764-5769.
32. Corning SMF-28 Optical Fiber. (2015). Retrieved 21 August 2015, from <http://ece466.groups.et.byu.net/notes/smf28.pdf>.

# Appendix A

The MATLAB code for sinusoidal wave fitting:

```
yu = max(y);
yl = min(y);
yr = (yu-yl);           % Range of 'y'
yz = y-yu+(yr/2);
zx = x(abs(yz) <= 0.0025); % Find zero-crossings
per = 2*mean(diff(zx)); % Estimate period
ym = mean(y);          % Estimate offset
fit = @(b,x) b(1).*(sin(2*pi*x./b(2) + 2*pi/b(3))) + b(4); % Function to fit
fcn = @(b) sum((fit(b,x) - y).^2); % Least-Squares cost function
s = fminsearch(fcn, [yr; per; -1; ym]) % Minimise Least-Squares
xp = linspace(min(x),max(x));
figure(1)
plot(x,y,'b', xp,fit(s,xp), 'r')
grid
[pks,locs]=findpeaks(fit(s,xp),xp);
```